Monitoring the degradation of PE pipes by IR-microscopy

Vom Fachbereich Chemie
der Technischen Universität Darmstadt
zur Erlangung des akademischen Grades eines

Doctor rerum naturalium
(Dr. rer. nat.)

genehmigte
Dissertation

vorgelegt von

Raquel Maria (Lic.)
Aus Lissabon, Portugal

Berichterstatter: Prof. Dr. M. Rehahn

Mitberichterstatter: Prof. Dr. M. Busch

Tag der Einreichung: 27th September 2013

Tag der mündlichen: 25th November 2013

Darmstadt 2014
D17

Diese Arbeit wurde unter der Leitung von Herrn Prof. Dr. Matthias Rehahn am Deutschen Kunststoff-Institut in der Zeit von Juli 2008 bis Juni 2012 durchgeführt.

To my parents,
Filipe and my grandmother

I would like to thank Prof. Dr. M. Rehahn who gave me the opportunity to work in his research group. I'm also thankful him for providing me a challenging research topic.

I sincerely thank my supervisor, Dr. Robert Brüll. His understanding, encouraging and personal guidance have provided a good basis for the present thesis. I also appreciate him for his optimistic discussions.

I acknowledge Christoph Brinkmann for his help with the SEC measurements.

I thank Frank Dorbath for his help with the OIT measurements at the Süddeutsches Kunststoff-Zentrum (SKZ).

I would like to express my gratitude to Karsten Rode for his friendship, moral support and scientific contribution during this study.

I'm thankful to all my past and present colleagues of DKI for the pleasant working atmosphere.

To Antonino Natoli and Sylvia Engel, I would like to thank their special friendship and to be there for us all the time.

I would like to thank my parents, Margarida and Deodato Maria, to whom I'm eternally grateful for their encouragement, support and patience during the course of my PhD as well their support to reach my goals during my life.

I am also thankful to Dolores and Carlos Natálio for their friendly and encouragement support.

A special thanks to my husband, Filipe Natálio, for his endless love, inspirations, support and tolerance throughout our life together and of course to all his patience during my PhD.

Index

1. Summary

Stabilisers, commonly hindered phenolic antioxidants (AO) and hindered amine light stabilisers (HALS), are added to protect polyolefins against thermo- and photo-oxidative degradation. Analysing the content of additives in polyolefin compounds or their residual stability is therefore essential to identify changes in these parameters as a result of application. High performance liquid chromatography (HPLC) and the oxidation induction time (OIT) are currently used for this purpose. In the case of polyolefin pipes concentration profiles of additives over the pipe wall can be obtained by mechanically abrasing layers and individually analysing these by HPLC and OIT. This approach is very labour intensive and, has a lower spatial resolution, and additionally a lower reproducibility.

Pipes are often exposed to different weathering conditions, either as semifinished product before installation or in final outdoor use. The elemental processes during weathering of polyethylene, i.e. extraction of antioxidants from the polymer and oxidation of the polymer, have been studied using the traditional aproach. However due to the mentioned deficits the data are insufficient and as a result of that these processes have not yet been correlated to the conditions of weathering. Therefore, the aim of this research project was, to develop an analytical method that allows to follow the degradation processes in the pipe wall during weathering. Particular focus was on the influence of UV radiation in the depletion of the phenolic long-term stabiliser, Irganox 1010.

IR-microscopy which combines the image analysis specificity of light microscopy with the chemical specificity of IR-spectroscopy fulfils the above requirements giving novel information about these elemental processes. Namely it is able to profile the concentration of antioxidants, degradation products of the polymer and the crystallinity of the pipe wall.

Pipes made from high density polyethylene (HDPE) were weathered under different climatic conditions. The pipes were stabilised with Irganox 1010 as phenolic AO and Irgafos 168 as processing stabiliser. To study the influence of different UV and light stabilising additives, additional pipes were stabilised with Tinuvin 327 as UV absorber, Tinuvin 770 as HALS, and with carbon black (CB).

Using IR-microscopy it could be shown that a loss of Irganox 1010 occurs upon weathering, with its extent depending on the climate chosen. It could be concluded that both temperature and UV radiation are the primary influence factors while humidity is of

minor significance.

To investigate in detail the correlation between the exposure to UV radiation and the loss of Irganox 1010, samples were exposed to artificial weathering. It was found that the loss of AO as determined by IR-microscopy and integrated over the pipe wall correlates linearily with the radiation dose. From the slope of the straight line the corresponding rate constants were calculated for the first time. As expected significantly higher values were found for the side exposed to radiation than for the unexposed one.

The disappearance of vinyl unsaturations originally present in PE, as well as the formation of *trans*-vinylene groups as unsaturated degradation products of PE, could also be quantified. The disappearance of vinyl unsaturations followed a first-order law and *trans*-vinylene unsaturations were formed proportionate to the dose of UV radiation on the side exposed to the radiation. At the same time the degree of crystallinity of the pipe remains unaffected and no breakdown of the molar mass occurs as shown by size exclusion chromatography (SEC).

HPLC analysis showed that the ratio of phosphite/phosphate decreases as a consequence of the exposure to UV radiation while the content of Irgafos 168 – i.e. the sum of phosphite and phosphate - remains constant.

Due to the fact that the phosphate has an absorption band which overlaps with the absorption band used to quantify the *trans*-vinylene groups, a new approach to calculate the amount of Irgafos and, following that, the content of *trans*-vinylene groups, was developed.

Adding a combination of the UV absorber Tinuvin 327 and the HALS Tinuvin 770 had no measurable effect on the loss of Irganox 1010. Interestingly HPLC analysis showed that Tinuvin 770 is also lost as a result of the UV exposure but to a lower extent than Irganox 1010. For the case of Tinuvin 327 no loss is observed as a result of the UV exposure.

In this study was also shown by IR-microscopy, that the presence of CB significantly prevents the loss of Irganox 1010. A relative decrease in the concentration of Irganox 1010 in the outer pipe wall by approximately 10 % after exposure to UV radiation was found in the presence of CB, compared to approximately 30 % without CB.In the case of the pipe stabilised with CB the triester of Irganox 1010 was identified as metabolite by HLPC analysis. This suggests that CB, apart from acting as a UV absorber, slows the loss of low molar mass metabolites of the AO.

Based on these results a mechanism for the photodegradation of Irganox 1010 in the presence of CB triggered by Norrish cleavage could be proposed.

1. Zussammenfassung

Stabilisatoren, im Allgemeinen sterisch gehinderte phenolische Antioxidantien (AO) und gehinderte aminische Lichtschutzmittel (HALS), werden Polyolefinen hinzugefügt, um sie gegen thermo- und photo-oxidativen Abbau zu schützen. Die Analyse des Additivgehaltes in Polyolefincompounds, bzw. deren nach Belastung durch den Abbau fördernde Parameter verbliebenen Anteilen, ist notwendig, um Veränderungen hinsichtlich des Stabilisierungszustandes zu identifizieren. Als Standardverfahren zur Gehaltsbestimmung von Stabilisatorenwerden gegenwärtig die Hochleistungsflüssigchromatographie (HPLC) und die Oxiddationsinduktionszeit (OIT) eingesetzt. Im Falle von Polyolefin-Rohren kann man Konzentrationsprofile von Additiven über die Wandung ermitteln, indem Schichten durch mechanische Abrasion separiert und einzeln mittels HPLC und OIT analysiert werden. Dieser Ansatz ist jedoch sehr arbeitsintensiv, unzureichend hinsichtlich räumlicher Auflösung, und zudem nur mäßig reproduzierbar.

Rohre werden oft unterschiedlichen Witterungsbedingungen ausgesetzt, entweder vor der Installation in Form des Halbzeugs oder bei Gebrauch im Außeneinsatz. Die Extraktion von AO aus dem Polymer sowie dessen Oxidation wurde bereits unter Verwendung des beschriebenen traditionellen Ansatzes untersucht. Jedoch sind die erhaltenen Datensätze sehr unzureichend und konnten aus diesem Grunde bisher nicht mit den Bewitterungsbedingungen korreliert werden. Daher war es das Ziel dieses Forschungsprojektes eine analytische Methode zu entwickeln, mit der man Veränderungen des Stabilisierungszustandes und des Polymers in der Wandung von Polyolefinrohren während der Bewitterung verfolgen kann. Besonderes Augenmerk lag dabei auf dem Einfluss von UV-Strahlung und deren Auswirkungen auf den Verlust und Abbau des phenolischen Langzeitstabilisators Irganox 1010.

Die IR-Mikroskopie, welche die Eigenschaften der lichtmikroskopischen Bildgebung mit den chemischen Informationen aus der IR-Spektroskopie verbindet, erfüllt die oben genannten Anforderungen und liefert grundlegende Informationen zu den elementaren Prozessen. Die Methode ist geeignet, um Konzentrationsprofile von AO und Abbauprodukten des Polymers sowie die Verteilung der Kristallinität über den Querschnitt

der Rohrwand zu ermitteln.

Rohre wurden aus Polyethylen hoher Dichte (HDPE) hergestellt und unter verschiedenen klimatischen Bedingungen bewittert. Die Rohre wurden mit Irganox 1010 als Langzeitstabilisator versetzt und zusätzlich für die Verarbeitung mit Irgafos 168 stabilisiert. Um den Einfluss von unterschiedlichen UV-und lichtstabilisierenden Additiven zu untersuchen, wurden zusätzliche Rohre mit Tinuvin 327 als UV-Absorber, Tinuvin 770 als HALS sowie mit CB stabilisiert.

Unter Verwendung der IR-Mikroskopie wurde gezeigt, dass bei Bewitterung ein Verlust von Irganox 1010 aus der Wandung auftritt, dessen Umfang von den klmatischen Bedingungen abhängt. Daraus ließ sich schließen, dass sowohl Temperatur- als auch UV-Strahlung die primären Einflussfaktoren sind, während Luftfeuchtigkeit von untergeordneter Bedeutung ist.

Um im Detail den Zusammenhang zwischen UV-Bestrahlung und Verlust von Irganox 1010 zu untersuchen, wurden die Proben einer künstlichen Bewitterung ausgesetzt. Mittels IR-Mikroskopie wurde durch Profilierung der AO-Konzentration über die Rohrwand festgestellt, dass der Verlust von AO linear mit der Strahlendosis korreliert. Aus der Steigung der Geraden wurde erstmalig eine Geschwindigkeitskonstante zum Verlust des AO berechnet. Für belichtete und unbelichtete Bereiche des Rohres konnten diese Geschwindigkeitskonstanten separat ermittelt werden. Wie erwartet, ist die Steigung der Geraden für die belichtete Seite des Rohres signifikant höher als für die unbelichtete Seite.

Desweiteren konnten der Verlust von ungesättigten Vinylgruppen, die ursprünglich in PE vorhanden waren, sowie die Bildung von trans-Vinylengruppen als ungesättigten Abbauprodukten von PE quantifiziert werden. Der Verlust der endständigen Vinylbindngen folgte einem Gesetz erster Ordnung während die ungesättigten trans-Vinylengruppen auf der belichteten Seite proportional zur Dosis der UV-Strahlung entstanden. Gleichzeitig bleibt der Kristallinitätsgrad des Kunststoffs in der Wandung unbeeinflusst. SEC-Analysen belegten, dass kein Abbau der Molmasse des Polymers auftritt.

Eine HPLC-Analyse des Verarbeitungsstabilisators Irgafos 168 zeigte, dass das Verhältnis von Phosphit/Phosphat als Folge der Einwirkung von UV-Strahlung abnimmt, während der Gesamtgehalt, - d.h. die Summe von Phosphit und Phosphat, konstant bleibt.

Aufgrund der Tatsache, dass die Absorptionsbande des Phosphates mit derjenigen für die

Berechnung der trans-Vinylengruppen verwendeten überlappt, wurde ein neuer Ansatz entwickelt, um den Gehalt von Irgafos 168 und der trans-Vinylengruppen separat zu quantifizieren.

Die Zugabe einer Kombination des UV-Absorbers Tinuvin 327 und des HALS Tinuvin 770 hatte keinen messbaren Effekt auf den Verlust von Irganox 1010. Interessanterweise zeigte die HPLC-Analyse, dass in Folge der Belichtung auch Tinuvin 770 verloren geht, wenn auch zu einem geringeren Ausmaß als Irganox 1010. Für Tinuvin 327 wurde kein Verlust aufgrund von UV-Bestrahlung beobachtet.

Zudem wurde in dieser Studie durch IR-Mikroskopie nachgewiesen, dass die Anwesenheit von Ruß den Verlust von Irganox 1010 aus der Rohrwandung signifikant verzögert. Nach UV-Bestrahlung wurde in Gegenwart von Ruß eine relative Abnahme der Konzentration von Irganox 1010 in der äußeren Rohrwand um ca. 10 % gefunden, verglichen mit 30 % ohne Ruß.

Im Fall des mit Ruß stabilisierten Rohres wurde mittels HLPC Analyse der Triester des Irganox 1010 als Metabolit identifiziert. Dies legt nahe, dass CB, abgesehen von der Wirkung als UV-Absorber, auch den Verlust von Metaboliten mit niedrigem MM verlangsamt.

Basierend auf diesen Ergebnissen konnte ein Mechanismus der Norrish-Spaltung für den Photoabbau von Irganox 1010 in Gegenwart von Ruß vorgeschlagen werden.

2. Introduction

2.1 An overview of polyolefins

Polyolefins are the most widely used synthetic polymers in the world. In recent decades they have replaced traditional materials like wood, ceramics or metal due to their superior and versatile mechanical properties, light weight, good processability and low cost. And it these features which make polyolefins highly suitable for numerous applications in the construction sector where high strength and durability are required. The most important polyolefins are polyethylene (PE) and polypropylene (PP). PE it is a light, versatile thermoplastic made by polymerisation of ethylene and can be found in a wide variety of applications ranging from pipes, packaging (detergent bottles, carrier bags, containers), toys, to household items such as laundry baskets and water buckets (Figure 1).

Figure 1: Representative applications of PE.

PE can be classified into several categories depending on its density and the method of synthesis [1]. Low density PE (LDPE) is produced in a free radical process by an autoclave or tubular process. It is characterised by a randomly long-chain branched structure also containing short-chain branches (SCB) of varying length [2]. The SCB, mostly between two and four carbons long, control the density of the product. Depending on the desired application, the molar mass distribution (MMD) can be varied [3,4]. Linear low density PE (LLDPE) which is produced via transition metal catalysis structurally differs from LDPE due to the absence of long chain branches. In LLDPE the SCB is introduced by copolymerising ethylene with a 1-olefin. High-density PE (HDPE) is linear, i.e. contains no long- and short-chain branches. Depending on the final application, the macroscopic properties can be modified by incorporating a small amount of SCB via adding comonomer. On a commercial scale both LLDPE and HDPE are produced using Ziegler-Natta- or metallocene-catalysts, which yield a relatively broad or narrow MMD respectively [5-15]. HDPE can be also produced by chromium based catalysts [16-18].

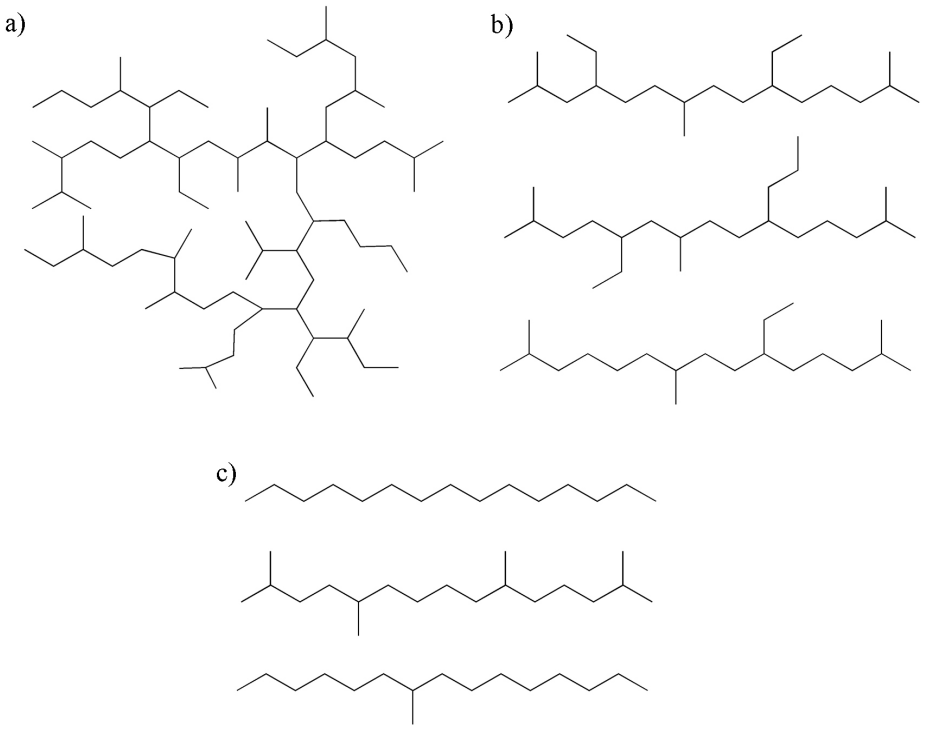

Figure 2: Structures of a) LDPE, b) LLDPE and c) HDPE.

PP is produced by transition metal catalysed polymerisation using either Ziegler-Natta or metallocene-catalysts. It is the fastest growing polyolefin and has a wide variety of applications including packaging and labeling, textiles (e.g. ropes and carpets), containers of various types, laboratory equipment and automotive components. From a commercial perspective simply referred to as PP, these materials can be classified based on their composition into the homopolymer (PP-H) and copolymers of propene and ethylene. Within PP-H the isotactic, syndiotactic and the atactic stereoisomer can be distinguished. In isotactic PP (i-PP) the methyl group has always the same configuration relative to the polymer backbone. In syndiotactic PP (s-PP) the methyl group has an alternating configuration with regard to the polymer backbone and in atactic PP (a-PP) the configuration is random (Figure 3).

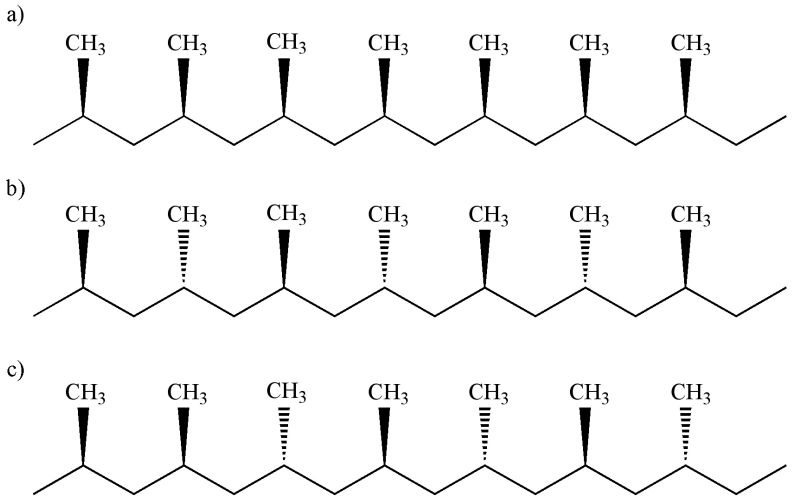

Figure 3: Chain structures of PP: a) i-PP, b) s-PP and c) a-PP

PP copolymers can be divided into random (PP-R) and high impact (hi-PP) copolymers. PP-R is manufactured by copolymerising propene with a small amount of ethylene. The random incorporation of ethylene results in a lowering of the melting point and glass transition temperature which ensures higher flexibility, particularly at low temperature. Hi-PP is manufactured in a two-stage process and contains phase-separated domains of ethylene-propylene (EP)-elastomer dispersed in a PP matrix. This morphology improves impact strength significantly, as the elastomeric phase can dissipate mechanical energy.

2.2 Polyolefins in pipe applications

Due to their previously mentioned advantageous properties polyolefins are widely used to produce pipes and successfully compete with metals or ceramics. Their good performance/cost ratio, low density, easy processability and durability towards corrosion make them suitable for a wide range of applications. The particular market for the individual polyolefins in the pipe sector is determined by the specific demands of the application. PP-H is frequently used in industrial pressure pipe systems, soil and waste water pipes as well as fittings. Due to its balanced combination of flexibility and pressure resistance, particularly at elevated temperatures, PP-R has found widespread application for domestic pressure pipe systems to transport hot and cold water. Hi-PP is, due to its combination of high stiffness and impact strength, especially at low temperatures, paired with good long term properties the favorite material for sewerage and drainage applications like for example revision chambers [19-21]. LDPE was used in the early 1950s for water pipe applications but only with limited success due to its poor stress crack resistance. At the same time a 1st generation HDPE based on Ziegler-Natta catalysts was developed which was more resistant towards hoop stress and had a greater stiffness than LDPE. However the resistance towards rapid crack propagation was poor which made further improvements necessary. This drawback was overcome by using chromium based (Philips) catalysts which produce PE with very high average MM and a broad MMD. In the early 1990s, a 3rd generation Ziegler-Natta based HDPE was developed by incorporating SCB in the high molar mass fraction. These materials are produced in a dual reactor process (cascade) and have a bimodal MMD consisting of a low MM linear homopolymer (HDPE) and a high MM copolymer containing SCB [22-24]. The so called inverse comonomer distribution results in an improved resistance towards hoop stress and crack propagation. It is common to classify HDPE for pipe applications based on its long term strength into PE 80 and PE 100. This is the minimum internal pressure (8 and 10 MPa respectively) the material has to withstand at 20 °C for 50 years [25]. In the field of hot water pipes, particularly in household installations, crosslinked PE (PE-X) is also widely used [19,20,26]. The crosslinking improves the mechanical properties including resistance to cold temperatures, cracking or brittleness on impact while retaining its flexibility. Three methods are used to crosslink PE for pipe applications: These are peroxide (Engel) curing, referred to as PE-X_a, silane crosslinking

(PE-X_b), and beta irradiation (PE-X_c). In the Engel process heat is used to activate the peroxide and thereby generate free radicals. In PE-X_b, crosslinking is achieved via silane bridges in two steps. The first step is to graft a silane onto the backbone of the PE and after the final product is formed adjacent silane branches react then in the presence of moisture, thus linking the PE chains. In the irradiation method free radicals are generated by an electron beam and thereby causing the crosslinking.

2.3 Polyolefins and degradation

As aliphatic hydrocarbons polyolefins are susceptible to degradation in every step of their lifecycle, i.e., during manufacturing (synthesis and processing) where they are exposed to high temperatures in the presence of oxygen, and during end-use. From a phenomenological point of view polyolefin degradation manifests itself in undesirable changes of the macroscopic physical and chemical properties [27-29] which eventually lead to premature failure [30]. Within the degradation of polyolefins the thermo-oxidative and photo-oxidative pathway can be distinguished. The term 'weathering' normally refers to an out-door accomplished process where degradation is triggered by a combination of factors like oxygen, temperature, humidity and UV irradiation [31-35]. Polyolefin degradation by oxidation (thermo-oxidative and photo-oxidative) is described by the classical free-radical chain mechanism consisting of initiation, propagation and termination. These steps will be considered in the following.

2.3.1 Initiation

The two reactions leading to the formation of radicals in the initiation step are abstraction of a hydrogen atom from the polymer backbone (reaction 1.1) or cleavage of a polymer chain to form terminal polymer radicals (reaction 1.2) as schematically represented in Scheme 1.

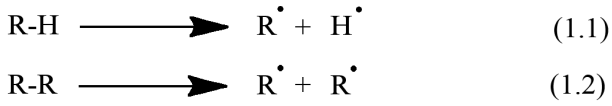

Scheme 1: Possible initiation steps for polyolefin degradation.

The C-C-cleavage (bond dissociation energy ~ 349 kJ/mol) is primarily caused by high temperatures or processing involving high shear, e.g. extrusion (reaction 1.2). C-H cleavage (bond dissociation energy ~ 410 kJ/mol) can be the result of a chemical or radiation attack, occurring more readily at elevated temperatures (reaction 1.1) [36-37]. The formed radicals may either recombine (as is the case during crosslinking), or react with other molecules present in the polymer matrix like for example molecular oxygen and continue the cycle of degradation (reaction 1.3). In the case of photo-oxidation in a polymer matrix consisting solely of saturated C-C- and C-H- bonds the initiation step can be attributed to the presence of molecules containing a UV absorbing group such as, impurities, catalyst residues or carbonyl groups as discussed in 2.3.

2.3.2 Propagation

During propagation, the alkyl radicals initially formed react with molecular oxygen to yield peroxy radicals (reaction 1.3).

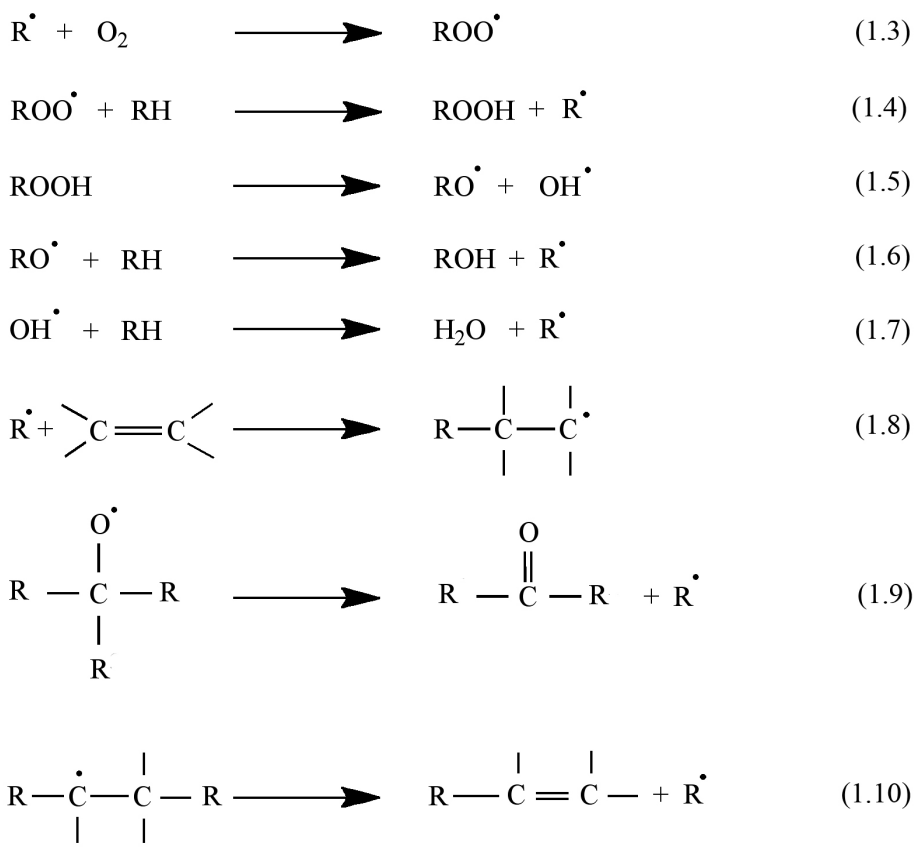

Scheme 2: Possible branching and propagation reactions in the degradation of polyolefins.

The peroxy radical abstracts a hydrogen atom from another polymer molecule (reaction 1.4) to form a hydroperoxide and generate another polymer radical. Hydroperoxides can be cleaved homolytically to yield an alkoxy- and a hydroxyl radical (reaction 1.5). Both are capable to abstract a hydrogen atom from adjacent polymer chains, resulting in the formation of water, an alcohol and more alkyl radicals capable of further reactions (reaction 1.6 - 1.8). Free radicals formed during the first two steps may also undergo further reactions leading to the insertion of various oxygen-containing groups. ß-cleavage (reaction 1.9) will lead to chain scission and a decrease of the MM.

2.3.3 Termination

Chain termination occurs by recombination or disproportionation of radicals. Potential steps leading to chain termination are reactions 1.11 - 1.15 (Scheme 3).

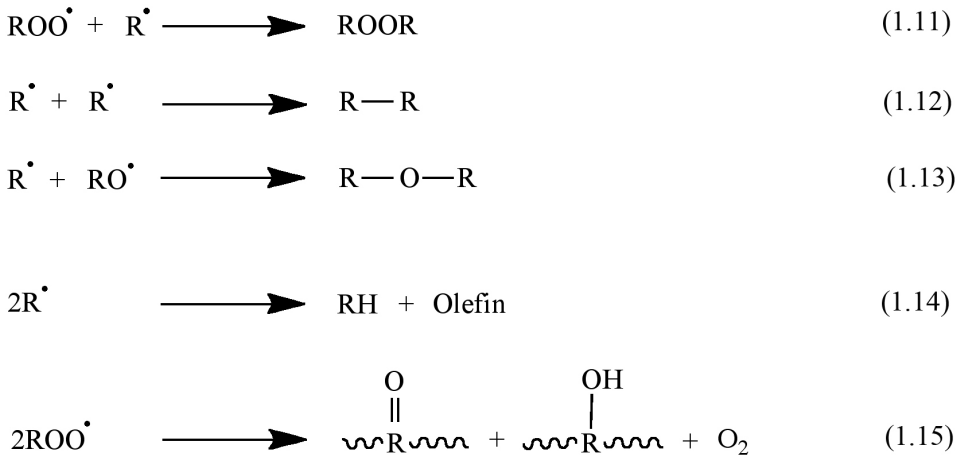

Scheme 3: Possible termination reactions in polyolefin degradation.

At high oxygen concentration and moderate temperatures chain termination proceeds by the recombination of peroxy radicals according to reaction 1.15. If the concentration of (R•) radicals is much higher than that of peroxy radicals (characteristic for processing of PE under oxygen depletion), chain termination is caused by recombination with other available radicals according to reactions 1.11 and 1.12.

The chain termination processes do not stop the thermo-oxidative reactions. The reaction products formed in the recombination reaction of peroxy radicals participate in further reactions.

2.3.4 Specific mechanism of degradation of PE

The degradation of PE has been studied extensively [38-43]. Since PE has only C-C and C-H bonds, it is at ambient temperatures relatively inert. However unsaturations may be formed during synthesis and processing which then facilitate the initiation of degradation. In the same sense different polymerisation catalysts may lead to varying amounts of

unsaturated end groups and in addition leave different types and levels of catalyst residues which in turn play an important role in the stability of the polymeric material [44-47]. The general degradation mechanism of PE consists also of the steps of initiation, propagation and termination as discussed in 2.3.1. In the initiation step, secondary alkyl radicals are formed under the influence of heat, shear, or UV radiation by chain scission (Scheme 4):

(1.16)

Scheme 4: Formation of an alkyl radical during initiation of PE degradation.

In the propagation step the alkyl radical will react with oxygen to form a hydroperoxide (reaction 1.17 and reaction 1.18).

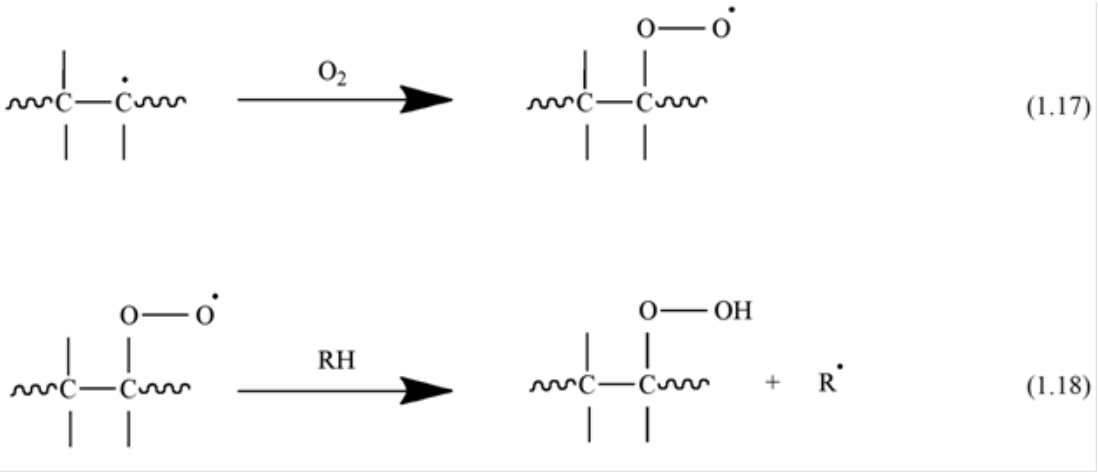

Scheme 5: Formation of a secondary hydroperoxide during initiation of PE degradation.

Hydroperoxides are unstable and their degradation, triggered by light or heat, will yield a carbonyl group and water. The main products of the photolysis are ketones (reaction 1.19) [48-50].

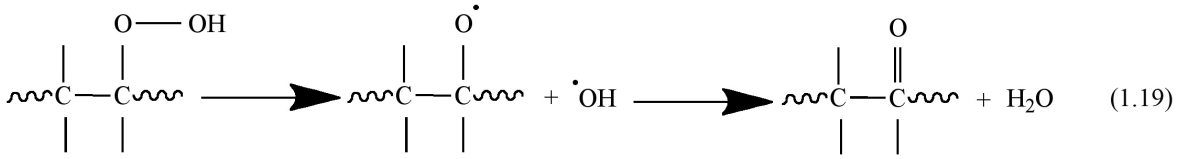

Scheme 6: Intramolecular photolysis of secondary hydroperoxides.

Ketones in turn can undergo Norrish type I (reaction 1.21) and II (reaction 1.22) photo-cleavage which result in backbone scission to yield free radicals capable to initiate photo-oxidation or undergo rearrangements (Scheme 7) [51-53].

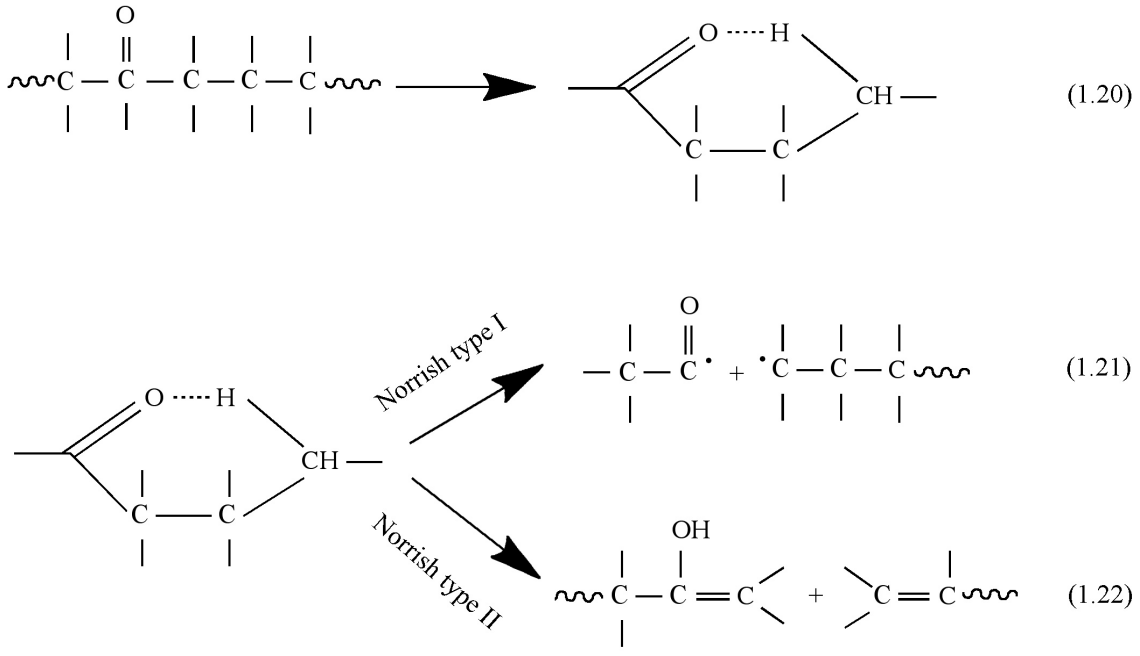

Scheme 7: Photolysis of PE, the Norrish reactions.

Secondary hydroperoxides may decompose yielding an aldehyde and a macroalkyl radical (reaction 1.23) [54].

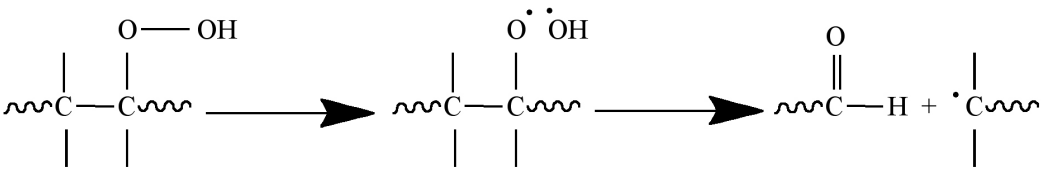

(1.23)

Scheme 8: Decomposition of the secondary hydroperoxide to an aldehyde.

Reaction with another chain segment (reaction 1.24) [31] will yield water and an internal (*trans*-vinylene) double bond.

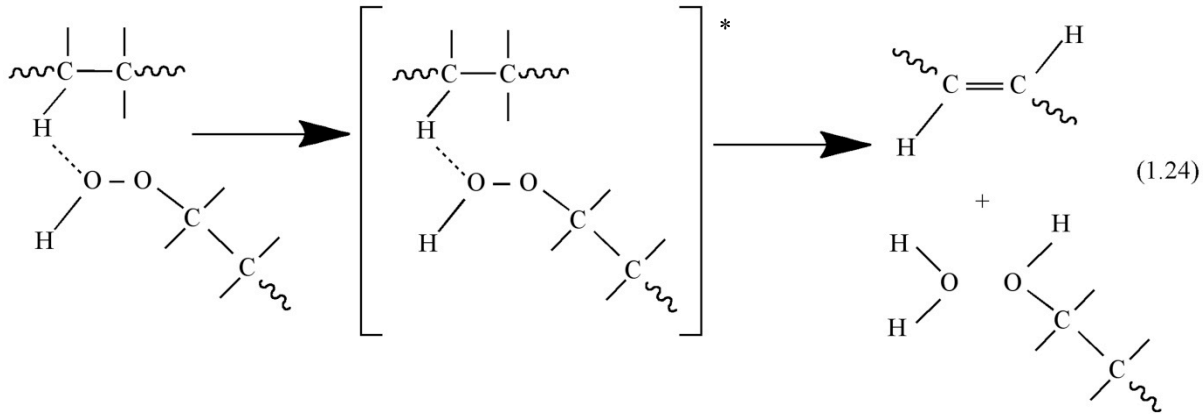

(1.24)

Scheme 9: Formation of *trans*-vinylene groups during degradation of PE.

β-scission of tertiary C-centered radicals will lead to vinylidene groups (reaction 1.25)[32,55].

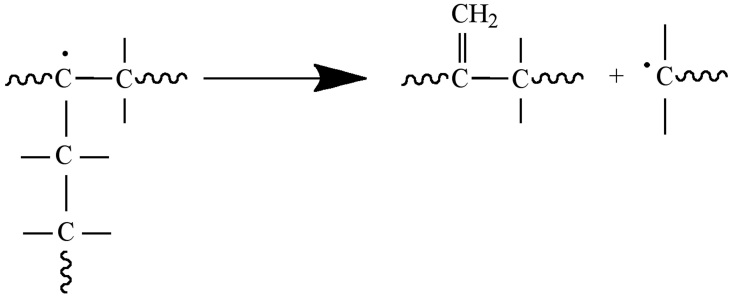

(1.25)

Scheme 10: ß-scission of a tertiary radical.

These can react with free radicals or absorb UV-radiation and may thus act as precursor for the formation of hydroperoxides.

2.4 Prevention of degradation/stabilisers

The success story of polyolefins in durable applications is only possible due to stabilising additives which are added to protect the polymer against degradation [56-57] during processing and long term use by trapping emerging free radicals or unstable intermediates. The general scheme of degradation with potential points of interception by stabilising additives is shown in Figure 4.

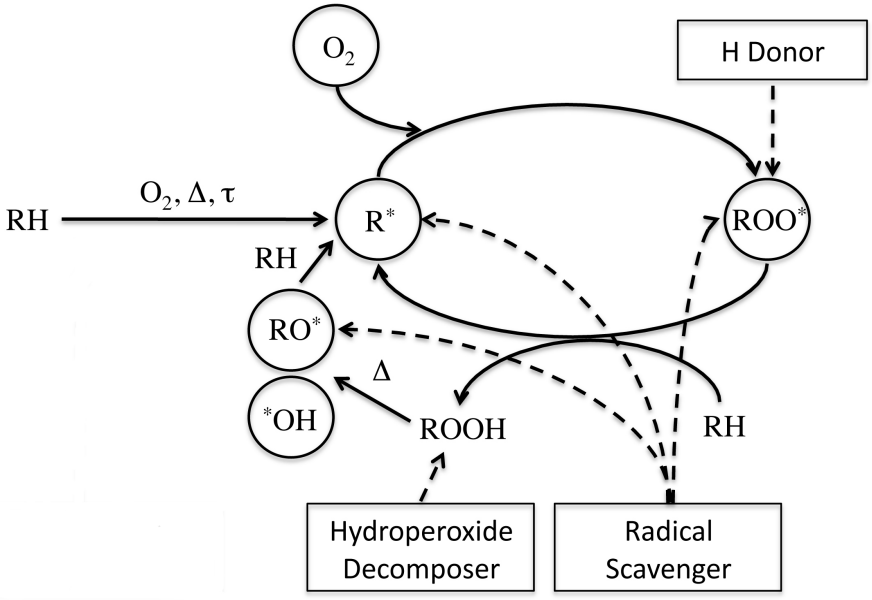

Figure 4: General scheme of inhibition of thermo-oxidative degradation[47].

Based on their mechanism of action stabilising additives for polyolefins can be classified into antioxidants (AO), light stabilisers and UV absorbers. Their detailed mode of action will be reviewed in the next section.

2.4.1 Antioxidants

Within the group of antioxidants primary (H-donors and free radical scavengers) and secondary (hydrogen peroxide decomposers) AO can be distinguished. Primary and

secondary AO are often used in combination to exploit synergistic effects. In the following their applications and mechanism of action will be described.

2.4.1.1 Primary antioxidants

The rate determining step in the autoxidation cycle is the abstraction of hydrogen by the peroxy radical from the polymer backbone to yield a relatively stable hydroperoxide. If therefore easily abstractable hydrogen is offered, this will react preferentially with the radical, thereby "saving" the polymer. Phenolic AO are the most extensively investigated primary AO for polyolefins and a wide variety of structurally different sterically hindered phenols [58-61] is commercially available. The structures of Irganox 1010, Irganox 1076 and Irganox 1330 – the workhorses of phenolic stabilisation - are shown in Figure 5.

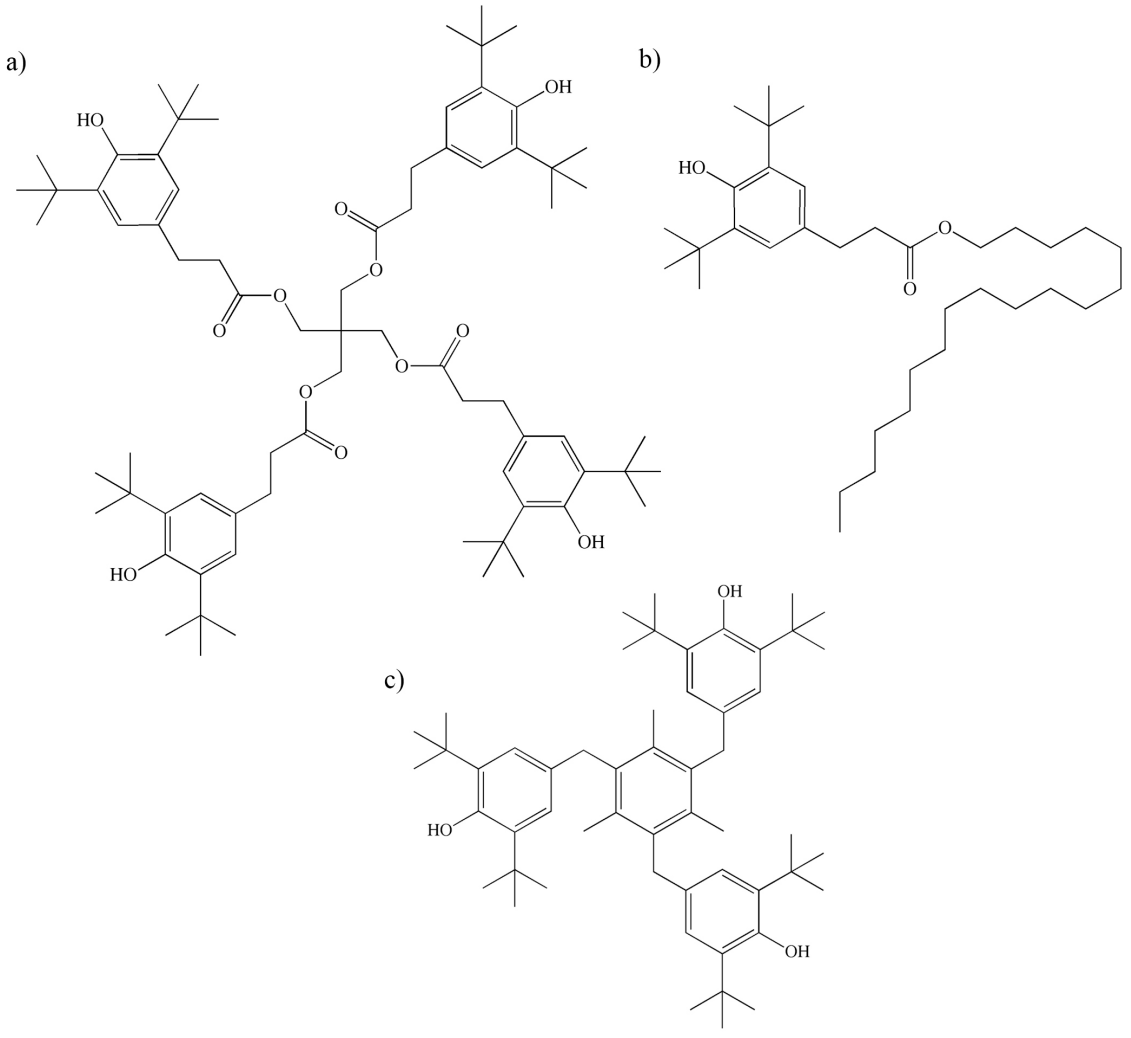

Figure 5: Structure of a) Irganox 1010, b) Irganox 1076 and c) Irganox 1330.

Phenolic AO react with O-centered peroxy radicals according to Scheme 11 [62-64].

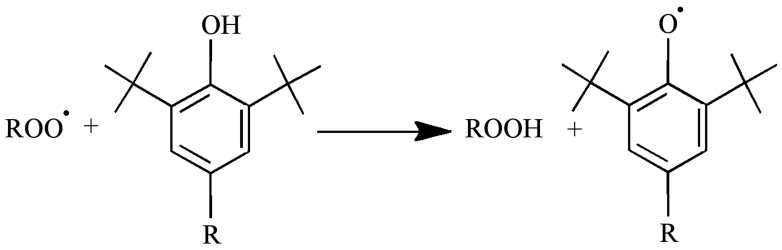

(1.26)

Scheme 11: Inhibition reaction involving sterically hindered phenols.

Thus from a mechanistic point of view they can only be active in the presence of oxygen and after chain scission has already taken place. The stability of the phenoxyl radical is governed by the sterical hindrance of the substituents in the 2,6-position and, depending on these, its reactivity in follow up reactions is significantly influenced [65,66].

Hindered Amine Stabilisers (HAS) based on derivatives of tetramethyl piperidine are efficient stabilisers against thermo-oxidative degradation of polyolefins [67,68]. Representative structures are shown in Figure 6.

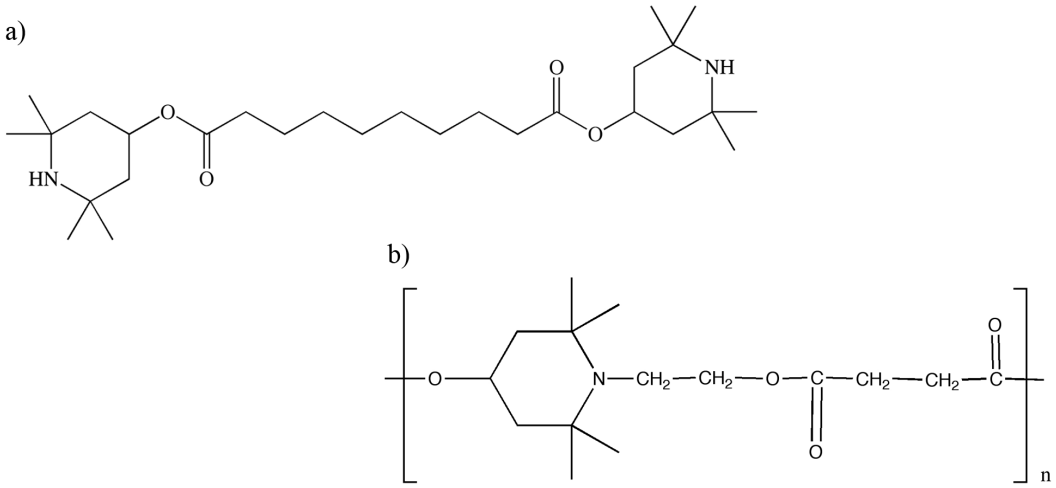

Figure 6: Structure of a) Tinuvin 770 and b) Tinuvin 622.

The active species responsible for the stabilising effect of HAS is a nitroxyl radical formed by oxidation of the parent amine (Scheme 12).

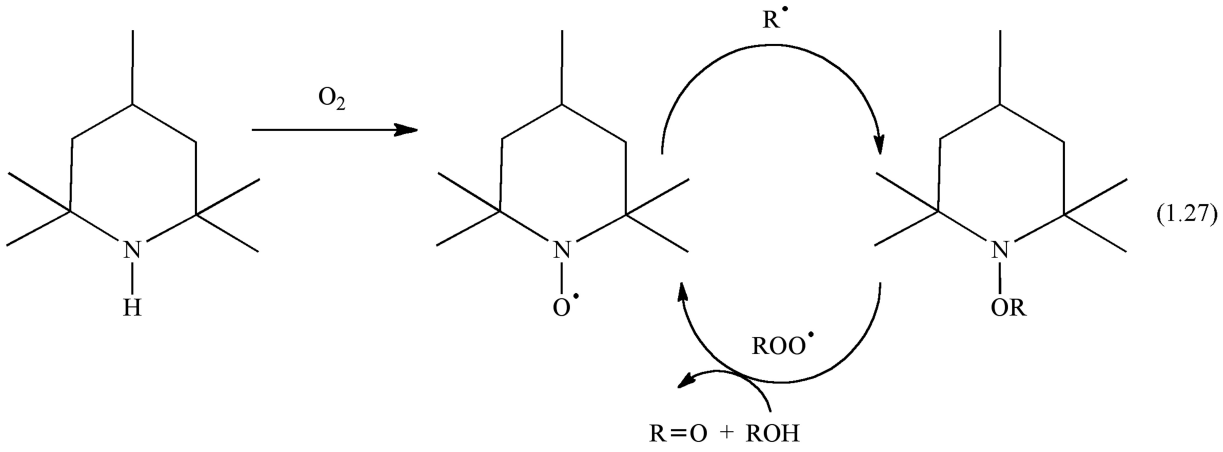

(1.27)

Scheme 12: Reaction of HAS with C-centered radicals.

The nitroxyl radical reacts with C-centered radicals to the hydroxylamine ether (NOR) which in turn reacts with a peroxy radical (ROO•) thus finally regenerating the nitroxyl radical[40]. Compared to hindered phenols, which solely act as scavenger for O-centered radicals, HAS react with both C- and O-centered radicals and consequently have a broader application spectrum [69]. The degradation behaviour of polymers stabilised with HAS and phenolic AO differs [70] and Figure 7 compares the mechanical properties as a function of time for a PE stabilised with phenolic AO and a HAS.

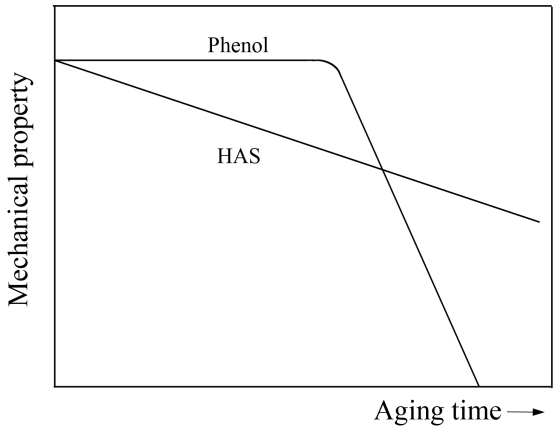

Figure 7: Mechanical property as function of time for PE stabilised with phenolic AO and HAS during ageing.

The phenolically stabilised material displays an abrupt loss its mechanical properties after an induction period while for samples stabilised with HAS the loss in mechanical performance is more gradual.

The third class of primary AO are secondary aromatic amines (SAAO). Representatively the structure of Irganox 5057 is shown in Figure 8.

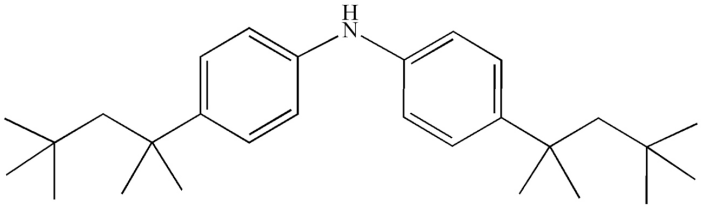

Figure 8: Structure of Irganox 5057.

The mechanism of action of SAAO as H-donor is shown in Scheme 13:

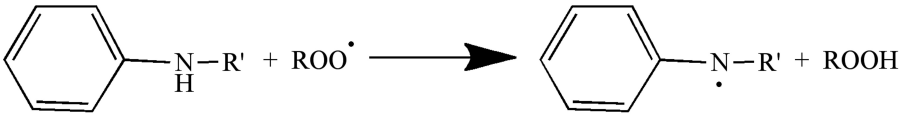

(1.28)

Scheme 13: Inhibition reaction involving aromatic amines.

Loss of the aminic hydrogen leads to the formation of aminyl and related mesomeric C-centered radicals which can undergo N-N, N-C, and C-C coupling. These compounds also exhibit AO properties and are further transformed into nitroxides or benzoquinone monoimides, which may scavenge C-radicals [71]. However as the coupling products discolour and stain the end product, their application is mainly limited to carbon black filled polymers.

2.4.1.2 Secondary antioxidants

An alternative option to hamper the degradation of polyolefins is to decompose the hydroperoxide itself. This is the task of hydroxide decomposers (HD), also referred to as secondary AO. The most common ones among them being sterically hindered phosphites, $P(OAr)_3$, and esters of 3,3-thiodipropionic acid. Representative structures of phosphites are shown in Figure 9.

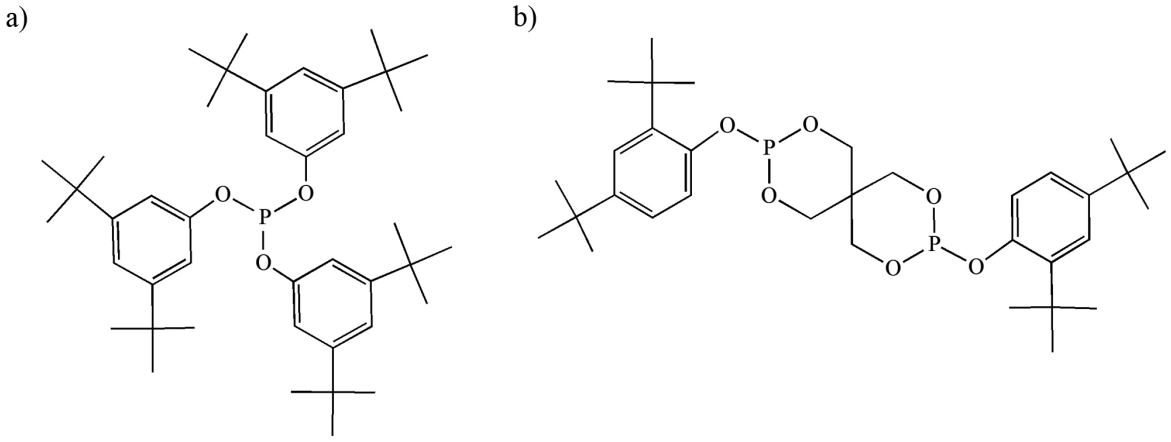

Figure 9: Structure of a) Irgafos 168 and b) Irgafos 126.

The phosphite reacts with a hydroperoxide (ROOH) to form an alcohol (ROH) while themselves being oxidised to the corresponding phosphate [72-78] (Scheme 14).

$$P(OAr)_3 + ROOH \longrightarrow O{=}P(OAr)_3 + ROH \quad (1.29)$$

$$P(OAr)_3 + ROO^{\bullet} \longrightarrow O{=}P(OAr)_3 + RO^{\bullet} \quad (1.30)$$

$$P(OAr)_3 + RO^{\bullet} \longrightarrow O{=}P(OAr)_3 + R^{\bullet} \quad (1.31)$$

$$P(OAr)_3 + RO^{\bullet} \longrightarrow RO{-}P(OAr)_2 + ArO^{\bullet} \quad (1.32)$$

Scheme 14: Hydroperoxide decomposition reactions by a phosphite.

Furthermore (ROO•) and (RO•) radicals can also be reduced by the reaction with trivalent phosphorus compounds. As phosphitic AO become only active above 150 °C they are used as processing stabilisers to protect the polymer against thermo-oxidative degradation during processing. They have no long term stabilising effect. Representative structures for esters of 3,3-thiodipropionic acid are shown in Figure 10.

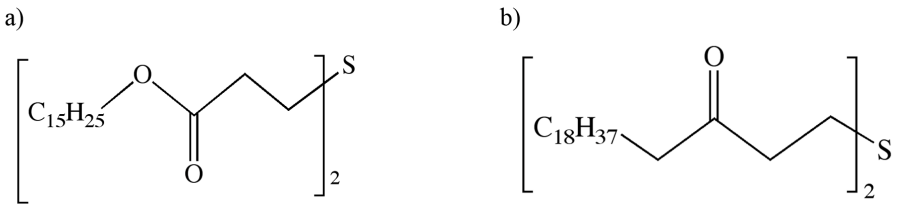

Figure 10: Structure of a) Irganox PS 800 and b) Irganox PS 802

The principal reaction is the formation of a sulfoxide which is then oxidised to a sulfenic acid [79].

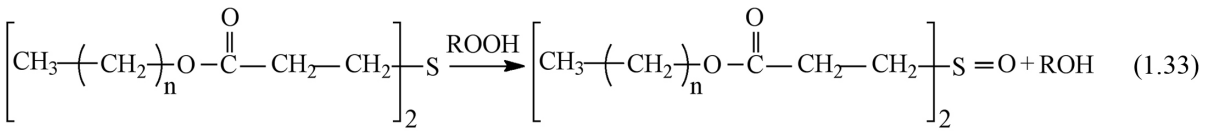

Scheme 15: Hydroperoxide decomposition reactions in the presence of thiodipropionate esters.

Sulphur containing stabilisers are highly efficient hydroperoxide decomposers. However, metabolites seriously limit the application of sulphur containing stabilisers in pipes for drinking water due to organoleptic problems (taste and odor). Thus they are mainly used in pipes for industrial applications or for drinking water pipes with a large SDR (main supply) with a regular exchange of the inner medium.

Primary and secondary antioxidants are often used in combination to exploit synergistic effects. Particular advantageous is the combination of primary and secondary AO in a single molecule as shown for example in Figure 11:

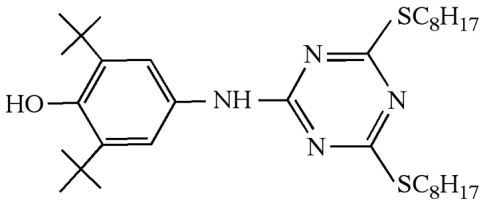

Figure 11: Structure of Irganox 565.

In this case the ratio of primary and secondary AO is given by the stoichiometry, and the proximity of the functionalities ensures maximum synergy.

2.4.2 Light stabilisers

Although polyolefins are – judging by the composition – not sensitive towards light due to the lack of chromophores in practice even the presence of minute impurities causes sensitivity towards UV radiation and thus makes an adequate stabilisation necessary for any outdoor application. The strategy is to absorb UV radiation before it can trigger degradation and simultaneously intercept the cycle of degradation.

2.4.2.1 Hindered amine light stabilisers (HALS)

Sterically hindered amines derived from 2,2,6,6-tetramethyl piperidines are highly efficient as light stabilisers and in this capacity referred to as Hindered Amine Light Stabilisers (HALS) [80-83]. Initially only low MM HALS were developed such as Tinuvin 770 (see Figure 6). They proved to be very efficient light stabilisers, however, due to their low MM they tend to diffuse or volatise from the polymer surface. This was overcome by the introduction of polymeric HALS. Figure 12 shows as example the structure of Chimassorb 944.

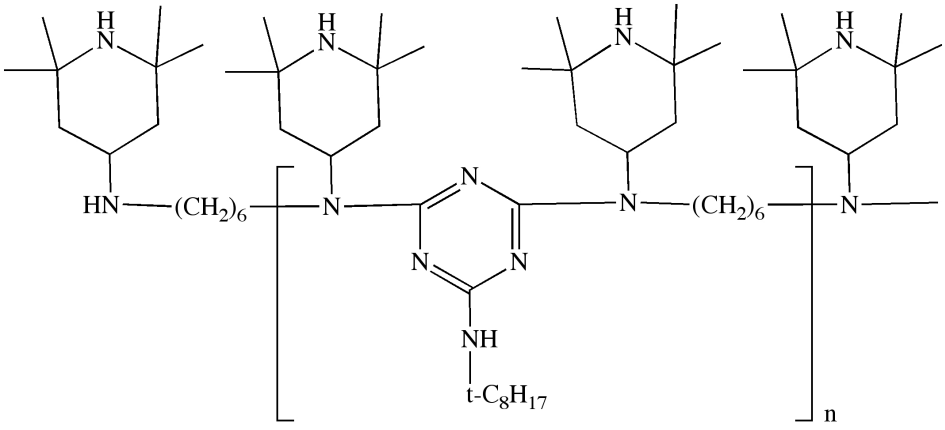

Figure 12: Structure of Chimassorb 944.

Originally their mechanism of stabilisation is believed to depend upon to their ability to form a stable nitroxyl radical which then scavenge macroradicals analogous to 2.4.1.1. However newer findings question this mechanism based on trapping of alkyl radicals. In fact because the ageing of polymers usually proceeds in air, the nitroxyl radical competes with oxygen for an alkyl radical. Hence unless photo-oxidation occurs under conditions leading to rapid oxygen starvation, the scavenge of alkyl radicals by nitroxyl radicals can be neglected. Another questionmark in this mechanism is the fact that nitroxyl radicals are stable at room temperature however at elevated temperatures they abstract hydrogen atoms from the polymer [65].

Later Sedlar et *al.* [84] attributed the effectiveness of HALS to their reaction with hydroperoxides. It regenerates a nitroxyl radical, but at the same time, a reactive alkoxy radical is formed [85]. The proposed mechanism is shown in Scheme 16.

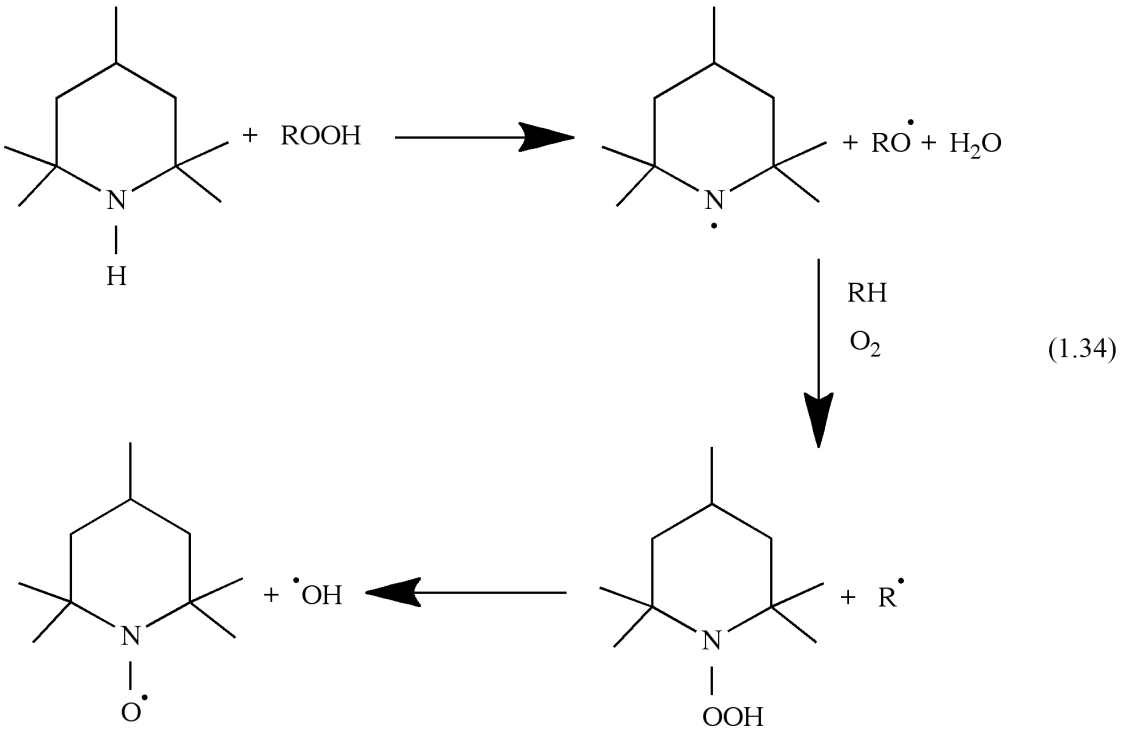

Scheme 16: Reaction of HALS with hydroperoxides.

HALS are a stabiliser of choice for polyolefins since they exhibit a multi-functional stabilisation activity and can protect the polymer against both thermo-oxidative and photo-oxidative degradation.

2.4.2.2 UV absorbers

An additional way to protect the polymer against the damaging effect of UV light is to absorb the radiation before it can initiate the degradation of the polymer, i.e. reduce the amount of light absorbed by chromophores. This can be achieved by adding UV absorbers to the polymer, which function by preferentially absorbing harmful UV radiation and dissipating it as thermal energy. 2-(hydroxyl phenyl)-benzotriazoles and 2-hydroxy benzophenones are the most extensively studied UV absorbers. Representative structures are given in Figure 13.

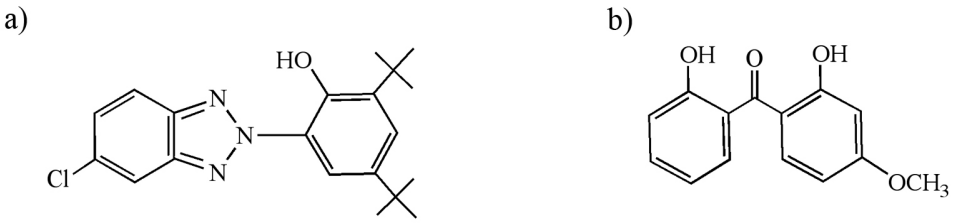

Figure 13: Structure of a) Tinuvin 327 and b) Cyasorb UV-24.

An essential criterion for UV absorbers is that they can rapidly dissipate the absorbed UV radiation via a suitable intramolecular rearrangement. Exemplarily the mechanism of interaction of benzotriazoles with UV light is illustrated in Scheme 17.

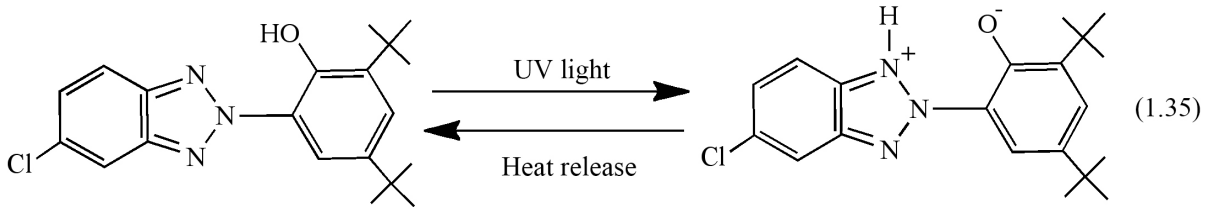

(1.35)

Scheme 17: Tautomeric rearrangement of 2-(hydroxyl phenyl)-benzotriazole as a result of UV-absorption.

Energy is absorbed via rapid tautomerisation at the excited state and dissipated as heat [86-90]. The wavelength of the absorbed light can be modified by the substituents on the aromatic ring.

Further novel light absorbers are 2-(2-hydroxy phenyl)-1,3,5-triazines which are characterised by a higher extinction coefficient compared to the benzotriazole UV absorber type [65,91]. Representative structures are given in Figure 14.

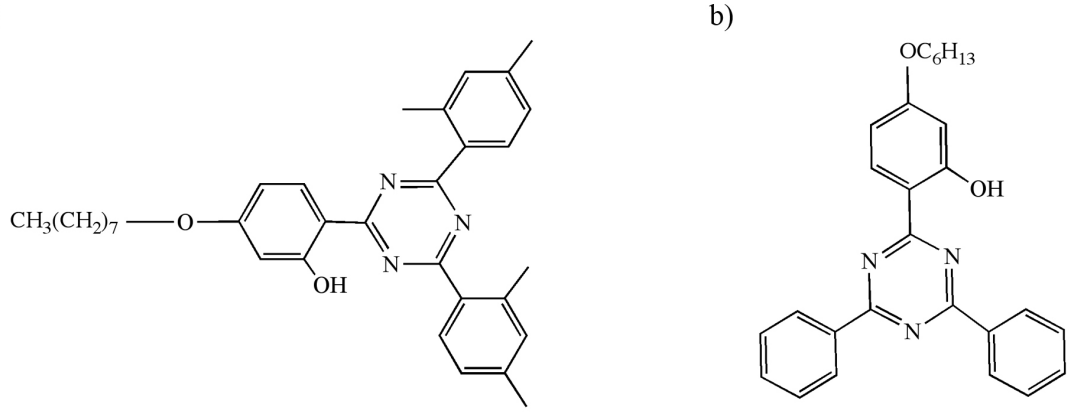

Figure 14: Structure of a) Cyasorb UV-1164 and b) Tinuvin 1577.

The properties and mechanism of action of this class of UV absorbers were investigated in detail. The crystal structure was determined by X-Ray diffraction, and from IR and NMR [94] data it could be concluded that the intramolecular hydrogen bond in these compounds is stronger than for the benzotriazole class.

Another widespread UV absorber is carbon black (CB) [53,93,95]. It is commonly referred to by the process or the source material from which it has been made, e.g. furnace black, thermal black, and channel black. The different grades differ in their particle size, surface area, porosity and type and amount of surface functionalities. The typical structure of CB is shown in Figure 15.

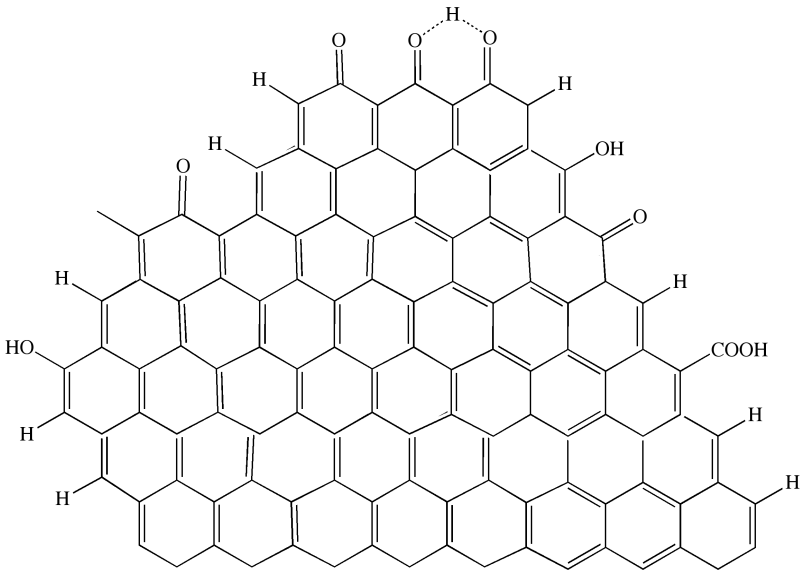

Figure 15: Structure of CB.

Due to its inexpensiveness CB has been an established light absorber for polyolefins since the early days, and as it contains functional groups (e.g. carboxylic acid, phenolic, quinone and lactones groups) it may also act as an AO [95]. However, due to the colour inferred its application is limited to cases where the colour of the final product does not play a role.

2.5 Analysis of degradation and stabilisation

Stabilisers are added to polymers to protect them against oxidation. However a loss of the stabiliser from the polymer matrix can occur for example during long term use which can change the polymer's properties and thereby reduce the life time of the final product. The solubility of stabilisers in polymers depends on the temperature and decreases dramatically during cooling [96]. As a result an oversaturated state is created at room temperature and a diffusion-controlled equilibrium slowly formed which can lead to blooming of the stabiliser at the surface [97,98]. Thus, a physical loss of the stabiliser can occur by diffusion, evaporation, or extraction [99,100]. A loss of stabiliser can also occur by photochemical reactions [101]. The physical loss of stabilisers depends upon numerous

factors, in particular the solubility of the compounds, the nature of the stabiliser, the environment, and the nature and geometry of the polymer samples.

The efficiency of stabilisers is commonly evaluated by a phenomenological approach using for example the time to embrittlement [102,103] or the yellowness index (YI) as indicators [104,105]. To determine the time to embrittlement polymer samples are exposed to different temperatures for an extended period of time and tensile tests are performed to determine the embrittlement endpoint. As degradation predominantly takes place in the amorphous regions, chain scission will result in a reduction of tensile strength, elongation at break and toughness of the sample.

The YI measures the discoloration of the polymer which arises from metabolites (mainly quinones) of phenolic AO resulting from the trapping of oxygen-centred radicals [66]. However in these accelerated ageing tests the visible damage is only the final result of chemical and physicochemical steps and an in depth understanding requires analytical techniques which take into account diffusion kinetics and chemical changes. Choosing the correct technique depends on the type of both, polymer and additive, and combinations of various techniques are often used which yield complementary information. In the next section an overview of methods to analyse stabilisers and the degradation of the polymer will be given.

2.5.1 Techniques to analyse stabilisers

2.5.1.1 Oxidative induction time (OIT)

It is common practice to analyse the content of active stabiliser by measuring the oxidative induction time (OIT) [106-109]. For its measurement the polymer sample is heated in a DSC-pan under nitrogen significantly above the melting temperature and then the purge gas is switched to air or oxygen. The heat flow between the sample and a reference is measured and the time from switching of the purge gas to the onset of an exothermic heat flow caused by oxidation of the polymer is referred to as OIT. A representative thermogram and the determination of the OIT are shown in Figure 16.

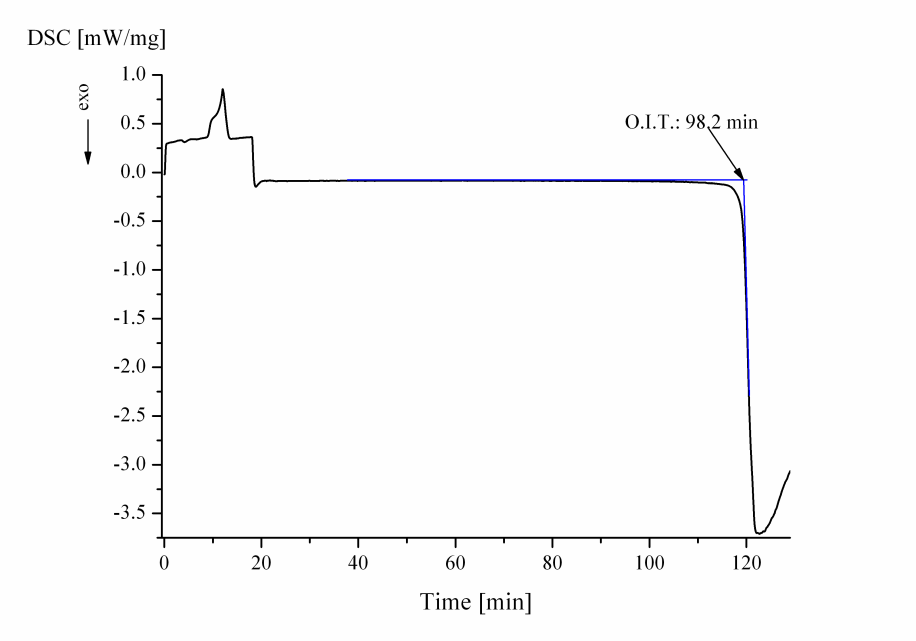

Figure 16: Example of an OIT curve.

OIT can be used to determine the level of hindered phenolic AO in polyolefins. Therefore a calibration is performed which correlates the OIT to the content of AO, yielding a straight line relationship [108]. In case that further components are present in the sample, strong deviations from the linear correlation may be observed as the OIT may be influenced in an unpredictable way as pointed out by several authors [110-112]. For example Billingham *et al.* singled out the influence of phosphite stabilisers on the OIT [113] and showed that phosphites influence the slope of the linear relationship, and that for each content of phosphite an individual linear relationship has to be applied. However, despite these limitations the OIT has found widespread use in industrial practice due to the inexpensiveness of the instrumentation as well as the simplicity of the measurement.

2.5.1.2 High Performance Liquid Chromatography (HPLC)

Different approaches can be used to analyse the content of stabilisers. Thin Layer Chromatography (TLC) is useful for a rapid analysis in a qualitative way. TLC is inexpensive as the costs only include solvents and TLC plates and no sophisticated instrumentation is required. However TLC is not a quantitative method, although with

reproducible sample introduction on the plates and a UV-Vis scanner which can detect the spots progress in the direction of quantification can be made.

Certainly the most comprehensive and universal approach is to extract a polymer sample and then analyse the content of stabilisers in the extract chromatographically. The most striking advantage of this procedure is that also complex mixtures of stabilisers can be analysed and that metabolites of the additives can be identified and quantified. A suitable extraction should isolate the stabilisers without degrading them and depending on the nature of the sample different methods are available. Due to its simplicity the Soxhlet method [114,115] found widespread use. To separate, identify and quantify the additives in the extract various chromatographic techniques can be used. In the case of volatile additives, gas chromatography may be the method of choice. However as the trend moves towards low volatile and even polymeric stabilisers high performance liquid chromatography (HPLC) gains more and more importance [116-119]. The combination of mobile and stationary phase has to be adjusted to the particular separation problem. Reversed phase chromatography using non polar stationary phases is broadly applicable for a wide range of commercially important stabilising additives. As the vast majority of stabilisers absorb UV radiation UV detectors are commonly used for detection, bringing the detection limit down to ppm level. The separated additives are identified by their retention time in the elugram. For quantification an internal standard is added prior to the extraction step.

2.5.1.3 Fourier Transform Infrared Spectroscopy (FTIR)

Infrared (IR)-spectroscopy uses the interaction of the IR-radiation with mass. This results in the absorption of light at specific wavelengths corresponding to the energy of transition between various vibrational-rotational states of molecules or groups of atoms in a molecule. Lambert Beer's law can be used for quantitative analysis of the IR absorbance in isotropic media. At constant sample thickness and a given wavelength, the absorption is proportional to the concentration of the absorbing species.

$$A = \varepsilon \, l \, c$$

where: **A** is the absorbance, **ε** is the molar absorptivity or molar extinction coefficient, **l** is the length of the optical path through the sample and **c** is the concentration of the absorbing species.

IR spectroscopy can be used to analyse the stabilisers in polyolefins in both, qualitative and quantitative manner. Most stabilisers have a unique IR spectrum and furthermore analysis in polyolefins is relatively easy because they present only few absorption bands. However, it must be taken into account that similarities between the spectra of comparable stabilisers as well as their low content in the matrix can seriously limit an unambiguous identification.Due to its high sensitivity IR-spectroscopy is a very powerful technique to quantify AO [120].

Models can be created for a series of IR spectra that are acquired as a function of the concentration of the additive in the polymer and a calibration curve is established. The main advantage of this technique is that the measurements can be performed directly on polymer films or plaques.

Thuet *et. al* [121] determined additives in PP, HDPE and LDPE by FTIR. Precisely defined concentrations of different stabilisers (Irganox 1010, Irganox 1076, Irgafos 168 and Chimassorb 944) were incorporated in the polymers and films of 1.0 mm thickness were manufactured and measured. Characteristic absorption bands of the stabilisers in the polymer (for example for the case of HDPE/Irganox 1010 at 1745 cm^{-1}, Irganox 1076 at 1740 cm^{-1} and Irgafos 168 at 849 cm^{-1}) were used to construct calibration curves in the range between 0.05 and 0.5 wt. %. However for such a univariate approach the composition of the measured sample must be known and specific wavelengths must be chosen for the studied stabilisers, which do not interfere with those of other additives.

Vigerust *et. al.* [122] used multivariate calibration and created a method to determine the content of three additives (silica, erucamide and butyl hydroxy toluene) in LDPE. Karstang *et. al.* [123] created a model to quantify three additives (Irganox 1010, Irgafos 168 and calcium stearate) in HDPE. The additives with concentration ranges between 0.0 and 0.2 wt. % were mixed with the polymer and films of 1.0 mm thickness were measured. The authors compared different calibration and scaling techniques and after validation of the calibration set with HPLC measurements, a suitable method to quantify additives in real production samples was established.

2.5.2 Techniques to analyse the degradation of the polymer

During oxidative degradation, the composition of the polymer changes due to the uptake of oxygen. Simultaneously chain scission or crosslinking take place, their extent depending on the specific conditions. On the physical side, the morphology of the polymer may change, resulting in changes of the degree of crystallinity and orientation of the polymer chains.

IR-spectroscopy is also widely used to study the degradation of polyolefins providing information about degradation products [124-127], chemical composition [128-129], and morphology (degree of crystallinity) [130-134] and orientation [135,136] of the polymer. As previously discussed a variety of oxygen containing functional groups can be formed during degradation which - like carbonyl and hydroxyl species - can be detected by IR-spectroscopy [137,138]. The degree of degradation of polyolefins is often described by the carbonyl index (CI) [139] which is defined as the ratio between the integrated area or height of the carbonyl absorption centered around 1714 cm^{-1} and an absorption of the polymer which is not influenced by degradation. In the case of PE the bands commonly used are those of the CH stretching vibrations around 1370, 1470 or 2020 cm^{-1} [140,142]. Plotting the CI against degradation time permits to assess the kinetics of oxidation. The degree of crystallinity can be calculated from the ratio between a band specific for the crystalline domains and one caused by the amorphous fraction. In the case of PE this can be calculated using the ratio between 729 and 719 cm^{-1} [143] or 1897 and 1304 cm^{-1} [144].

During degradation chain scission or crosslinking may occur which will result in changes of the MMD [145,146]. In the case of PE crosslinking predominates in the absence of oxygen while chain scission becomes more important in the presence of oxygen [147,148].

To monitor changes in MM viscosimetry or size exclusion chromatography, SEC, are widely used to determine the average MM or MMD respectively [149-153].

DSC is frequently used to analyse the melting behavior of polyolefins. The degree of crystallinity can be derived from the heat of melting.

2.6 Practical aspects of polyolefin pipes

2.6.1 Production and testing

Polyolefin pipes are produced by extrusion. The polyolefin compound is either used as obtained from the raw material producer or specially batched by the pipe manufacturer. Figure 17 shows the scheme of an extrusion line.

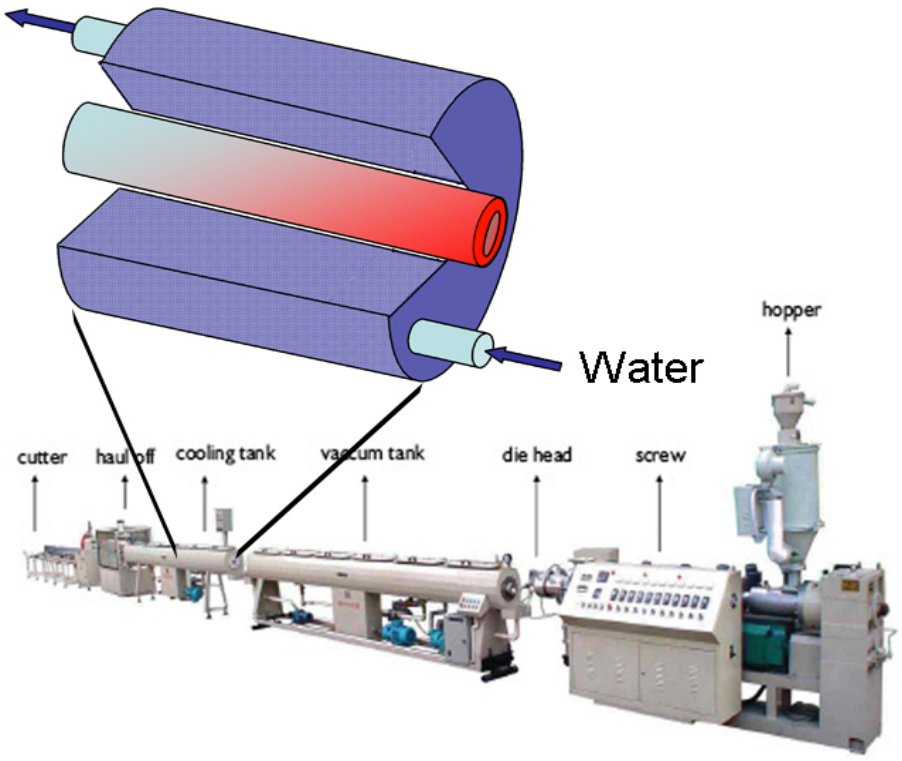

Figure 17: Pipe extrusion line and an enlargement of the cooling bath.

After passing the die of the extruder the not yet solidified pipe passes a water bath, whereby it is cooled on the outside (Figure 17). Within the water bath a so called calibration path is placed where an external vacuum is applied to bring the pipe to the desired dimension. The output of the extruder, the temperature of the melt and the cooling conditions are parameters that enable the manufacturers of pipes to maximise their productivity. The processing conditions also set the morphology of the polymer and thereby determine the short-term properties (mechanics) of the pipe and as well as its long-term behaviour.

The service life of plastic pipes and the factors influencing it have been the subject of considerable interest. The lifetime of pipes is usually predicted by hydrostatic pressure tests [154-157] in which the pipe is subjected to different hoop stress at various temperatures and the time to rupture is measured according to ISO 1167-1 [158]. The time to failure is recorded and the data is plotted in a double logarithmic plot (Figure 18).

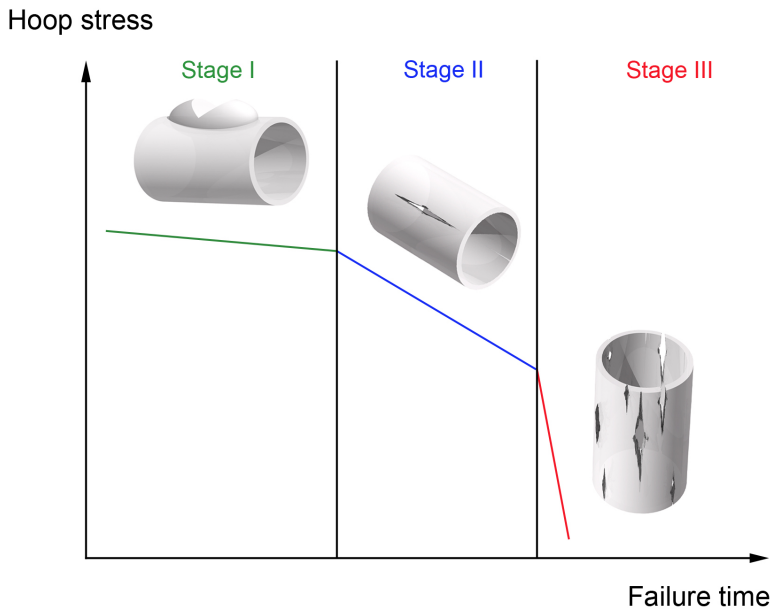

Figure 18: Stress rupture scheme [159].

Three different modes of failure can be distinguished: In stage I ductile failure occurs. Here the stress in the pipe wall exceeds the yield stress of the material and leads to failure through deformation. In stage II, the so called brittle region, micro-cracks are formed by random defects which lead to mainly brittle failure at intermediate stress levels. And finally in stage III, the so called oxidative region, the thermo-oxidative degradation of the polymer occurs, manifesting in a rapid loss of MM and mechanical stability. Hydrostatic pressure tests measure the integral ageing behaviour of the pipes but as phenomenological tests they do not provide information about the elemental processes occurring in the pipe wall during ageing namely the loss of AO, oxidation of the polymer and changes of the morphological structure [160,161].

2.6.2 Ageing of polyolefins pipes

The residence time of stabilisers in the pipe wall is influenced by the type of AO, i.e. its MM and polarity, the morphology of the polymer, and the conditions of service. When pipes are filled with a liquid inner medium, the AOs are gradually extracted into the latter and concentration gradients of the stabilisers are formed across the pipe wall. Additionally the AO is consumed by oxidation. Once the concentration of AO falls below a critical level, free radical oxidation of the polymer sets in, leading to the formation of degradation products (ketones, aldehydes, lactones, carboxylic acids, esters and peroxides). At the same time the average MM of the polymer is reduced as a result of chain scission, leading to embrittlement and eventually failure of the product. Both processes are linked and their kinetics depend to a large extent on the permeability of the polymer. The model for the diffusion step assumes that the AO migrates in the amorphous regions of a semi-crystalline matrix [162]. The crystalline domains form a lattice and the permeability of the polymer depends on the degree of crystallinity, i.e. the ratio of crystalline to amorphous phase and the crystallite structure (average size and size distribution) of spherulites. In the case of pipes one has additionally take into account that the morphological parameters are anisotropic, due to the different cooling rates on external and internal wall surface after the extrusion and the shear field in the die.

Since the 1980s efforts have been undertaken by various groups to monitor the process of ageing in walls of polyolefin pipes during hydrostatic pressure testing using analytical techniques such as HPLC, OIT or IR-spectroscopy [163-167]. As the process of pipe ageing occurs locally heterogeneous spatially resolving analytical techniques are needed for its analysis. This has been achieved by mechanical abrasion of layers (e.g. by grinding) and then analysing the obtained samples individually with regard to their content of AO using HPLC or OIT. The average MM of the polymer can be determined by viscosimetry or SEC and the status of the polymer degradation derived from the CI. Using this approach Kramer *et al.* analysed poly-1-butene (PB) pipes and found that the content of stabiliser as determined by OIT in the wall is reduced during service and that a concentration gradient of the AO perpendicular to the pipe axis is formed [168-170]. Allen *et al*. studied the performance of two different phenolic AO (Irganox 1010 and Irganox 1330) in PE pipes exposed to water at different temperatures [171]. It was shown that both AOs were extracted

from the pipe surface and that the loss of AO increases with temperature and time of exposure. The extractability of Irganox 1330 was lower than that of Irganox 1010 (see Figure 15). Karlsson *et al.* studied pressure tested medium density polyethylene (LDPE) pipes as a function of temperature, hoop stress and exposure time and showed by IR-spectroscopy that oxidation starts in the inner wall just prior to failure[162]. The same authors also studied pressure tested poly-1-butene pipes [172] under the same conditions and found that the oxidation is initiated at the outer wall. Gedde *et al.* studied pressurised PE-X pipes at 110 °C and showed by IR-spectroscopy the formation of carbonyl and hydroxyl groups at the inner wall [173]. Later the same authors [174] analysed LDPE-pipes after different exposure times and showed by OIT that the concentration profile of a phenolic AO in the pipe wall is a function of the testing conditions, namely higher temperature leading to an accelerated loss of AO. Diffusion coefficients calculated from the OIT data over the pipe wall for two AOs showed that the temperature dependence of the diffusion follows Arrhenius' law. Hoàng *et al.* exposed a PE 100 pipe stabilised with a phenolic AO, a HALS and an UV absorber to hydrostatic pressure at various temperatures and showed that the depletion of AO is strongly related to the type and content of AO [159]. Recently Thörnblom *et al.* studied the migration of Irganox 1330, Irganox 1010 and Irganox 1076 in HDPE, LDPE and PE-X pipes during water extraction without pressure at elevated temperatures (95 – 100 °C) [175]. Layers were mechanically prepared and analysed by HPLC and OIT. For all samples a decrease in the amount of the AOs with prolonged extraction time was observed, however the behaviour of the individual AOs differed. For the case of Irganox 1330 transformation products were found and since the content of AO determined by HPLC was larger than the corresponding loss in OIT the authors concluded that these metabolites also have antioxidant capacity. For the samples stabilised with Irganox 1010 and 1076 no transformation products were found. It was suggested that Irganox 1010 and 1076 which both contain ester groups (Figure 15) are hydrolysed and the low MM products of the hydrolysis are better extractable due to their higher polarity and lower MM.

Summarily it can be stated that by combining mechanical abrasion with follow up analysis of the samples by OIT, HPLC or IR-spectroscopy it could be shown that during ageing of pipes under hydrostatic pressure extraction of the AO into the inner medium takes place. It could also be shown that the rate of extraction depends on the type of AO and the specific

running conditions like temperature and the type of inner medium. Nethertheless, quantitative data are very sparse in the literature and in case they exist are not comparable with those from other references.

Pipes are also frequently exposed to weathering, for example in outdoor installations or when the extruded pipes are stored in the open before their installation. The effect of weathering on the polymer is the consequence of the combined action of UV-light, temperature and moisture as described in section 3.3. Allen *et al.* [176] exposed LDPE pipes outdoor for 2 years and showed by mechanical abrasion of layers and subsequent OIT measurements that the degradation starts at the outer surface and gradually progresses into the bulk of the material. FTIR measurements showed that carbonyl functions were formed on the surface of the pipe. Nevertheless in all these studies the mechanical sample preparation infers poor reproducibility and limited spatial resolution [177,178]. A much more elegant way would be therefore to use a single analytical technique which is able to monitor the concentration of stabilising additives, the oxidation of the polymer and the morphology of the polymer.

2.6.3 IR-microscopy

Taking into account the previous chapters, IR-microscopy, which combines the image analysis specificity of light microscopy with the chemical specificity of IR-spectroscopy could potentially be very useful for this purpose. IR-microscopes became widely available due to advances in instrumentation [179-181] in the 1980s. The scheme of an IR-microscope is shown in Figure 19a.

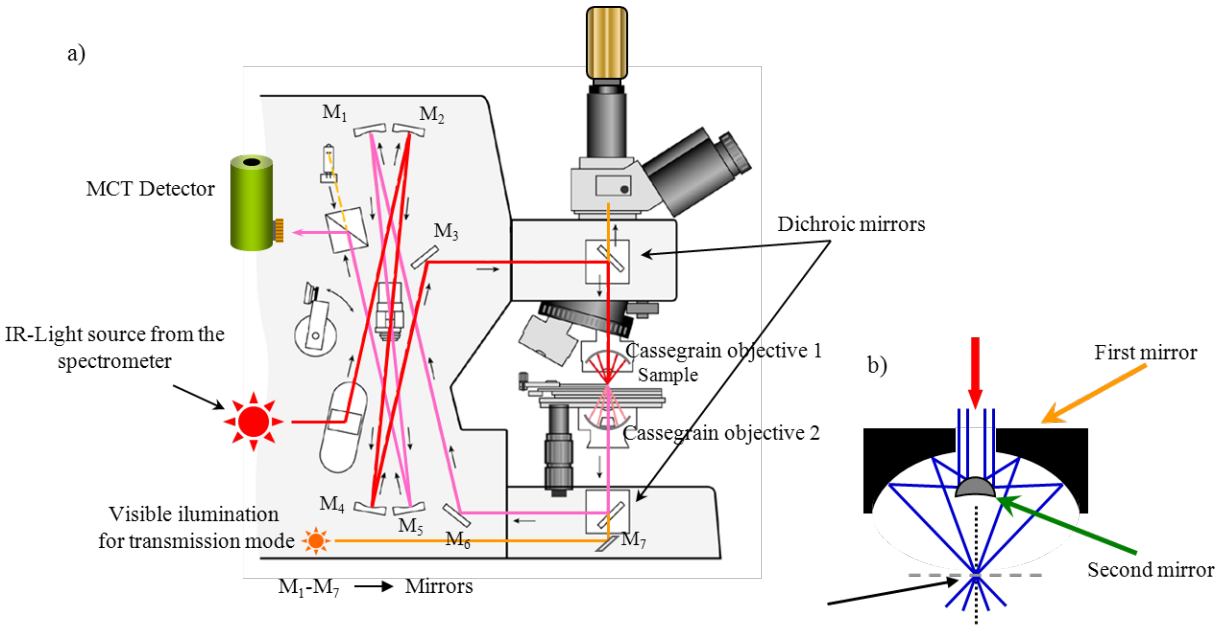

Figure 19: a) Scheme of an IR-microscope and b) detail of the Cassegrain objective (adapted with permission from [182].

The IR beam is focused on the sample via Cassegrain objectives and condensers and a mercury cadmium telluride (MCT) element is used for detection of the light which can be collected either in transmission or reflection mode. Two apertures – one before and another after the sample - are used, thus providing a resolution which is superior compared to a single aperture. Depending on the wavelength the spatial resolution limit is around 10 µm [179,180]. For measurement the sample is positioned on a movable, software controlled XY-table. Based on the alignment of measurement points one can distinguish line scans and area maps. The line scan and area map define a series of spectra to be collected in one or two dimensions and providing an infrared image which can be directly correlated with the visual one. For a line scan spectra are collected along a given line. This is time saving, however, information is only collected in one dimension, i.e. heterogeneities in the other dimension cannot be determined [183]. The data can be visualised as waterfall plot or as colour coded contour plot (Figure 20).

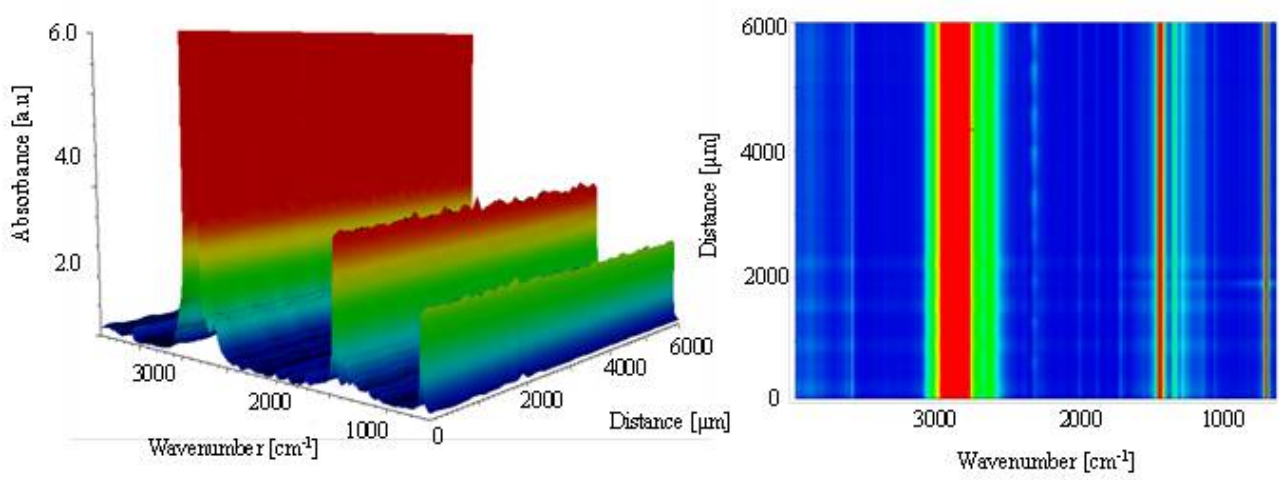

Figure 20: a) Waterfall and b) colour coded contour plot of a line scan over the wall of an unaged commercial HDPE pipe.

Alternatively the chemigram of a particular wavenumber along the analysed line can be generated as shown in Figure 21 for Irganox 1010 over the wall of an unaged HDPE pipe.

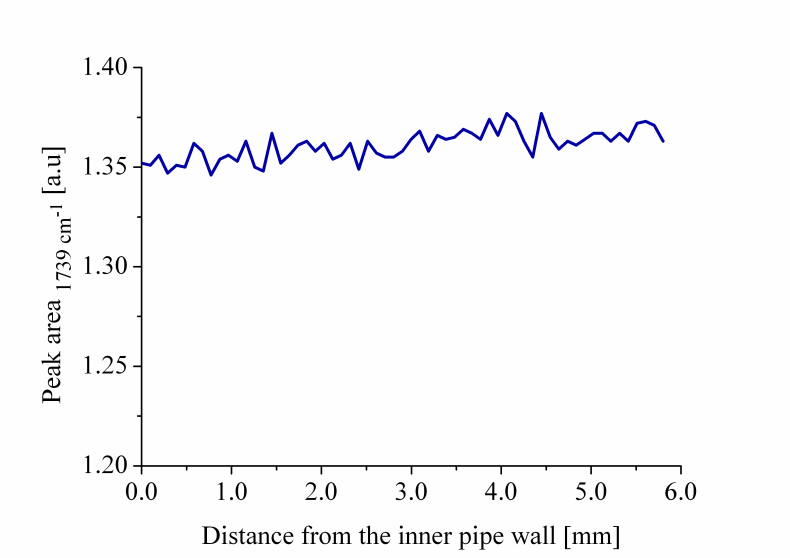

Figure 21: Intensity of the carbonyl band at 1739 cm^{-1} characteristic for Irganox 1010 over the wall of an unaged HDPE pipe.

IR-microscopy has been widely used to assess heterogeneities in polymers [184-186]. The capability to perform spatially resolved chemical analyses of microscopic regions of samples makes it a powerful technique to identify additives and contaminants [187,188], monitor the diffusion of AOs [192], the local heterogeneity of polymer degradation [190-192], as well as morphology and orientation [193].

In many cases IR-microscopy is used in a qualitative manner as for example Gravila *et al*. rate the extent of degradation by profiling the carbonyl groups in different regions of cross sections of PP irradiated in air for 15 years [194], but only few examples exist for quantitative applications. Hsu *et al.* profiled the concentration of the UV-stabiliser Cyasorb UV 531 in PP [195] using IR-microscopy. Hirt *et al*. determined the loss rate of the slipping agent erucamide from a PE-film using synchrotron IR-microscopy [196]. Later they compared the diffusion rate of erucamide between multilayer PE and PE-PP films [197], and between PE and polyolefin plastomer films by microtoming slices perpendicular to the surface and profiling the concentration of the additive [198]. In the field of pipes Brüll *et al.* showed for the first time that IR-microscopy enables to profile both the concentration of AO and the morphology of the polymer across the wall of PP-R pipes [199,200]. It was shown that the processing conditions as well as the composition of the compound influence the distribution of the degree of crystallinity through the pipe wall. With the same technique Geertz *et al*. monitored the extraction of Irganox 1010 from the wall of PP-R-pipes as well the oxidative degradation of the polymer [201]. For the first time the influence of the hoop stress and extrusion rate on the migration of Irganox 1010 in PP-R pipes could be visualised.

2.7 Aim of the research

In the field of analytical polymer chemistry, the development of a fast and accurate method to evaluate polymer degradation and in a qualitative and quantitative manner still remains an unmatched goal. The individual elementary processes that occur during photo-oxidation of PE - the extraction of antioxidants and oxidation of the polymer - have been subject of innumerous studies. However, in the field of polyolefin pipe degradation a correlation

between these elementary processes and the ageing conditions has been a subject of scarce research. This information is crucial to drive new developments in this area and improve the current performance of polyolefin-based pipes. The aim of the Ph.D. thesis is to use IR-microscopy to obtain information on elemental processes occurring in the wall of HDPE pipes during ageing, as for example, the loss of AO, oxidation of the polymer and consequently the morphological changes intrinsically associated.

3. Experimental Procedure

3.1 Materials

Pipes of PE-80, PE-100 and PE-Xa as shown in Table 1 were kindly donated by the manufacturers. A fresh batch of the production of orange pipe PE-100 (labelled as B_1) was analysed in comparison and was designated as B_2.

Table 1: Labelling and properties of the pipes used in this study.

Sample	Material	Dimension
A	PE-80 (yellow)	SDR11 63 x 5.8 mm
B_1	PE-100 (orange)	
B_2	PE-100 (orange)	
C	PE-Xa (blue)	
D	PE-Xa (yellow)	
E	PE-Xa (yellow)	SDR11 110 x 10 mm
F	PE-100 (black)	SDR17 110 x 6.6 mm

The corresponding images are shown in Figure 22.

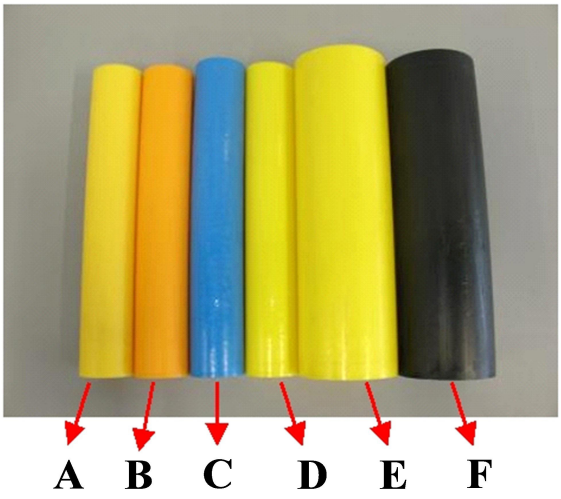

Figure 22: Photographs of the pipes.

3.2 Ageing

3.2.1 Natural weathering on the roof

The natural weathering was carried out from May 2009 to July 2009 in Würzburg (Germany) on the roof of the Süddeutsches Kunststoff-Zentrum (SKZ). Figure 23 shows the arrangement of the different pipes fixed on a wood pallet to prevent slipping, twisting or rolling. This assures that a defined part of the pipe surface is always exposed to the zenith.

Figure 23: Weathering on the roof.

During the weathering, temperature, precipitation, relative humidity, duration of sun light and radiation exposure were registered daily for the exact location of the SKZ (49 ° 46 'N / 09 ° 58' E). The daily values were averaged for each month. The data as obtained from the German Weather Service (DWD) are summarised in Table 2.

Table 2: Climatic parameters as obtained by averaging the daily values provided by the German Weather Service (DWD) for the exact location of SKZ.

	May	**June**	**July**
Temperature [°C]	15.0	16.5	19.0
Precipitation [mm]	1.4	1.4	2.6
Relative humidity [%]	71.9	68.0	71.9
Sunshine duration [h]	207	206	201
Radiation [kJ/m^2]	36000	36200	35400

3.2.2 Artificial weathering in an ageing chamber

Artificial weathering was carried out based on the data in Table 1. Accordingly, different doses of UV radiation, temperature and relative humidity programs were independently implemented in order to determine their individual influence on the integrity of different pipes as described in Table 3. The following programs were used: **May double** contains the double amount of UV radiation compared to the natural ageing conditions found for May. In **May without sun** the pipes were not exposed to UV radiation to assess its effect on the material integrity. The **May dry** program was used to understand the influence of moisture and thus the relative humidity was reduced to half of the standard values. In **May-July**, the natural weathering conditions were used. To study extreme conditions, the **Subtropical** program simulated very warm and humid climate to determine the influence of moisture at high temperature without UV radiation. Finally, the **Arizona** program simulated an equally

very warm but dry climate in order to determine the influence of temperature in the absence of moisture.

Table 3: Conditions of artificial weathering.

Climate scenario	Radiation Dose (kJ/m^2)	Temperature (°C)		Relative humidity (%)	Time (h)
		Set	Real		
May	30 000	28.0	35.2	71.6	144
Double May	60 000	28.0	35.8	71.8	288
May without sunlight	0	28.0	35.3	71.9	144
May dry	30 000	28.0	37.2	45.8	144
May-July	107 600	28.0	35.5	70.5	504
Subtropical	0	40.0	38.5	89.9	144
Arizona	60 000	50.0	49.8	12.4	288

Artificial weathering was carried out in an accelerated ageing chamber Suntest XXL+ (Atlas Material Testing Technology, Linsengericht, Germany) equipped with a Xenon lamp (Atlas Material Testing Technology, Linsengericht, Germany, Figure 24a). The different pipes were arranged in the chamber as depicted in Figure 24b. As for the natural ageing procedure, the pipes were ensured to stay in the same position to maximise the UV light exposition of a defined part of the pipe surface to the different conditions.

a) b)

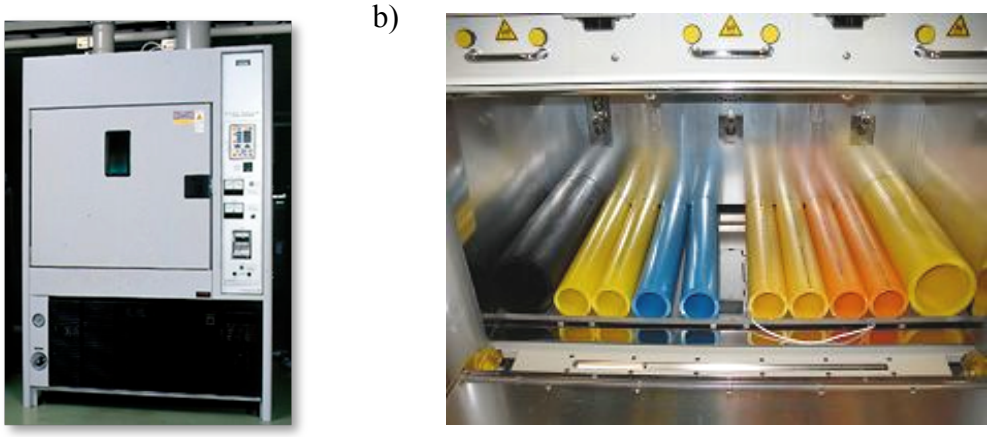

Figure 24: a) Artificial ageing chamber and b) arrangement of different pipes in the chamber.

Considerable differences between the set temperature and the real one were observed. This is due to the lack of a cooling system which could discharge the heat generated by the UV lamp.

3.3 Characterisation

3.3.1 Fourier Transform Infrared Spectroscopy (FTIR)

All measurements were performed on a Nicolet 8700 FTIR spectrometer from Thermo Fisher Scientific (Madison, WI, USA) equipped with a DGTS-detector and a single bounce diamond ATR accessory. 64 scans were accumulated per spectrum with at a spectral resolution of 4 cm^{-1}. Data acquisition and evaluation were done by means of the OMNIC Continuμm software version 7.3 (Thermo Electron, Waltham, USA).

3.3.2 Fourier Transform Infrared Microscopy (μ-FTIR)

All measurements were performed on a Continuum IR- microscope from Thermo Fisher Scientific (Madison, WI, USA) equipped with a cryogenically cooled mercury cadmium

telluride (MCT)-detector (narrow band mid-IR: 4000 - 650 cm^{-1}). The microscope was coupled to a Nicolet-Nexus 670 FTIR spectrometer as beam source (Figure 25). The aperture was set to 100 x 100 μm^2. The step width of the line scans was 100 µm. All measurements were performed in transmission mode at a spectral resolution of 4 cm^{-1} and 100 scans were collected for each spectrum. Data accumulation and processing were done by means of the OMNIC software version 7.3 (Thermo Fisher, Waltham, USA).

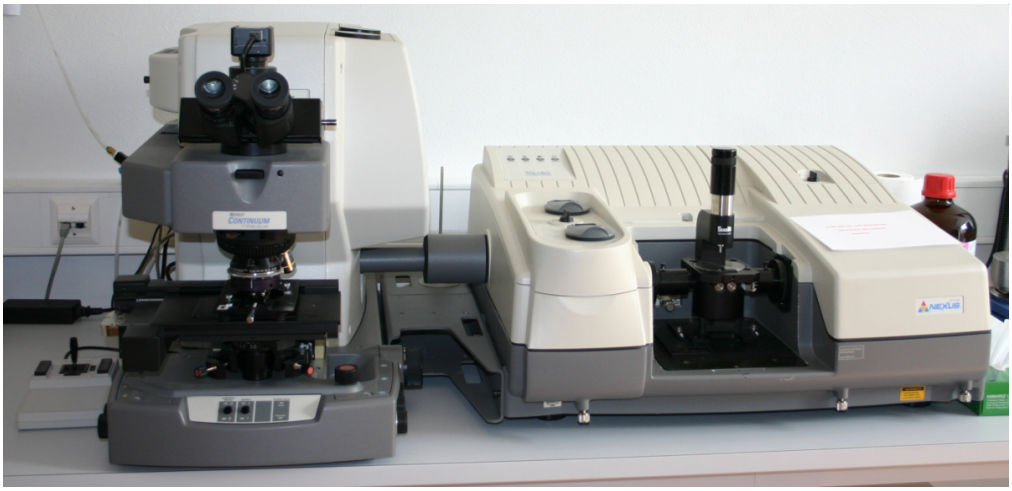

Figure 25: IR-microscope Continuum, Thermo Nicolet coupled to a Nicolet-Nexus 670 FTIR spectrometer.

3.3.2.1 Sample preparation

Samples of 200 ± 5 µm were prepared using a Leica RM2245 microtome. The preparation of the cuts and the direction of the line scan are shown in Figure 26.

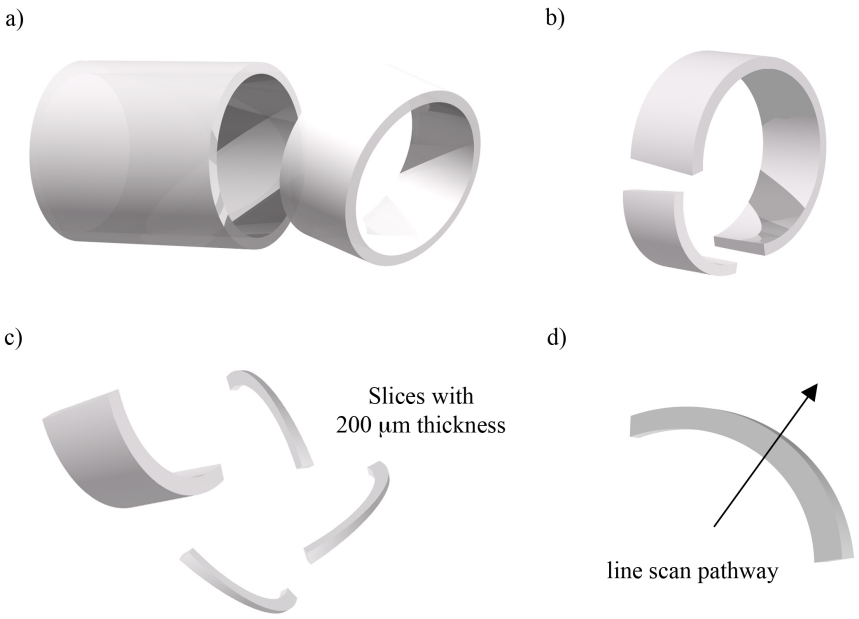

Figure 26: Schematic representation of sample preparation.

The thickness of all slices was determined by a microgauger to ensure reproducible and comparable results with a small systematic deviation of +/- 5 μm.

Each cross-section was clamped stress-free in a micro-vice sample holder, which fits into the X-Y-movable stage, allowing for precise control over the position of the sample during scanning (Figure 27).

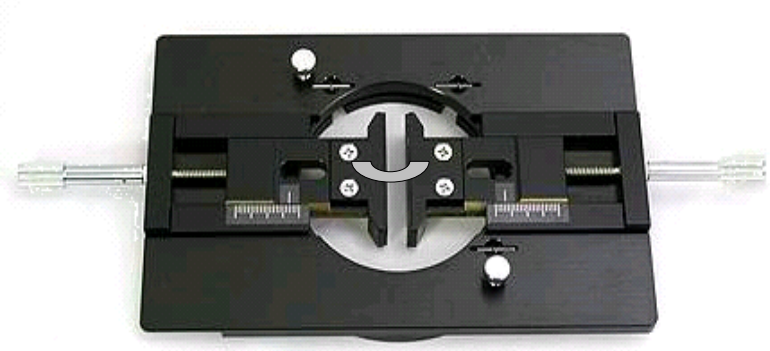

Figure 27: Micro-vice sample holder.

3.3.2.2 Calculation of the peak areas

The peak areas were calculated using a fixed two-point baseline. The details will be given in chapter 4.

3.3.3 Differential Scanning Calorimetry (DSC)

Circular samples with a diameter of 5 mm and a thickness of 200 μm (ca. 5 mg) were peeled from the outer surface of the pipe. The oxidative induction times (OIT) of the samples were measured isothermally in a DSC 204 Phönix (Netzsch). At the beginning of the measurement the sample is kept at 200 °C under nitrogen for 2 minutes to ensure that the sample is heated uniformly. Subsequently, the purge gas was changed to air. The OIT values were calculated according to DIN EN 728:1997 [202].

3.3.4 Chromatographic techniques

3.3.4.1 Extraction of additives

Additives (stabilisers and pigments) present in the samples were extracted from the polymer matrix using the reflux technique with toluene as solvent and methanol as co-solvent [116-119]. The measurements were carried out by BASF Schweiz AG (Basel, Switzerland).

3.3.4.2 High Performance Liquid Chromatography (HPLC)

After solvent extraction and subsequent filtration through a PTFE 0.45 μm syringe filter the resulting solutions were injected into the HPLC-UV system. The analyses were performed on a Shimadzu LC20 system equipped with two LC20AD pumps, an SIL-20A auto-sampler, a CTO-20AC column oven and a photodiode array SPD-M20A detector. The stationary phase was Agilent Zorbax ODS 150 mm x 4.6 mm, 5 μm (Agilent Techologies, Böblingen,

Germany). The quantification was done at a wavelength of 270 nm using the internal standard technique.

3.3.4.3 Size Exclusion Chromatography (SEC)

A high temperature chromatograph PL 220 (Polymer Laboratories, Agilent Inc, Church Stretton, England) was used to determine the MMD. The temperature of the injection block and the column compartment was set to 140 °C. Three mixed bed Olexis columns (Polymer Laboratories, Agilent Inc, Church Stretton, England) with dimensions 30 x 0.8 cm i.d. were used. The flow rate of the mobile phase was 1 mL/min. The samples were dissolved for 2 h in 1,2,4-trichlorobenzene TCB, stabilised with butyl hydroxy toluene (0.2 mg/mL), at a concentration of 1 mg/mL and a temperature of 150 °C. 200 µL of the sample solution were injected. Narrow disperse polystyrene standards (Polymer Standards Service, Mainz, Germany) were used for calibration. WinGPC software (Polymer Standards Service GmbH, Mainz, Germany) was used for data acquisition and processing.

4. Results and discussion

The aim of this work was to develop an analytical method based on IR-microscopy to study the ageing processes, namely the loss of AO, degradation of the polymer and change of the crystallinity in PE pipes, which were exposed to different doses of UV radiation. For this purpose pipes made from different types of PE (PE 80, PE 100 and PEX) were used as obtained from the manufacturers. They were stabilised with Irganox 1010 as primary AO and Irgafos 168 as secondary AO, and were exposed to different (natural and artificial) weathering conditions.

With IR-microscopy line scans were performed over the pipe wall and at the surface and the loss of the long term stabiliser Irganox 1010 during ageing was determined. Degradation products and spectral crystallinity were also profiled.

Some pipes samples were additionally stabilised with light stabilisers and UV absorbers and the behaviour of Irganox 1010 in combinations with these compound was studied. To verify the results from IR-microscopy the content of stabilisers was determined by extraction and subsequent HPLC-UV-analysis.

4.1 Characterisation of the unaged pipes

4.1.1 High performance liquid chromatography (HPLC)

The additives in the pipes were analysed using extraction and HPLC. A representative chromatogram of the additives present in B_2 is shown in Figure 28 and their content is summarised in Table 4.

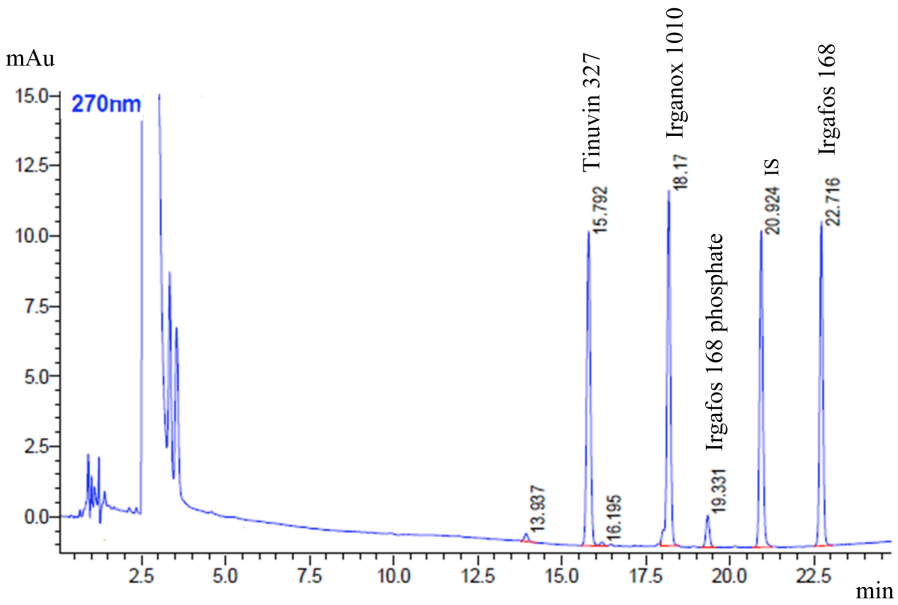

Figure 28: Chromatogram of the additives presents in the samples detected by UV-light at 270 nm wavelength.

Table 4: Additive content in the pipe samples as determined by HPLC-UV.

Sample	Primary AO [wt. %]	Secondary AO (Irgafos 168 as phosphite and phosphate) [wt. %]	UV protector [wt. %]
A	< 0.002 Irganox 1010	0.035 phosphite 0.113 phosphate	-
B_1	0.122 Irganox 1010	0.116 phosphite 0.024 phosphate	-
B_2	0.130 Irganox 1010	0.120 phosphite 0.024 phosphate	0.070 Tinuvin 327 0.069 Tinuvin 770
C	0.007 Irganox 1010	0.154 phosphite 0.115 phosphate	-
D	0.003 Irganox 1076	0.019 phosphite 0.081 phosphate	-
F	0.123 Irganox 1010	0.081 phosphite 0.031 phosphate	-

A, B_1, B_2, C and F contain a phenolic AO, Irganox 1010 (pentaerythritol tetrakis-3-(3,5-di-tert.-butyl-4-hydroxyphenyl) propionate) as primary stabiliser and Irgafos 168 (tris-(2,4-di-t-butylphenyl)-phosphite) as secondary stabiliser. D contains a phenolic AO, Irganox 1076 (octadecyl-3-(3,5-di-tert.butyl-4-hydroxyphenyl)-propionate), as primary stabiliser as well Irgafos 168 as secondary stabiliser. In addition, B_2 contains Tinuvin 327 (2,4-di-tert-butyl-6-(5-chlorobenzotriazol-2-yl) phenol) as UV absorber and Tinuvin 770 (bis (2,2,6,6,-tetramethyl-4-piperidyl) sebacate) as light stabiliser (HALS). F contains additionally 2 wt. % CB as UV absorber. *Yellow 181* and *Yellow 13* were identified as pigments for B_1 and B_2 respectively. Significant amounts of oxidised Irgafos 168 (phosphate) are present in A, C and D, while lower levels were found in the other samples. The high fraction of oxidised Irgafos in A, C and D is the result of severe processing conditions, i.e. high temperatures during extrusion. Although it must be noted that in these samples the primary AO (Irganox 1010, Irganox 1076) is either completely degraded (A) or only trace levels are present (C and D). Those samples stabilised with quite reasonable formulations (more than 0.1 wt. % Irganox 1010) are B and F. Since D and E (see section 4.1) differ only in their dimensions and the investigations will focus on D.

4.1.2 IR-microscopy

In the study of polymer degradation IR-spectroscopy is one of the most widely used techniques because of its high sensitivity. It provides not only the qualitative and quantitative composition of the polymer but also gives morphological information such as the degree of crystallinity or degree of orientation.

4.1.2.1 Identification of the pure additives and pure PE

Initially, the pure additives - Irganox 1010, Tinuvin 327, Tinuvin 770 and Irgafos 168 - and an unstabilised PE sample were analysed by FTIR in ATR mode. Figure 29 shows the IR-spectra.

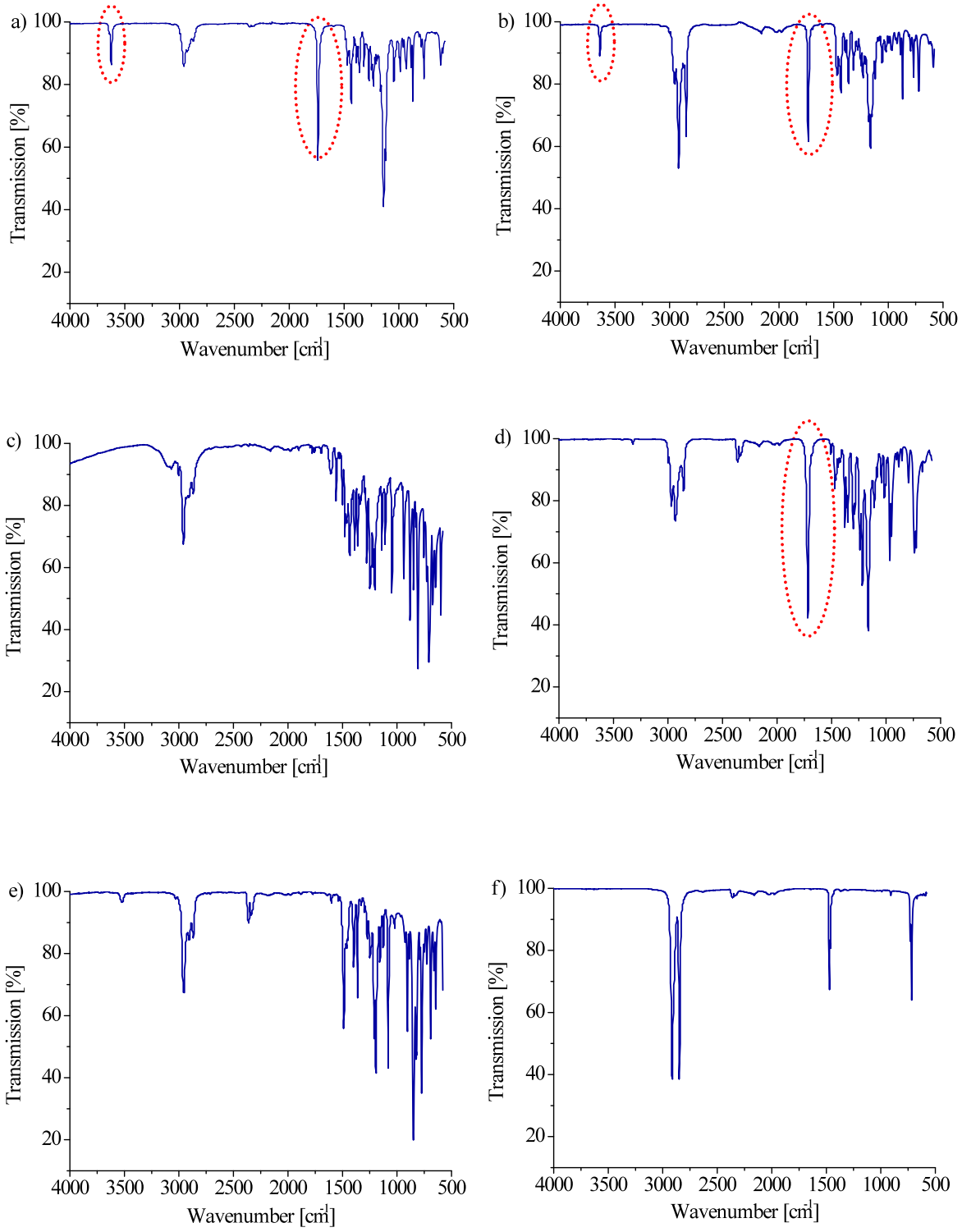

Figure 29: FTIR spectrum of a) Irganox 1010, b) Irganox 1076 7, c) Tinuvin 327, d) Tinuvin 770, e) Irgafos 168 and f) HDPE.

The IR-spectra of Irganox 1010 and Irganox 1076 show a characteristic absorption at 1739 cm^{-1} assigned to the stretching vibration of the carbonyl group ($\nu_{C=O}$). In addition, for both AOs a double band at 3604 and 3644 cm^{-1}, caused by the stretching vibration of hydroxyl groups (ν_{OH}), is visible. Tinuvin 770 also shows a characteristic carbonyl band ($\nu_{C=O}$) at 1717 cm^{-1}. The assignment of selected vibrational bands of the additives is presented in Table 5.

Table 5: Selected IR-vibrations of the additives.

Wavenumber [cm^{-1}]	**Intensity**	**Vibration Mode**
1739	s	Carbonyl vibration of an aliphatic ester (Irganox 1010) ($\nu_{C=O}$)
1736	s	Carbonyl vibration of an aliphatic ester (Irganox 1076) ($\nu_{C=O}$)
1717	s	Carbonyl vibration of an aliphatic ester (Tinuvin 770) ($\nu_{C=O}$)
1219	w	N-H stretching vibration of the amine (Tinuvin 770) (ν_{N-H})
1122, 1135	s	C-O *asym.* ester vibration (Irganox 1010) (ν_{C-O})
3604	w	stretching vibration of the OH group of the phenol (hydrogen bonded OH) (Irganox 1010 and Irganox 1076) (ν_{OH})
3644	w	stretching vibration of the OH group of the phenol (free OH) (Irganox 1010 and 1076) (ν_{OH})

(w = weak, m = medium, s = strong)

The IR-spectrum of PE shows strong bands at 2800 - 3000 cm^{-1} which are assigned to the stretching mode of CH_2, $\nu_{a(CH2)}$ and $\nu_{s(CH2)}$, at 1465 assigned to the bending mode, $\delta_{(CH2),}$ and at 731 and 721 cm^{-1} assigned to rocking mode $\gamma_{r(CH2)}$ [203]. The assignment of all bands to the vibrational modes of the PE is presented in Table 6.

Table 6: IR-vibrations of PE.

Wavenumber [cm^{-1}]	**Intensity**	**Vibration Mode**
2897	m	CH_2 *asym.* stretching $\nu_{a(CH2)}$
2851	vvs	CH_2 *sym.* stretching $\nu_{s(CH2)}$
1894	w	Combination 1168/726
1473	vs	CH_2 bending $\delta_{(CH2)}$
1463	vs	CH_2 bending $\delta_{(CH2)}$
1368	m	CH_2 wagging $\gamma_{w\ (CH2)}$
1305	m	CH_2 wagging $\gamma_{w\ (CH2)}$ amorphous region
966	vvw	*Trans* RCH=CHR
908	m	$RCH=CH_2$
888	vw	$R\text{-}CH_3$
731	vs	CH_2 rock $\gamma_{r\ (CH2)}$
721	vs	CH_2 rock $\gamma_{r\ (CH2)}$

(w = weak, m = medium, s = strong, v = very → Example vvs = very very strong)

4.1.2.2 Determination of the Irganox 1010 calibration curve in PE

Using the carbonyl absorption $\nu_{C=O}$ at 1739 cm^{-1} and the hydroxyl absorption ν_{OH} at 3644 cm^{-1} of Irganox 1010 enables to determine its concentration in the samples. Therefore PE standards with well-defined concentrations of Irganox 1010 between 0.02 and 0.60 wt. % were prepared and microtome slices of 200 µm thickness of those analysed. Figure 30a shows an enlargement of the carbonyl absorption ($\nu_{C=O}$) and Figure 30b an enlargement of the hydroxyl absorption (ν_{OH}) of the PE standards with different concentrations of Irganox 1010.

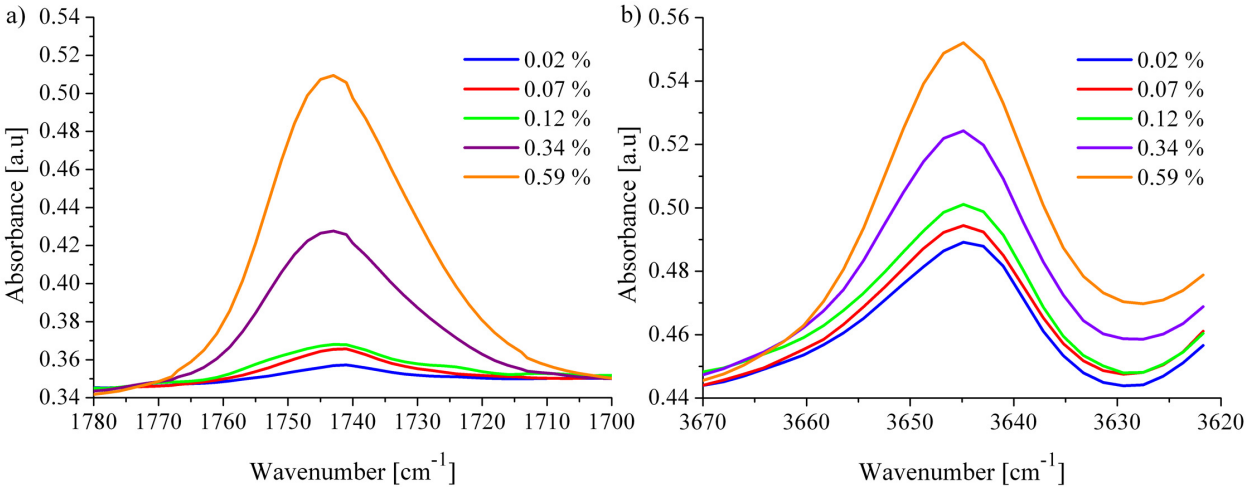

Figure 30: Enlargement of the IR-spectrum of PE standards containing different concentration of Irganox 1010 ranging from 0.02 - 0.6 wt. % and measured on 200 µm thickness slices in the a) $\nu_{C=O}$ region (1744 cm^{-1}) and b) ν_{OH} region (3644 cm^{-1}).

As can be noticed the carbonyl vibration of Irganox 1010 in the PE standards displays a shift of 5 cm^{-1} towards lower wavenumbers when compared to the pure Irganox 1010 (Figure 29a). A possible reason for this may be the fact that Irganox 1010 can crystallise in different polymorphs depending on the solvent [204,205], temperature [206,207] or polymer matrix [208,209]. In detail three crystal modifications (form I, II and III) were characterised by X-ray diffraction. These differ in their extent of intermolecular hydrogen bonding between the ester and hydroxyl groups, which in consequence leads to a different position of the carbonyl vibration in the IR-spectrum.

In order to convert the intensity of the carbonyl absorption into an absolute content, the area of the absorption was calculated [201] using the integration limits as shown in Figure 31.

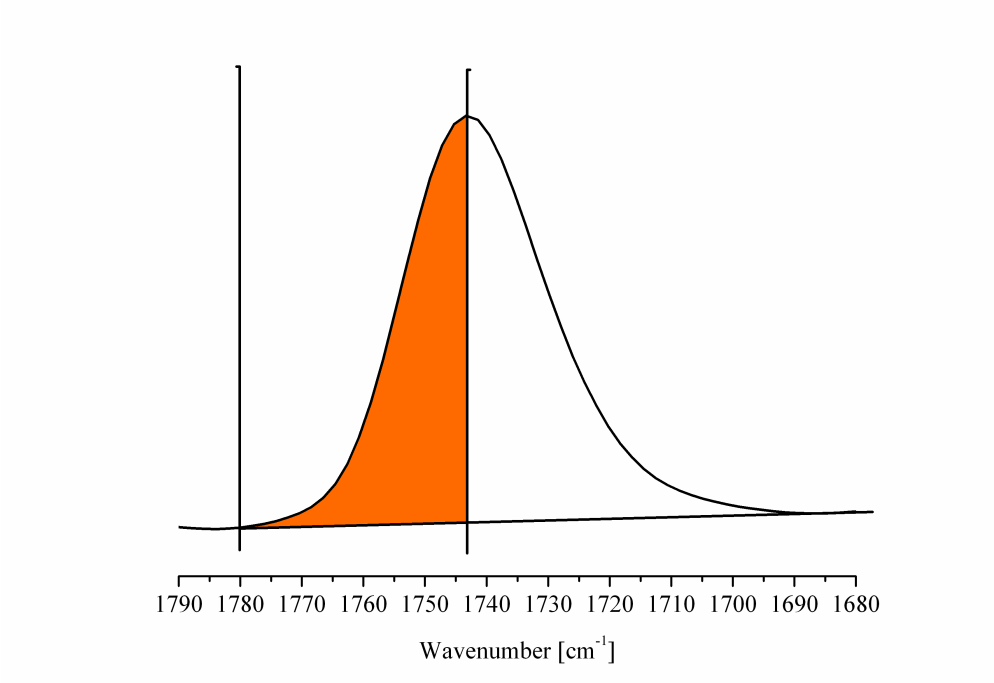

Figure 31: Integration limits of the carbonyl band in the IR-spectrum of the PE standards.

The half width of the peak area was used for integration to avoid errors caused by overlapping absorption bands of possible degradation products around 1710 cm-1. The same integration limits were used for the pipe samples.

At a constant thickness, the area of the band at 1744 cm^{-1} ($A_{1744cm-1}$) depends on the concentration of Irganox 1010 ($C_{Irganox1010}$) in the PE slices and a proportionality factor *k* can be established by equation 1.36.

$$C_{\text{Irganox 1010, 200 µm}} = \frac{1}{k} A_{\text{1744 cm-1, 200 µm}} \qquad (1.36)$$

The proportionality factor is calculated with $k = \varepsilon_{1744cm-1} \bullet d$ where $\varepsilon_{1744cm-1}$ is the absorption coefficient at 1744 cm^{-1} and d is the thickness of the irradiated film. This factor is determined from the calibration measurements. Multiple points (10 points) of the PE-

standards slices were measured for each sample, averaged and a calibration curve was built. Figure 32a shows A $_{1744cm-1}$ and Figure 32b A $_{3644cm-1}$ as a function of the AO content.

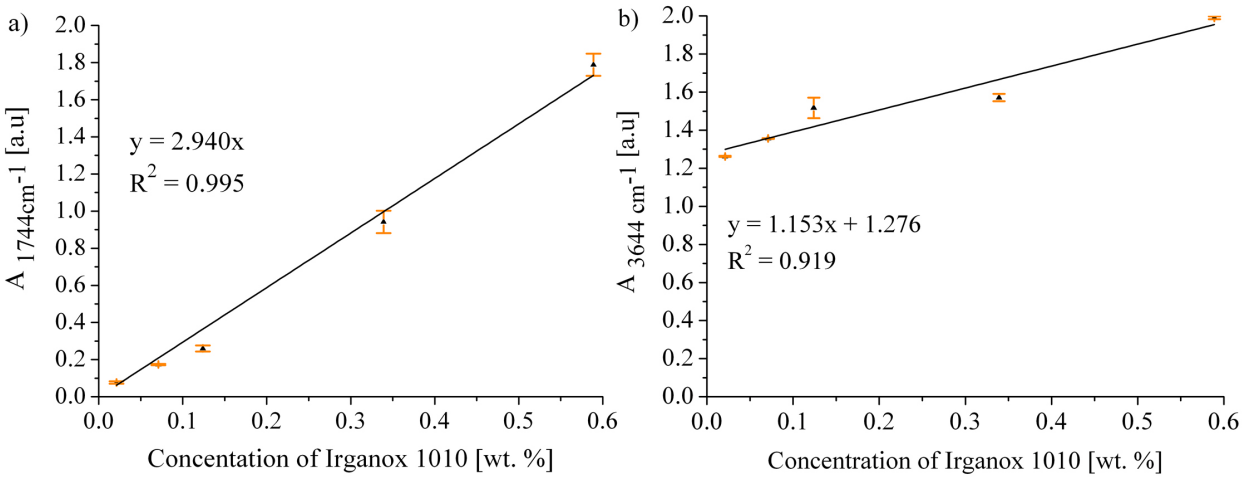

Figure 32: Calibration curve for Irganox 1010 of a) A $_{1744\ cm-1}$ and b) A $_{3644\ cm-1}$ vs. concentration in the PE standards with concentrations of Irganox 1010 ranging between 0.02 and 0.6 wt. %.

For the carbonyl band, the straight line intersects the origin of the coordinate system which is not the case for the hydroxyl band. This can be explained by the adsorption of water from the surrounding air during the measurement or alternatively the Irganox 1010 used to prepare the standards contained traces of moisture which were not completely removed during the extrusion process. Therefore only the carbonyl band calibration was used for further calculations. With the slope of the calibration curve of the carbonyl band (Figure 32a) k is determined and $A_{1744\ cm-1}$ can now be converted to the content of Irganox 1010 in the PE standards according to equation 1.37.

$$k_{200\,\mu m} = \frac{2.940}{\text{wt. \%}} = 294$$

$$C_{\text{Irganox 1010, 200 µm}} = \frac{A_{1744\ cm-1,\,200\,\mu m}}{k_{200\,\mu m}} \qquad (1.37)$$

Furthermore, the slope provides a value for the extinction coefficient (ε), which is theoretically independent of d and can be determined as follows:

$$\varepsilon_{1744cm-1} = \frac{k}{d} = \frac{294}{200\ \mu m} = \frac{1.47}{\mu m}$$

This calculation assumes that the absorption of IR light due to scattering is constant on all PE standards. The region of linear response for the detector is typically below an extinction of 1.5, which is the case for all PE-standards. However, all absorption bands of PE which could potentially be used as a reference band for quantification, i.e. the CH stretching vibration either around 2800 or at 1465 cm^{-1}, have extinction values higher than 1.5. Thus it was not possible to calculate the concentration of Irganox 1010 in relation to a fixed polymer band and the calculated additive concentration will depend on the thickness of the irradiated layer.

4.1.2.3 Identification of the additives and quantification of Irganox 1010 in the samples

Figure 33 shows the enlargement of the IR-spectrum in the carbonyl region for the unaged pipes.

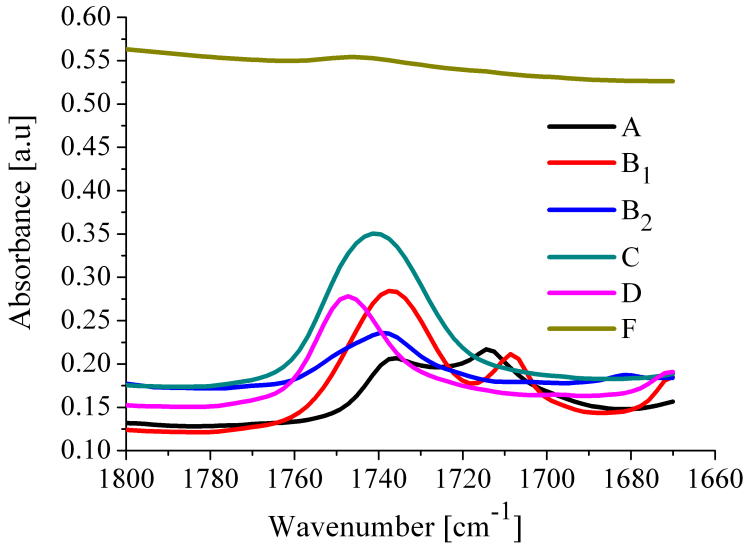

Figure 33: Enlargement of the IR-spectrum in the carbonyl region of A, B_1, B_2, C, D and F.

A shows a double band in the carbonyl region with maxima at 1737 cm^{-1} and 1717 cm^{-1} respectively. According to the results from the extraction (section 4.1.1) the Irganox 1010 was strongly degraded and only 0.002 wt. % of AO was present in the sample. Thus the band at 1737 cm^{-1} cannot be attributed to the Irganox 1010. Therefore both bands can be attributed to pigments and degradation products formed due to the processing conditions.
Two bands appear for B_1 in this region, one at 1737 cm^{-1} attributed to carbonyl vibration of the Irganox 1010 as confirmed by HPLC (concentration in the sample was 0.122 wt. %), and the other at 1709 cm^{-1} which can be assigned to the amide group of the pigment Yellow 181 (identified by mass spectrometry). In the latter the carbonyl vibration causes two characteristic bands at 1709 cm^{-1} ($\nu_{L\ C=O}$) and 1727 cm^{-1} ($\nu_{H\ C=O}$) [210-212]. The structure of *Yellow 181* is shown in Figure 34.

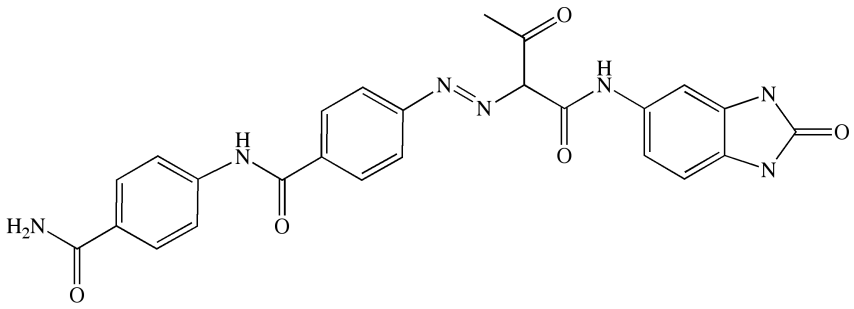

Figure 34: Structure of Yellow 181.

In B_2 the band of the carbonyl vibration is broadened due to overlapping of the carbonyl bands of Irganox 1010 and Tinuvin 770. In this sample the pigment *Yellow 13* (Figure 35) was identified, meaning that no additional bands are expected in this region.

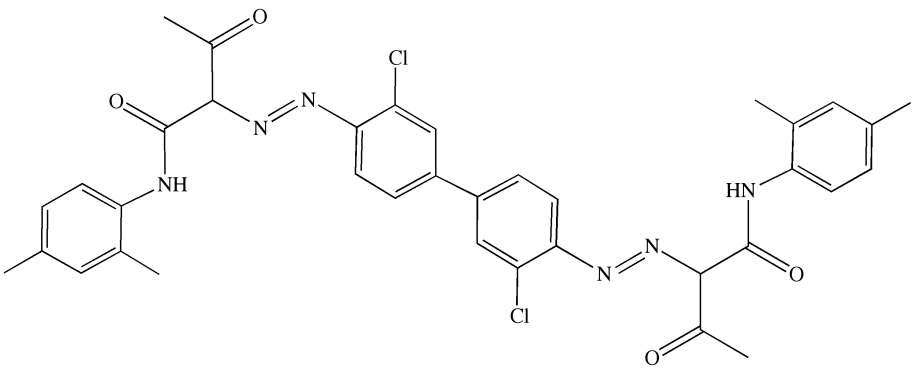

Figure 35: Structure of Yellow 13.

For C and D intense absorptions at 1740 cm^{-1} and 1750 cm^{-1} are observed. These cannot be attributed to AO since the extraction results (section 5.1.1) show a very low concentration of AO. PE-Xa (section 2.2) is commonly produced by the Engel method where peroxides are used as initiator. The bands at 1740 cm^{-1} and 1750 cm^{-1} can be attributed to reaction products from the production or to pigments which were not detected by HPLC. For F, a shift to higher extinction is observed over the entire spectral range due to the presence of CB. Although the absorption of the carbonyl band for Irganox 1010 at 1744 cm^{-1} is lower, it is still in the region of the linear response of the detector.

As described, A, C and D show very low concentrations of stabiliser. Therefore B and F, which have a higher content of AO were selected for further studies.

4.1.2.4 Determination of the concentration of Irganox 1010 for B_1

The IR-spectrum of B_1 shows a band at 1727 cm^{-1} ($\nu_{H\ C=O}$) which can be attributed to the pigment *Yellow 181* in turn overlaps with the carbonyl band of Irganox 1010. Due to this fact, the total observed carbonyl absorbance (A) consists of the contribution $\nu_{C=O}$ of Irganox 1010 and that of *Yellow 181*.

From the HPLC results of the unaged B_1 a value of 0.122 wt. % of Irganox 1010 was found which corresponds to a carbonyl absorbance of 0.359 (A_0). With this information and the assumption that the content of *Yellow* 181 does not change during weathering, the initial calibration (see Figure 32a) can be adjusted by adding an offset, $\Delta A = A - A_0$, as shown in Figure 36 (line b).

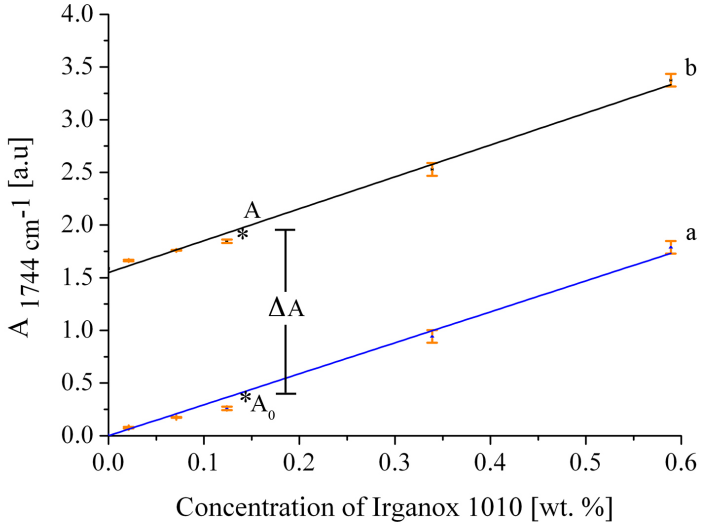

Figure 36: Calibration curve of A $_{1744\ cm\text{-}1}$ vs. concentration for Irganox 1010: line a) in a PE matrix and line b) corrected by taking into account the contribution of the pigment Yellow 181 as offset.

With the adjusted calibration curve the peak area can now be converted into concentration values of Irganox 1010. In Figure 37 an example for the concentration profile of Irganox 1010 over the pipe wall for B_1 is depicted.

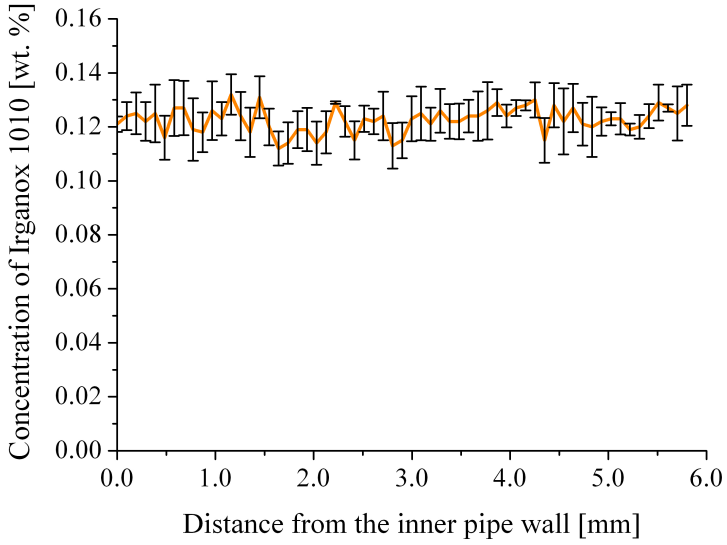

Figure 37: Concentration profile of Irganox 1010 over the wall for B_1.

The reproducibility was evaluated by preparing microtome cuts of 200 µm thickness of the unaged sample and measuring them individually. The standard deviation determined from four independent measurements was 0.007.

4.1.2.5 Degree of spectral crystallinity

The degree of spectral crystallinity across the pipe wall was profiled using the ratio of the bands at 1897/1304. The band at 1897 cm^{-1} is caused by crystalline sequences in PE and is a combination of the $\gamma_{r\ (CH2)}$ 1168, 720, 730 cm^{-1} bands. The band at 1304 cm^{-1} is assigned to the CH_2 twisting mode in the amorphous chain segments [133,144]. The area of the bands was evaluated by integration using a fixed two point baseline as shown in Figure 38.

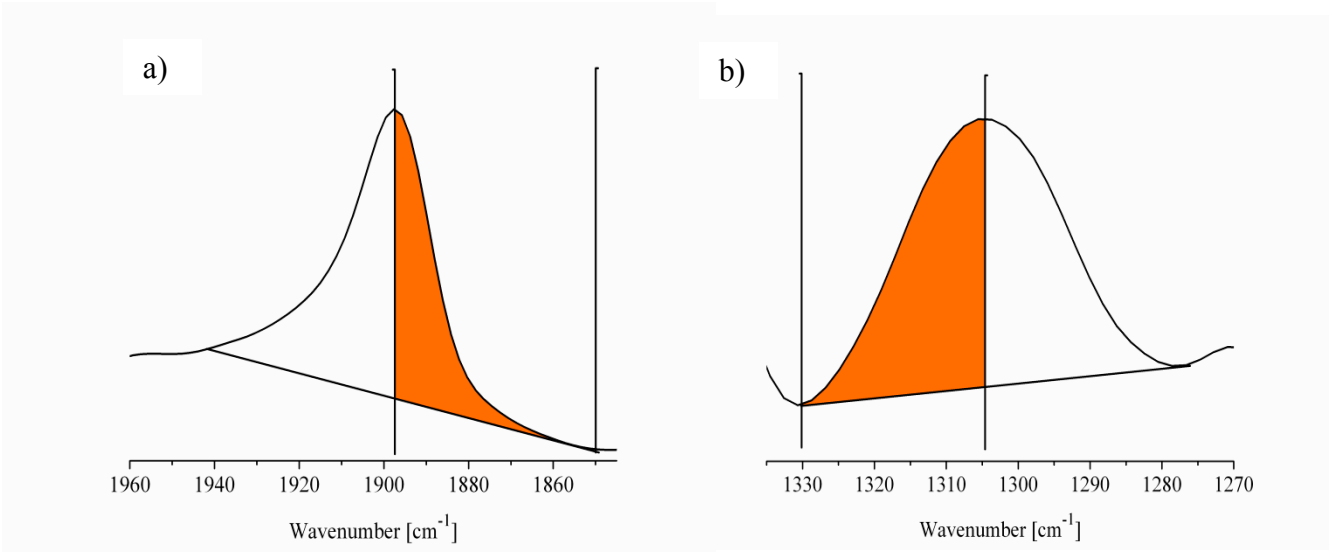

Figure 38: Integration limits of IR bands of PE at a) 1897 cm^{-1} and b) 1304 cm^{-1}.

The profiles of the degree of spectral crystallinity over the wall of A - D are shown in Figure 12.

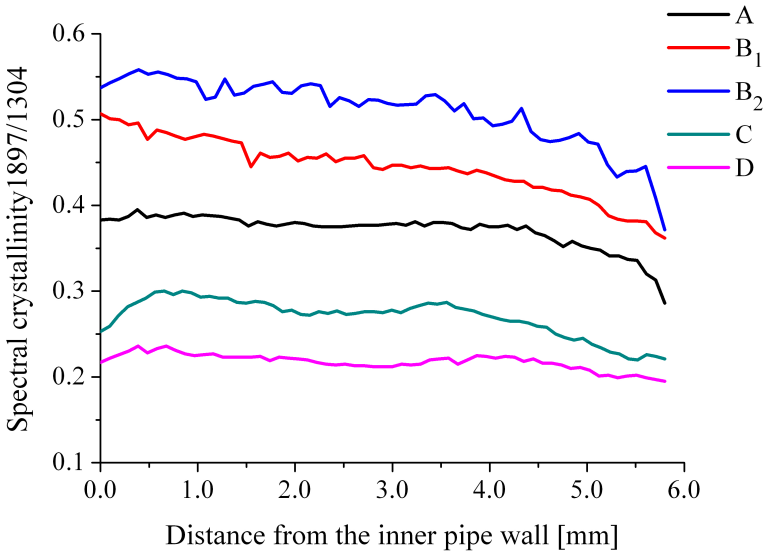

Figure 39: Distribution of the degree of spectral crystallinity derived from the peak area ratio 1897/1304 over the wall for A - D.

A gradual decrease in the degree of spectral crystallinity from the inner to the outer surface is observed. This can be explained by the fact that the cooling of the freshly extruded pipe starts from the outer surface thus preventing a proper crystallisation of the polymer. Differences in the spectral crystallinity between the samples can be due to the individual processing conditions and additionally stem from the different pigments. It was shown [213-217] that pigments can act as nucleating agents leading to the formation of a higher number of smaller spherulites and increasing the final crystallinity. In the case of F the spectral crystallinity was not determined because the absorption band at 1897 cm^{-1} is influenced by the absorption of CB.

4.1.3 Oxidative induction time (OIT)

Despite its lower resolution and accuracy compared to IR-microscopy OIT is still a simple approach to roughly estimate the residual content of phenolic antioxidant. It has to be pointed out that since A, C and D are already degraded (section 4.1.2.3) the OIT measurements were performed only for B_1, B_2 and F by peeling thin slices (200 µm) from the outer pipe surface. The results are shown in Figure 40.

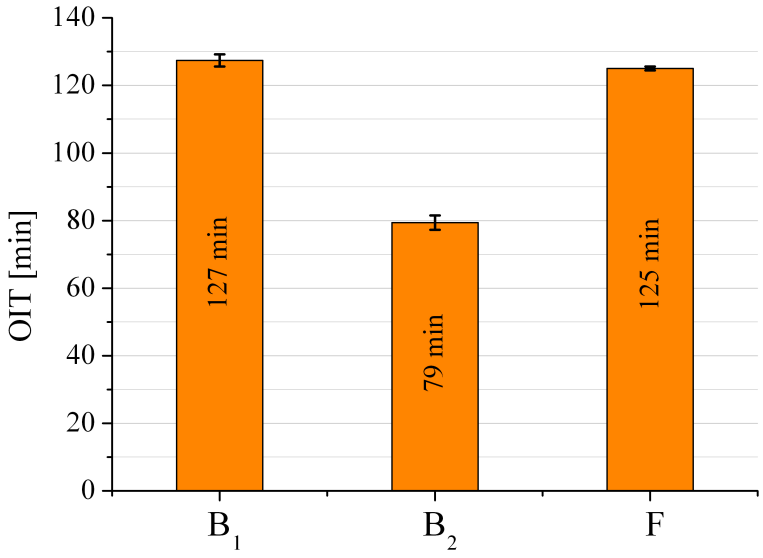

Figure 40: OIT measurements of 200 µm peeled slices of B_1, B_2 and F.

It can be observed that B_1 and F have an OIT of around 125 min. A higher OIT value for F would have been expected in comparison with B_1 since it has been established that CB can retard thermal oxidation, either by acting as a mild AO or by influencing the activity of other antioxidants. The mechanism of action is believed to be reactions between polar groups (carboxylic and phenolic functionalities) of CB and PE free radicals and/or antioxidants [95,218,219]. However the precise nature of the interactions between CB, PE and AO depends on the nature and amount of polar groups present on the surface of the CB (section 2.4.2.2). For the case of B_2, the observed value is much lower, namely 80 minutes. Some authors [220,221] studied the effect of the combination of Irganox 1010 and Tinuvin 770 and found that it can have either a synergistic or an antagonistic effect. From the data shown here, the combination of these AO exerts an antagonistic effect. This can be attributed to one or a combination of the following possible processes:

1) Oxidation of the phenol to the corresponding quinone by the nitroxyl radical

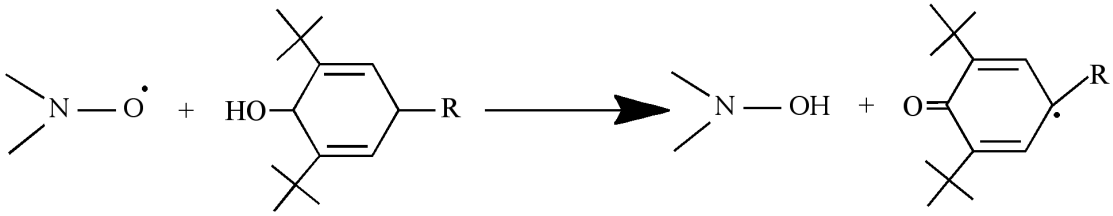

2) Reaction of the nitroxyl radical with a radical intermediate from the phenol

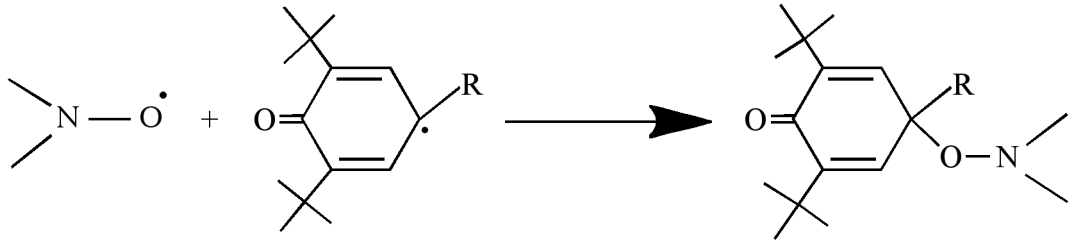

3) Formation of a salt between the acidic phenolic AO and the basic HALS.

These effects are significantly influenced by factors such as processing of the polymer, content and ratio of the additives as well as the presence of pigments.

In order to convert the OIT into absolute concentration, a calibration curve was constructed using the same PE standards (section 4.1.2.2) with well-defined amounts of Irganox 1010 between 0.02 and 0.60 wt. %. The OIT averaged from 3 independently prepared slices is shown as a function of the AO content in Figure 41.

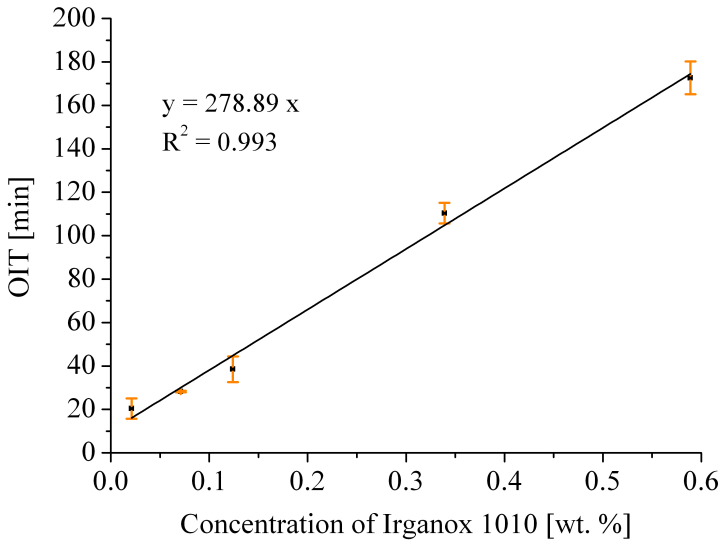

Figure 41: Calibration curve OIT times vs. concentration in the PE standards with concentrations of Irganox 1010 ranging between 0.02 and 0.6 wt. %.

Since the content of Irganox 1010 determined by HLPC (section 4.1.1) for B_1, B_2 and F was 0.122, 0.130 and 0.123 wt. % respectively, an OIT value of around 37 min was expected. However an increase of the expected OIT value to 128 min is visible for B_1 and F and to 80 min in the case of B_2. As mentioned in section 3.5.1.1.1 the linearity between the OIT and the content of phenolic AO is solely possible for the combination of a single phenolic AO with PE. Since in the investigated pipes further components are present, such as Irgafos 168 and HALS these can influence the OIT in an unpredictable way [222,222]. For B_1 and F it may be assumed that the presence of Irgafos 168 increases the OIT. In the case of B_2 an additional interaction of the HALS with the phenolic AO can also influence the OIT values.

Independent from the fact that the calibration curve cannot be used to quantify the phenolic AO in B_1 and F, the OIT will be measured for the aged samples to monitor the loss of stabiliser from the polymer.

4.2 Characterisation of the aged B_1, B_2 and F

4.2.1 Characterisation of B_1 aged by natural and artificial weathering

In this section the influence of different weathering scenarios on the surface of B_1 will be probed by IR-microscopy and complementary by HPLC and OIT.

4.2.1.1 IR-microscopy

4.2.1.1.1 Spatial concentration of Irganox 1010

As previously mentioned, an important prerequisite for the correct conversion of the spectral information into the content of Irganox 1010 is the assumption that the contribution of the pigment to the carbonyl absorption does not change during ageing. Pipes were exposed to UV light in a natural (on the roof) and in an artificial (weathering machine) environment under different conditions (section 3.2). Line scans were performed on microtome cuts of 200 µm thickness on the exposed and unexposed side to the UV radiation (Figure 42a). The concentration profiles of Irganox 1010 over the pipe wall were calculated for the side that was unexposed to the UV radiation in Figure 42b and for the side exposed to the UV radiation in Figure 42c.

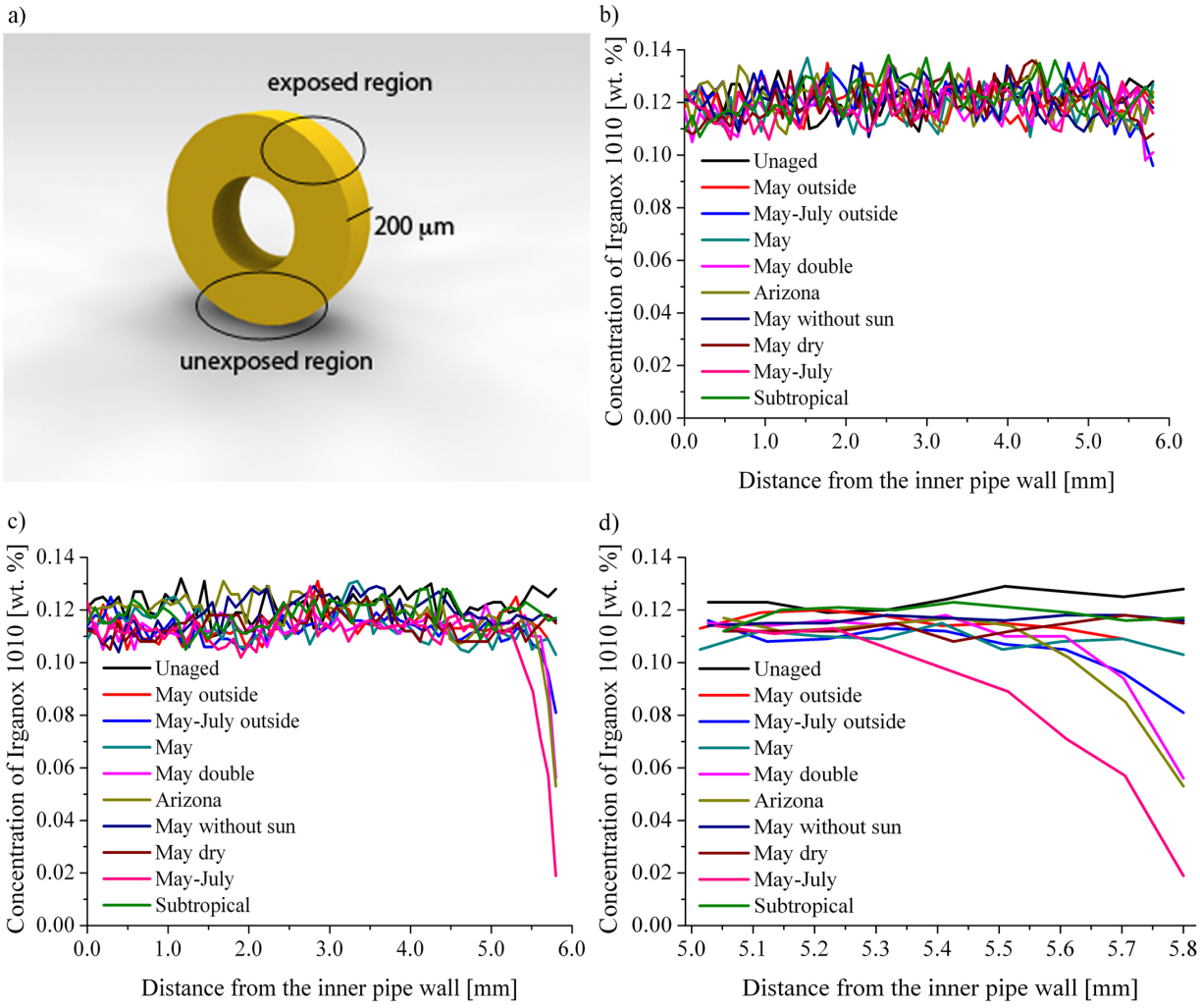

Figure 42: a) Illustration of the analysed regions, concentration profiles of Irganox 1010 over the wall of B_1 on the side b) exposed and c) unexposed to the UV-radiation at different weathering scenarios, d) enlargement of the outer pipe wall for the exposed side.

A loss of AO occurs in the outer part of the pipe wall after natural and artificial weathering in all samples, pronouncedly on the side that has been directly exposed to UV radiation, which is in agreement with previous results [171-176]. To better visualise the effect an enlargement of Figure 42c representing the outer part of the pipe wall is shown in Figure 42d.

For $B_{1\textbf{Subtropical}}$ which was exposed to high humidity (90 %) without UV radiation, for $B_{1\textbf{May dry}}$ which was exposed to lower humidity (45 %) and a lower dose of UV radiation and for $B_{1\textbf{May without sun}}$, no significant changes in the concentration profile of the AO are

observed. This suggests that UV radiation is very likely responsible for the depletion of the AO rather than humidity *per se*. Comparing $B_{1\textbf{May outside}}$ and $B_{1\textbf{May-July outside}}$ a serious depletion of AO in the outer pipe wall occurs after 3 months of exposure to the UV radiation. Since $B_{1\textbf{May-July outside}}$ and $B_{1\textbf{May-July}}$ were exposed to approximately the same amount of UV radiation with the only difference being that $B_{1\textbf{May-July outside}}$ was exposed to natural and $B_{1\textbf{May-July}}$ to artificial weathering, no major differences in their stabiliser profile should be expected. It is however interesting to note that the depletion of the stabiliser is higher for the artificially weathered sample than for the naturally weathered one. Since the dose of UV radiation was the same the observed difference can be attributed to a higher surface temperature in artificial weathering. The depletion of stabiliser in $B_{1\textbf{May double}}$ is almost the double than in $B_{1\textbf{May}}$ which leads to the assumption that a correlation between the dose of UV radiation and the extent of stabiliser loss exists. The **Arizona** conditions are used to study the interaction between UV radiation and temperature. In comparison with the **May double** program, the additional effect of high temperature may lead to a higher depletion of stabiliser. Taken together, it can be concluded that both temperature and UV radiation play an important role in the loss of AO.

4.2.1.1.2 Degradation products

As a result of the loss of the stabiliser, the polymer becomes unprotected and degradation products can be formed. Hydroperoxides, formed in the early stages of oxidation, are unstable and provide a source of free radicals for further initiation, chain scission, and crosslinking. The primary decomposition products are ketones or - going through ß-scission - aldehydes and macroalkyl radicals (section 3.3.2). These groups absorb IR radiation at around 1710 cm^{-1} and with secondary oxidation products in the later stages of oxidation the range extends to 1790 cm^{-1}. For monitoring $A_{1709\ cm\text{-}1}$ attributed to degradation products of the PE, a fixed two point baseline as shown in Figure 43 was used.

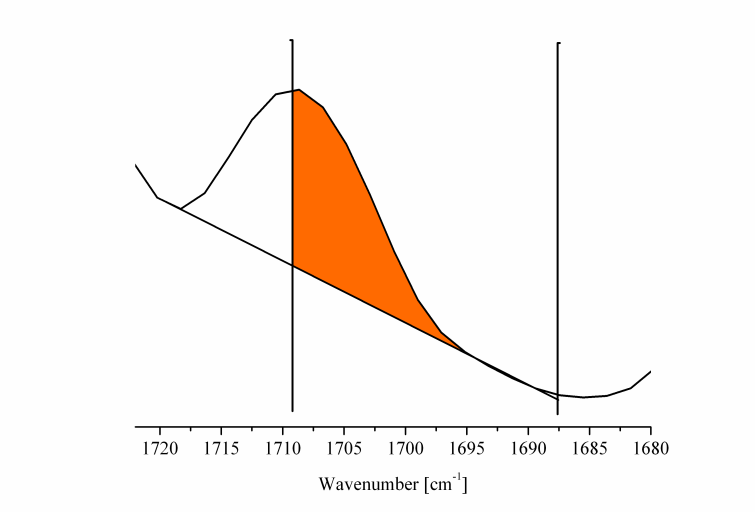

Figure 43: Integration limits of the carbonyl region characteristic for degradation products of PE.

An average over the wall of B_1 for all the different weathering scenarios is shown in Figure 44a. Since there were only minor changes for the carbonyl absorption at 1709 cm^{-1} for unaged and aged B_1 only representative absorption profiles of samples which were exposed to more extreme conditions, i.e., $B_{1\textbf{May-July outside}}$, $B_{1\textbf{Arizona}}$ and $B_{1\textbf{May-July}}$ are presented in Figure 44b.

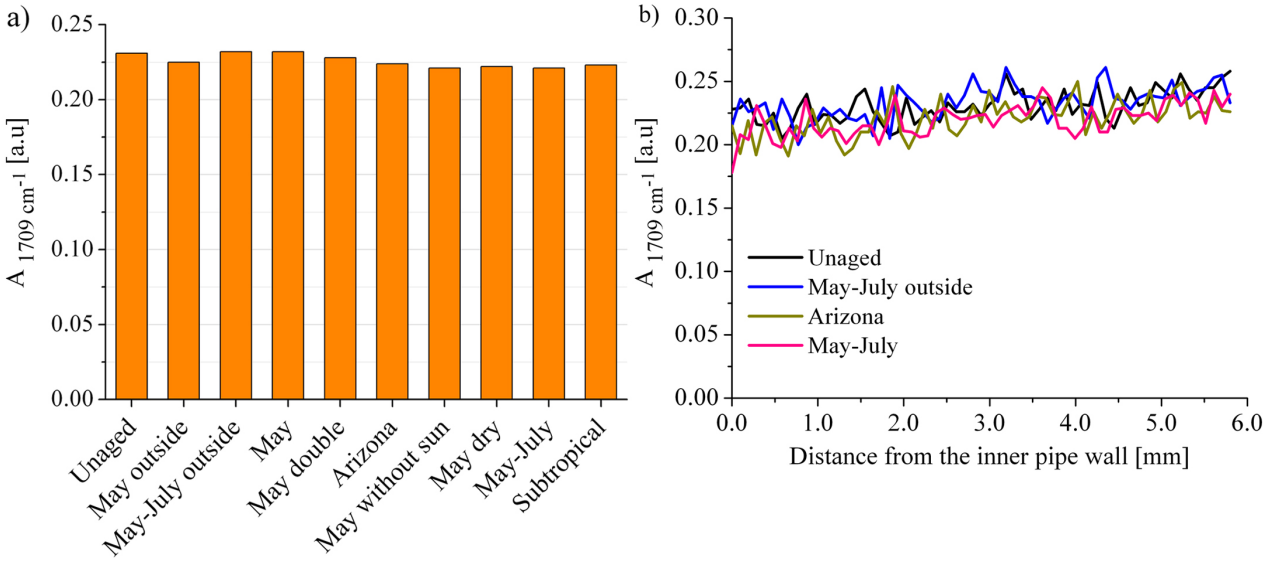

Figure 44: a) Averaged $A_{1709\ cm\text{-}1}$ over the pipe wall for all weathering scenarios and b) representative $A_{1709\ cm\text{-}1}$ over the pipe wall for the unaged B_1 and for the exposed side of B_1 at extreme weathering scenarios.

Since *Yellow 181* has a carbonyl group ($\nu_{L\ C=O}$) (Figure 34) which absorbs in the IR spectrum at 1709 cm^{-1} an initial offset of the carbonyl absorption has to be taken into account for B_1. No major differences are observed in the peak area between the samples which consolidates the assumption that the concentration of pigment is constant after natural and artificial weathering. It can be recognised that no additional carbonyl functionalities are formed after exposure to the different climate scenarios.

During photodegradation of PE *trans*-vinylene groups can be formed as described in section 3.3.2 [4,223]. Vinyl-groups are present in the polymer due to its catalytic synthesis caused by elimination of the polymer chain from the catalyst. Vinyl- and *trans*-vinylene groups show an IR absorption at 908 and 966 cm^{-1}, respectively. $A_{908\ cm\text{-}1}$ and $A_{966\ cm\text{-}1}$ were calculated in an analogue manner using a fixed two point baseline with the integration limits as shown in Figure 45.

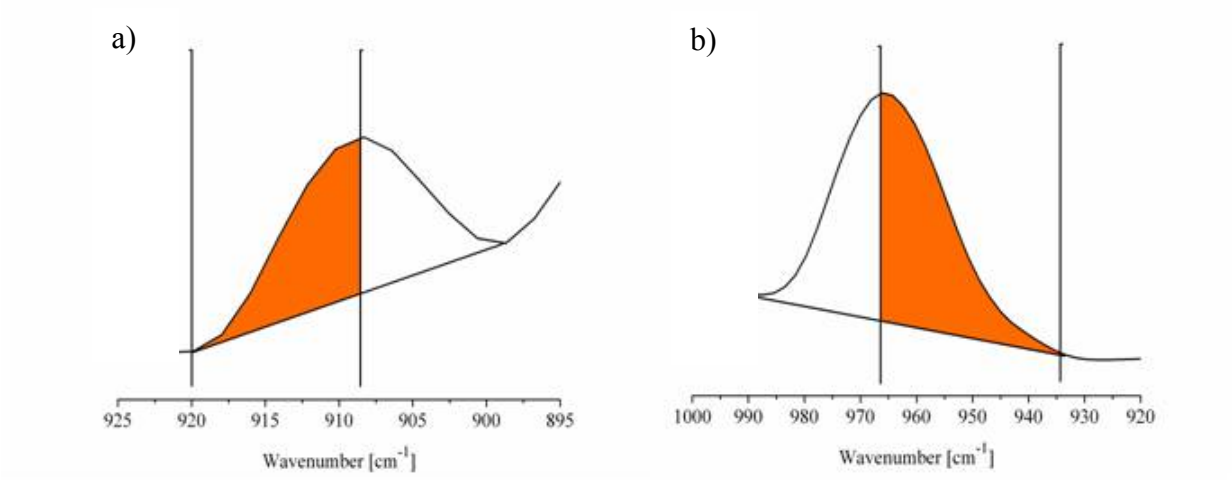

Figure 45: Integration limits of the a) vinyl and b) trans-vinylene band in the B_1 pipe samples.

Since the photodegradation occurs only at the outer region of the pipe wall the next results will focus on the outer 1.8 mm of the pipe wall. $A_{908\ cm\text{-}1}$ on the exposed and unexposed side of B_1 is shown in Figure 46a and 46b. Figure 46c and 46d show $A_{966\ cm\text{-}1}$ at the outer surface of B_1.

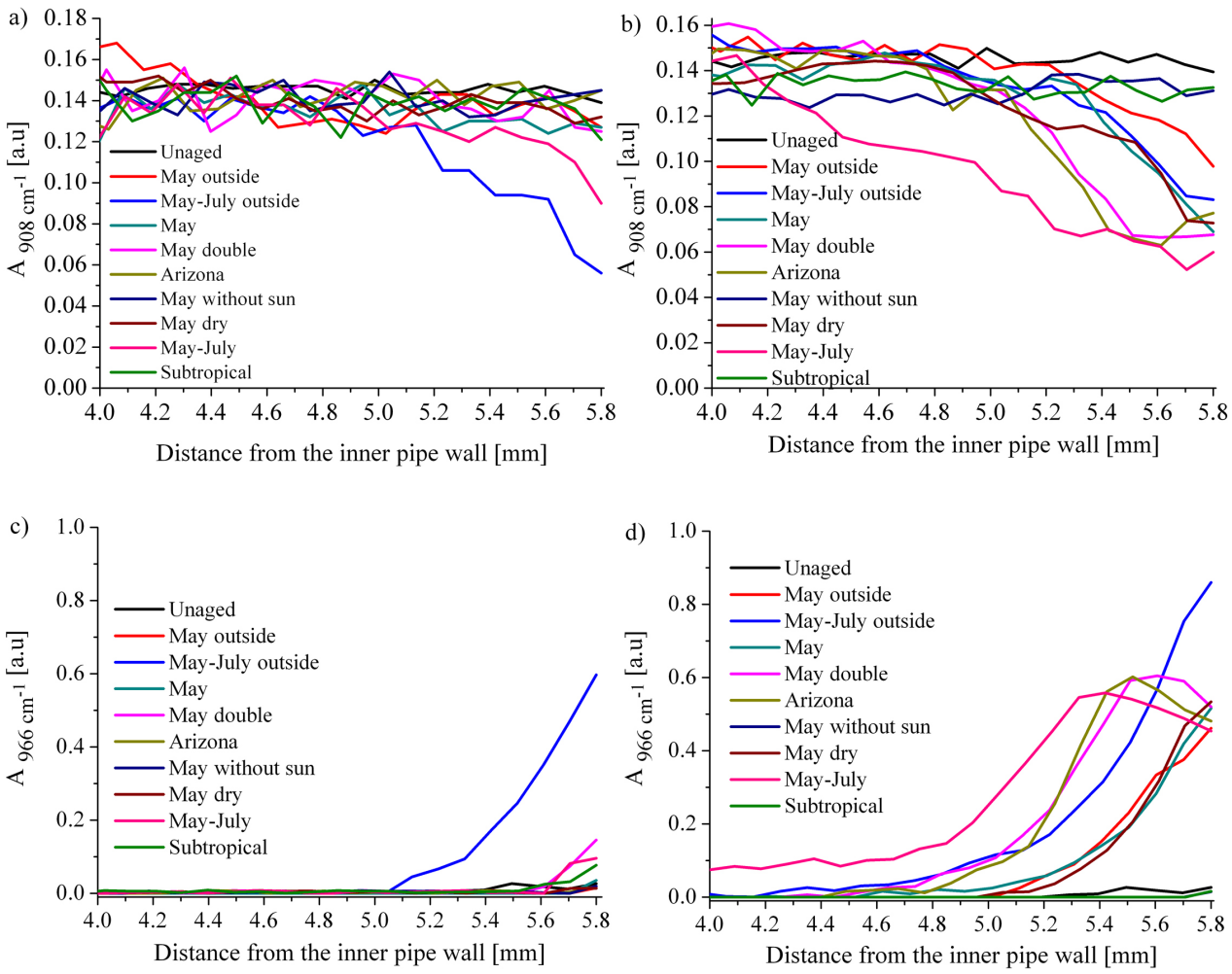

Figure 46: A $_{908\ cm\text{-}1}$ at the outer surface of the wall of B_1 on the side that was a) unexposed and b) exposed to UV radiation at different weathering conditions, and A $_{966\ cm\text{-}1}$ at the outer surface of the B_1 pipe wall on the side that was c) unexposed and d) exposed to different weathering conditions.

Vinyl groups are present in the native polymer as a result of its catalytic synthesis [5] (Figure 46a and 46b). Their content decreases with prolonged UV exposure. Worth to note that for $B_{1\textbf{May-July outside}}$ (aged on the roof for three months) a significant decrease of the vinyl groups on the unexposed side is also observed. Given the cylindrical nature of the pipe this fact can be attributed to sun rotation throughout the day.

On the other hand, *trans*-vinylene groups are formed as the pipe ages under all weathering conditions (Figure 46c and 46d). The *trans*-vinylene groups can be formed by the loss of

hydrogen atoms from adjacent methylene groups [224-226] through the mechanism described in 3.3.4. As expected, for $B_{1\text{May-July outside}}$ a significant increase of the content of *trans*-vinylene groups on the unexposed side was also observed due to the sun rotation as previously discussed.

For those samples which were exposed to a very low dose of UV radiation or even no radiation at all ($B_{1\text{Subtropical}}$, $B_{1\text{May dry}}$, $B_{1\text{May without sun}}$) no significant formation of degradation products (e.g. vinyl and *trans*-vinylene) is observed. Again, these results suggest that UV radiation plays an important role in PE pipes degradation.

4.2.1.1.3 Degree of spectral crystallinity

Figure 47 shows the profile of the degree of spectral crystallinity for B_1 after exposure to different weathering scenarios.

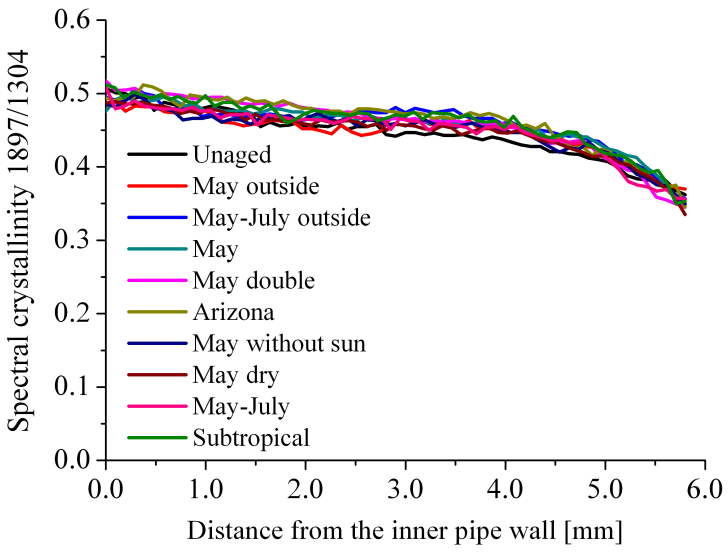

Figure 47: Distribution of the degree of spectral crystallinity derived from the peak area ratio 1897/1304 over the pipe wall for B_1 after exposure to UVradiation at different weathering scenarios.

No significant changes in the crystallinity profile occur as a result of weathering.

4.2.1.2 High performance liquid chromatography (HPLC)

In order to confirm the observations from IR-microscopy an independent analytical technique was chosen as a reference. For this purpose, thin slices (200 µm) from the outer surface exposed side of the unaged and aged pipes were peeled off and subjected to extraction and subsequent HPLC analysis as described in section 4.3.4.2. Table 7 shows the data of two representative samples, one under extreme conditions (**May-July**) and another one without exposure to UV radiation (**Subtropical**) obtained by extraction/HLPC and IR-microscopy. The weight percentage of Irganox 1010 obtained by IR-microscopy was determined by averaging the values over the outer 200 µm of the exposed side.

Table 7: Content of Irganox 1010 obtained from extraction/HPLC in the peeled outer 200 µm (exposed side) and that from averaging the Irganox 1010 content as obtained by IR-microscopy (200 µm from the surface, exposed side) for the unaged B_1 and two representative weathering scenarios.

Sample	Irganox 1010 content [wt. %]	
	Extraction / HPLC	IR-microscopy
Unaged	0.122	0.121
May-July	< 0.005	0.019
Subtropical	0.091	0.117

The content of Irganox 1010 obtained from both approaches is in agreement. Differences may be due to the lower spatial resolution of the mechanical abrasion compared to the step width of the microscope. These results show that the extent of AO depletion directly depends on the climate conditions especially if UV radiation is one of the considered parameters, i.e., the loss of Irganox 1010 under subtropical conditions without exposure to UV radiation is much lower than for $B_{1\textbf{May-July}}$ which was exposed to a high radiation dose.

The presence of the processing stabiliser (Irgafos 168 as phosphite and phosphate) was equally assessed by means of extraction/HPLC and is shown in Table 8.

Table 8: Determination of the content of processing stabiliser (Irgafos 168 as phosphite and phosphate) in the peeled outer 200 µm (exposed side) for the unaged B_1 and two representative weathering scenarios by extraction/HPLC.

Sample	Extraction / HPLC	
	Secondary AO (Irgafos 168 as phosphite and phosphate) [wt. %]	**Σ Irgafos 168 as phosphite and phosphate [wt. %]**
Unaged	0.116 phosphite 0.024 phosphate	0.140
May-July	0.011 phosphite 0.119 phosphate	0.130
Subtropical	0.103 phosphite 0.036 phosphate	0.139

The total content of phosphite and phosphate remains constant, i.e. no loss occurs as a result of evaporation. An interesting observation from the analysis by extraction/HPLC is the fact that the ratio of phosphite/phosphate decreases as a consequence of the exposure to UV radiation. Moreover the content of Irgafos 168 decreases upon ageing in the same extent as that of the phosphate increases, and the total molar concentration of both components is equivalent to the original Irgafos 168 (as phosphite and phosphate) content. Similar results were also observed by Dörner et *al*. [227] who studied the content of stabilisers in HDPE pipes aged in air at temperatures from 40 to 105 °C by HPLC.

4.2.1.3 Oxidative induction time (OIT)

Despite the fact that the OIT calibration cannot be used due to the presence of varying amounts of processing stabiliser in the samples (see section 4.1.3), the loss of stabiliser efficiency in B_1 was monitored by performing additional OIT measurements to the samples exposed to the different weathering scenarios. For this purpose, peeled thin slices (200 µm) from the unexposed and exposed outer pipe surface were obtained and analysed by OIT. The results are shown in Figure 48.

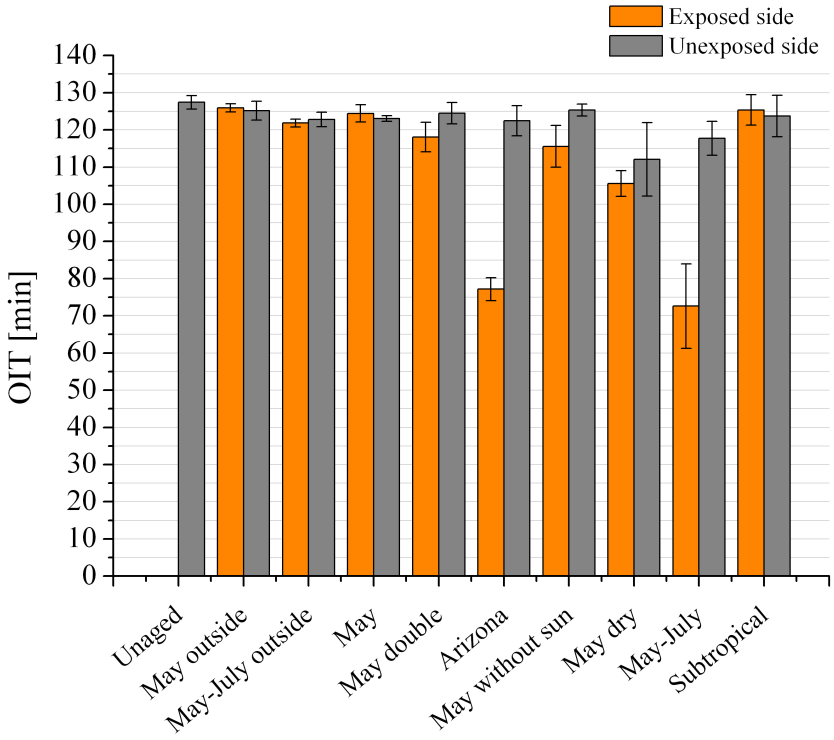

Figure 48: OIT measurements of peeled thin slices (200 µm) from the unexposed (grey bars) and exposed (orange bars) outer surface of B_1 surface after exposure to UV-radiation at different weathering scenarios.

While for most of the samples the differences in OIT between the exposed and not exposed side are statistically insignificant, for $B_{1\mathbf{Arizona}}$ and $B_{1\mathbf{May\text{-}July}}$ differences in the OIT between the exposed and unexposed side are observed which are in agreement with the results from IR-microscopy (see section 4.2.1.1). Since the major differences are seen in the samples

which were exposed to high doses of UV radiation these underline once more that UV radiation plays an important role in the depletion of the AO. It should be noted that for $B_{1\textbf{May-July outside}}$ a depletion of the AO in the outer wall can be observed by IR-microscopy but however not be detected by OIT measurement.

4.2.2 Correlating the loss of stabiliser with the radiation dose

In order to establish the relation between the loss of stabiliser and the dose of radiation, B_1 was subjected to UV radiation and samples were taken at different doses (20 000 - 100 000 kJ/m^2) and analysed by IR-microscopy. Complementary SEC measurements were performed to analyse changes to the MMD.

4.2.2.1 IR-microscopy

4.2.2.1.1 Spatial distribution of Irganox 1010

The spatial distribution of Irganox 1010 in the exposed and unexposed side over the pipe wall of B_1 was determined as described above (see section 4.2.1.1.1). However since the major differences were in the outer pipe wall, Figure 49a and 49b show the concentration profiles in the outer of the pipe surface (0.8 mm) for the side exposed and unexposed to the radiation respectively, and Figure 49c and 49d the average values over the outer pipe surface for the side unexposed and exposed to the UV radiation respectively.

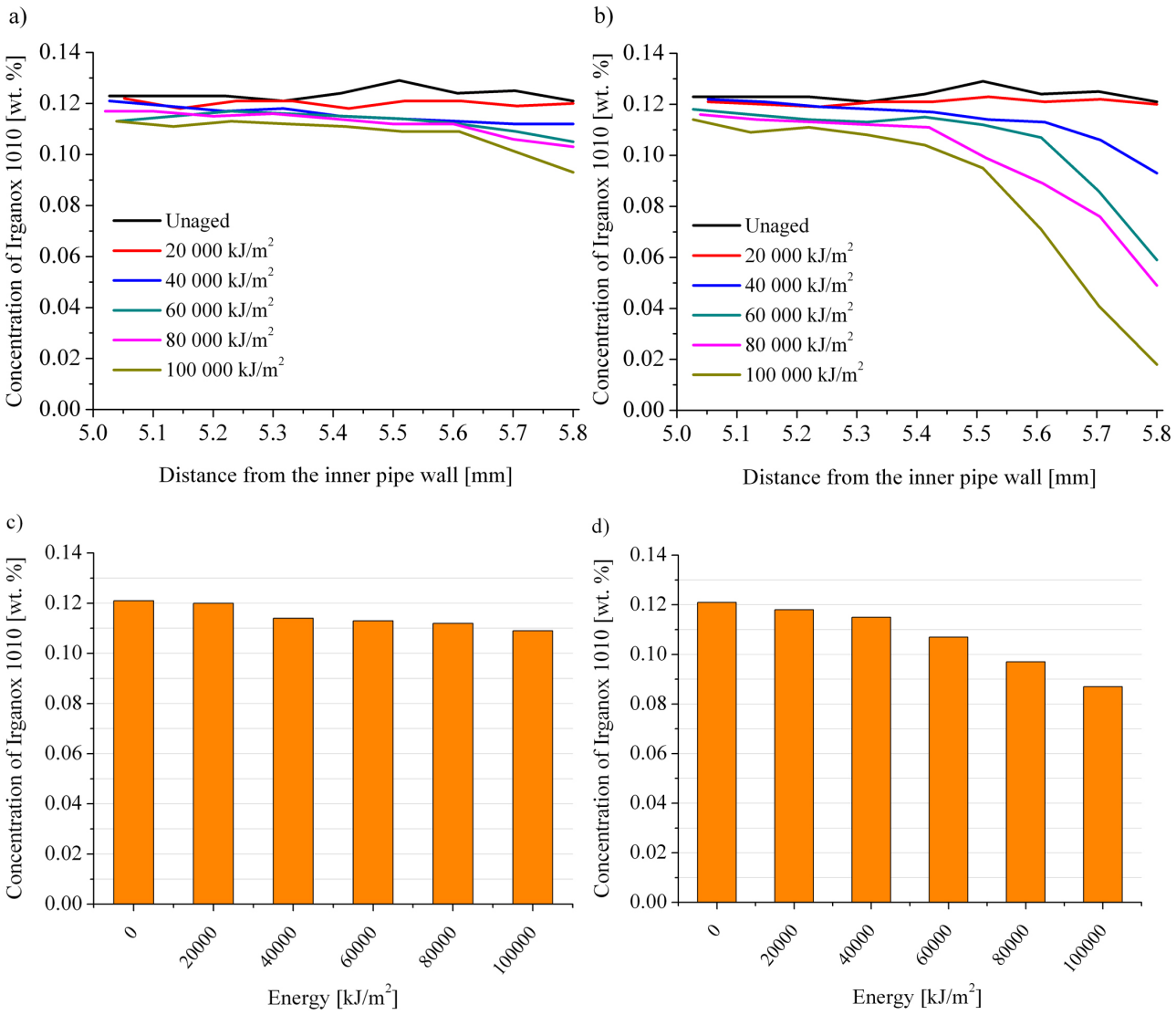

Figure 49: Spatial distribution of Irganox 1010 in the outer wall of B_1 a) exposed and b) unexposed to different doses of UV radiation and c) and d) the corresponding average values over the outer 0.8 mm of the pipe wall.

It is observed that there is some depletion of Irganox 1010 in the unexposed side especially for higher values of energy (e.g. 100 000 kJ/m^2). On the other side, the exposed side, as expected, is far more affected by the loss of stabiliser and the depletion reaches to a depth of 0.4 mm. The correlation between the radiation dose and the averaged relative content of Irganox 1010 over the outer 0.4 mm of the pipe wall is shown in Figure 50.

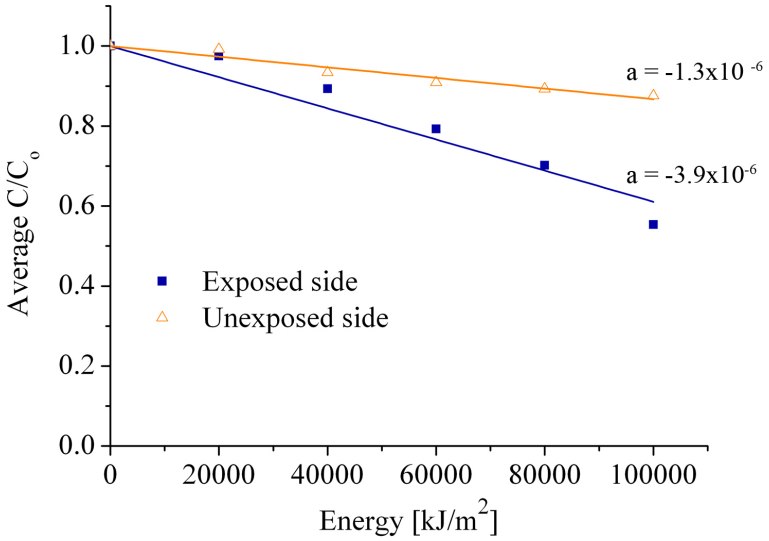

Figure 50: Correlation between the averaged relative content of Irganox 1010 and the UV dose in the outer 0.4 mm of B_1 for the unexposed and exposed side.

An almost linear correlation exists between the content of Irganox 1010 and the radiation dose for both, the exposed and the unexposed side. The slope is significantly higher for the side exposed to radiation than for the unexposed one. These results confirm again the assumption that photochemical reactions are responsible for the loss of stabiliser.

4.2.2.1.2 Degradation products

A $_{1709\ cm\text{-}1}$ was evaluated as previously (section 4.2.1.1.2) described for different doses of UV radiation. An overlay of the intensity profile of A $_{1709\ cm\text{-}1}$ for the unaged B_1 and after exposure to a UV dose of 100 000 kJ/m^2 is shown in Figure 51.

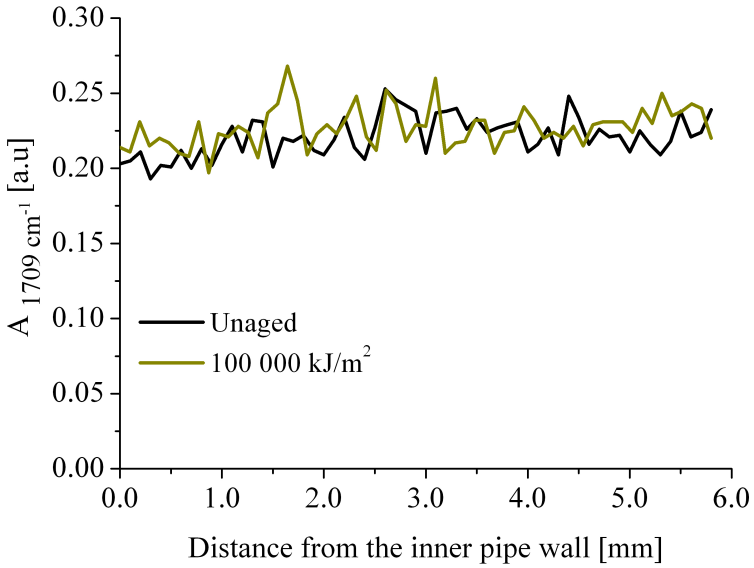

Figure 51: Overlay of A $_{1709\ cm\text{-}1}$ for the unaged B_1 and the side exposed to a UV radiation dose of 100 000 kJ/m^2.

An initial intensity of A $_{1709\ cm\text{-}1}$ can be observed for the unaged B_1 due to the presence of *Yellow 181*. However it can be recognised that no additional carbonyl functionalities are formed during the UV exposure.

A $_{908\ cm\text{-}1}$ (Figure 52a and b) and A $_{966\ cm\text{-}1}$ (Figure 52c and d) were profiled for the unexposed and exposed side as well.

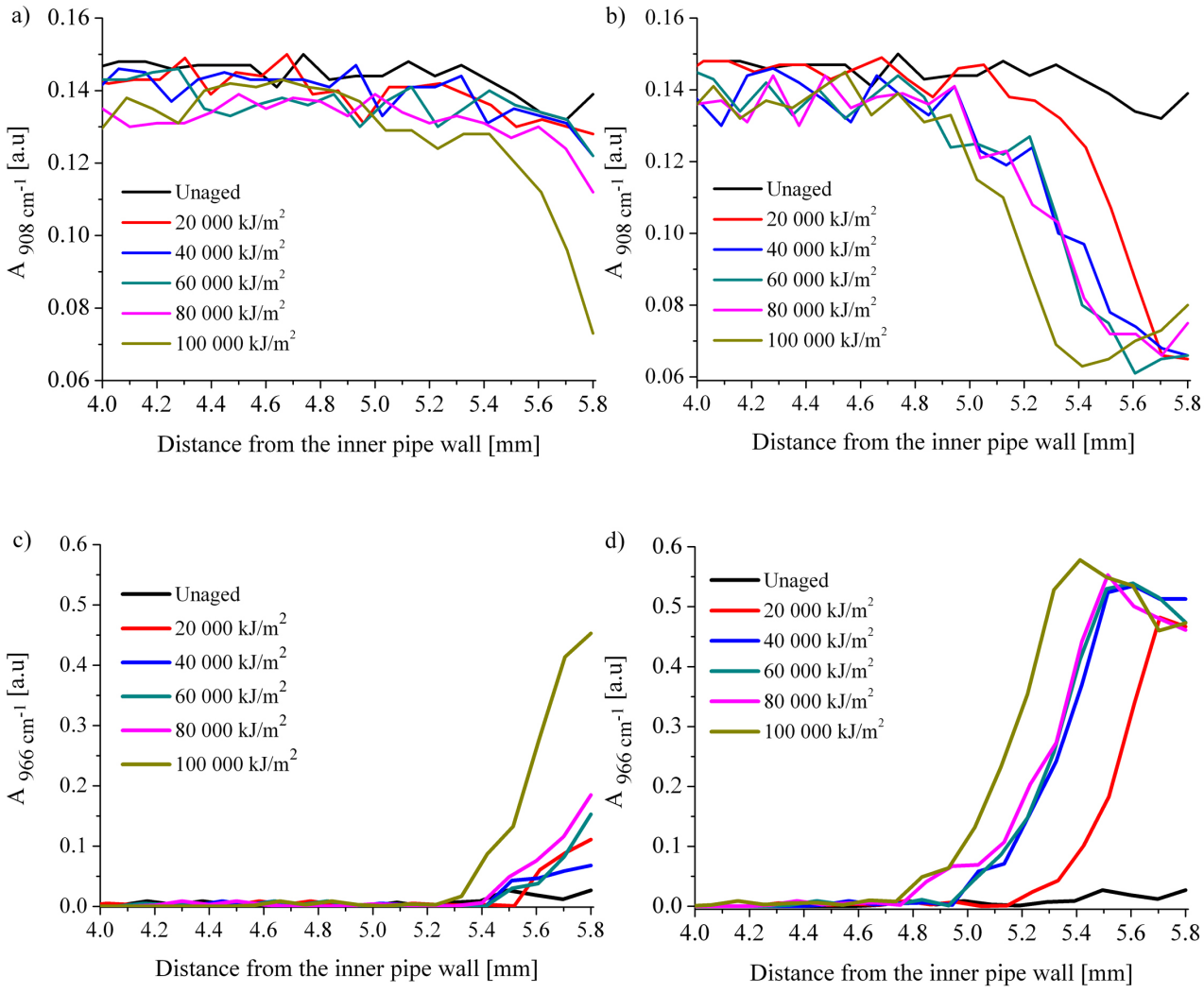

Figure 52: A $_{908\ cm\text{-}1}$ at the outer surface of the pipe wall on the side a) unexposed and b) exposed to different doses of UV radiation and A $_{966\ cm\text{-}1}$ at the outer surface on the side c) unexposed and d) exposed to UV radiation.

The content of vinyl groups decreases with prolonged UV exposure while *trans*-vinylene groups are formed. Additionally, the concentration profile of the *trans*-vinylene group passes a maximum at a certain depth, and then decreases towards the surface. With increasing dose of UV radiation the onset of the profile as well as the maximum is located deeper in the pipe wall. It may be assumed that the decrease of the *trans*-vinylene content towards the wall surface is due to secondary reactions like oxidation or crosslinking.

HPLC analysis showed that during ageing the phosphite is degraded to the corresponding phosphate (section 4.2.1.2). Irgafos 168 has an absorption band ($\nu_{asym\ P(-O-)3}$) at 849 cm^{-1} and upon degradation to the phosphate an absorption band ($\nu_{asym\ \ O=P(-O-)3}$) at 964 cm^{-1} appears. Unfortunately, the latter overlaps with the absorption band of the *trans*-vinylene groups at 966 cm^{-1} and thus the observed $A_{966\ cm\text{-}1}$ is the sum of the contributions of $A_{\nu\ asym\ \ O=P(-O-)3)}$ and $A_{\nu\ RCH=CHR}$. Despite this overlapping the vibration ($\nu_{asym\ P(-O-)3}$) of the phosphite at 849 cm^{-1} [228,229] can be used to determine quantitatively the content of phosphite. $A_{849\ cm\text{-}1}$ was calculated in an analogous manner, using a fixed two point baseline with the integration limits as shown in Figure 53.

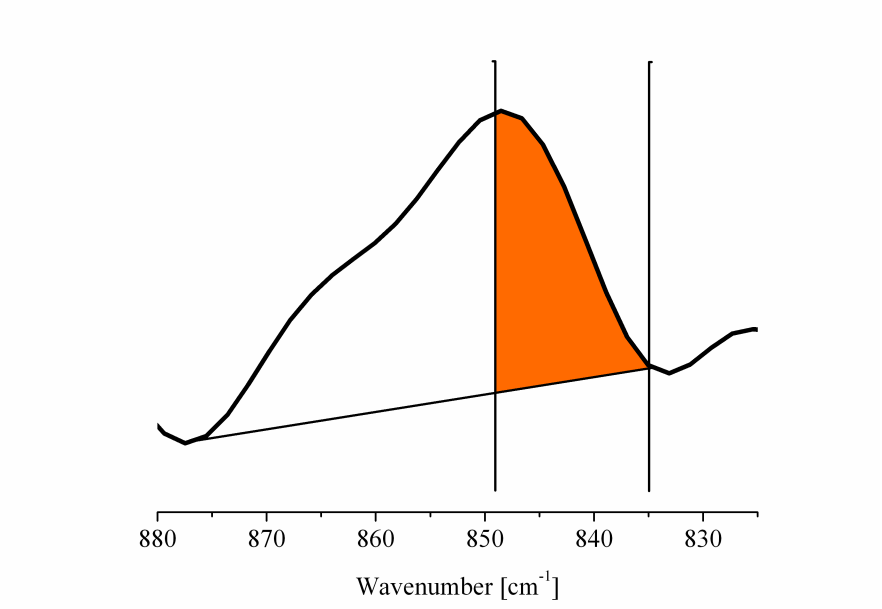

Figure 53: Integration limits of the band at 849 cm^{-1}.

The profile of $A_{849\ cm\text{-}1}$ at the outer wall surface for the unexposed and exposed side is shown in Figure 54.

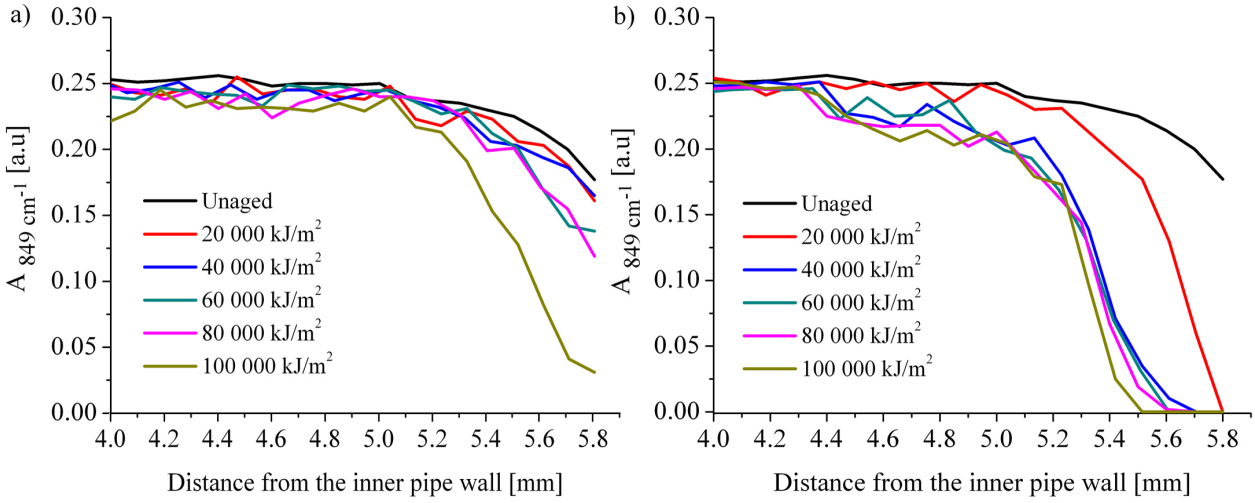

Figure 54: A $_{849\ cm\text{-}1}$ at the outer surface of the pipe on the side a) unexposed and b) exposed to different UV radiation doses.

A decrease of A $_{849\ cm\text{-}1}$ in the outer pipe wall can be observed in both sides after ageing, being however more pronounced for the exposed side than for the unexposed one. These results reveal that UV radiation plays an important role in the oxidation of the phosphite and simultaneously confirm the HPLC analyses.

As shown in Table 8 the content of Irgafos 168 decreases upon ageing in the same extent as that of the phosphate increases, and the total molar concentration of both components is equivalent to that of the original Irgafos 168 content. Considering this fact, and the fact that the extinction coefficient of both bands ($\nu_{asym\ P(\text{-}O\text{-})3}$ and $\nu_{asym\ O=P(\text{-}O\text{-})3}$) is approximately identical, as was shown by Karstang *et al.* [123], the loss in A $_{849\ cm\text{-}1}$ corresponds to the gain in A $_{966cm\text{-}1}$ of the $\nu_{asym\ O=P(\text{-}O\text{-})3}$.

Thus the profile of A $_{966\ cm\text{-}1}$ caused by $\nu_{asym\ O=P(\text{-}O\text{-})3}$ (A $_{966cm\text{-}1,\ phosphate}$) at the outer wall surface can be calculated by subtracting the values from the unaged sample from those of the aged samples (Figure 55).

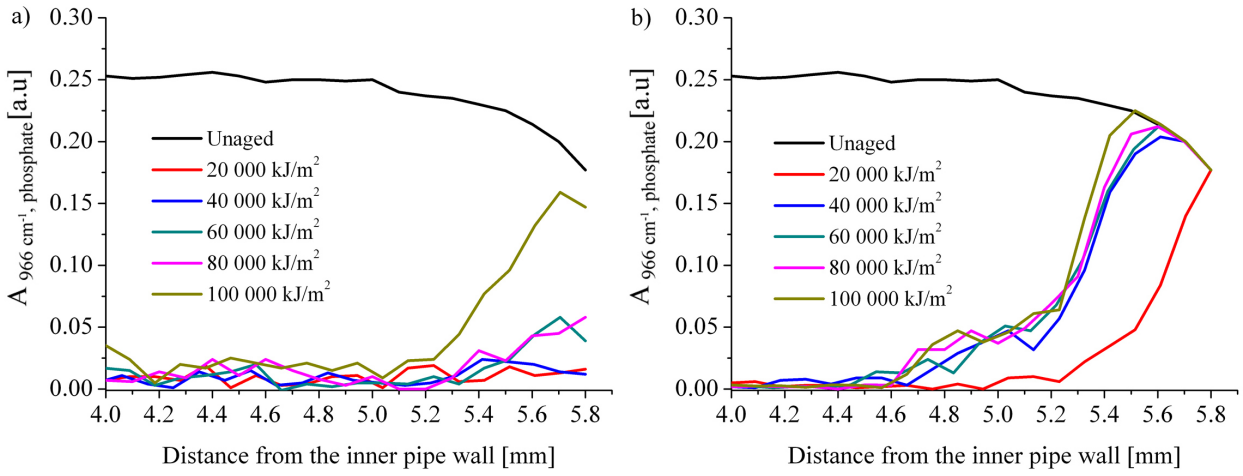

Figure 55: A $_{966\ cm\text{-}1,\ phosphate}$ at the outer surface of the pipe on the side a) unexposed and b) exposed to different UV radiation doses.

As expected an increase of A $_{966\ cm\text{-}1,\ phosphate}$ in the outer pipe wall can be observed in both sides after ageing as a result of the oxidation of the phosphite. As the contribution of the phosphate to A $_{966cm\text{-}1}$ has now been singled out, the contribution of the *trans*-vinylene groups to the absorption at 966 cm^{-1} can also be calculated (A $_{966\ cm\text{-}1,\ \textit{trans-vinylene}}$). Therefore the values of A $_{966\ cm\text{-}1,}$ were subtracted from the total A $_{966\ cm\text{-}1}$ calculated in Figure 52. The thus calculated portion of the absorption at 966 cm^{-1} due to the *trans*-vinylene band (A $_{966cm\text{-}1,\ \textit{trans-vinylene}}$) at the outer surface on the unexposed and exposed side to the different UV radiation doses is shown in Figure 56.

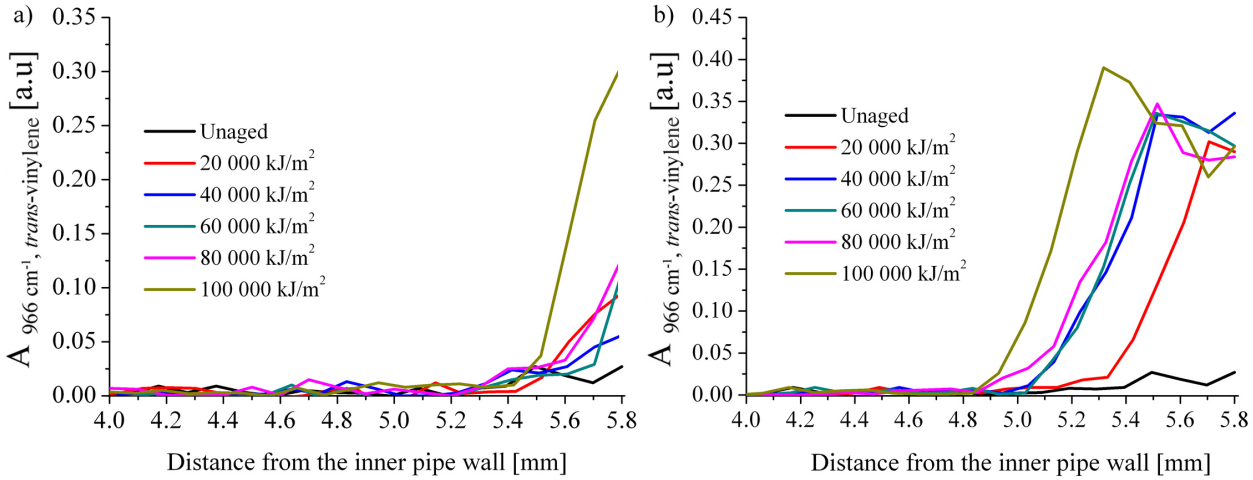

Figure 56: A $_{966cm-1,\ trans-vinylene}$ at the outer surface of the pipe wall on the side a) unexposed and b) exposed to different UV radiation doses.

In order to establish a correlation between the dose of UV radiation and changes in the content of vinyl- and *trans*-vinylene groups, the relative intensity of the bands at 908 cm^{-1} and 966 cm^{-1} respectively averaged over the pipe wall is shown in Figure 57.

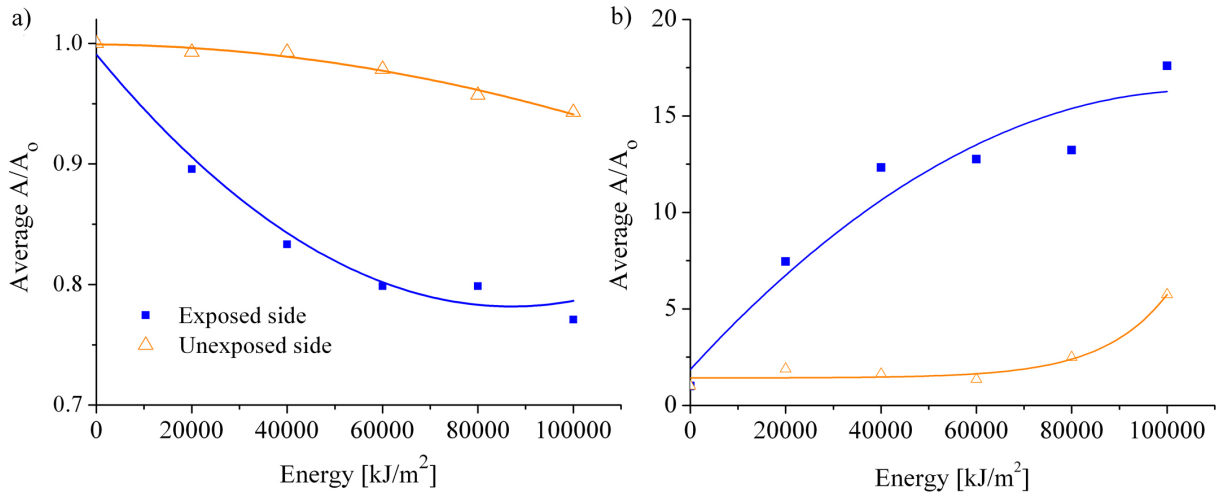

Figure 57: Correlation between the dose of UV radiation and a) A $_{908\ cm-1}$ and b) A $_{966cm-1,\ trans-vinylene}$ averaged over the outer pipe surface for the exposed and unexposed side.

The content of terminal vinyl unsaturations decreases with the dose of UV radiation which may be due to either oxidation or crosslinking (Figure 57a). Since no increase in the content of carbonylic oxidation products at higher radiation was observed (see Figure 51) it may be concluded that crosslinking occurs preferentially. For the *trans*-vinylene double bonds initially an almost linear increase with the UV radiation dose takes place on the exposed side that tapers out after a certain dose of UV radiation. On the unexposed side the increase is exponential after an initial lag phase (Figure 57b). Similar observations were found for γ-irradiation of PE films where it has been shown that the disappearance of vinyl unsaturations originally present in PE follows a first-order law and that *trans*-vinylene unsaturations are formed proportional to the UV radiation dose [225].

4.2.2.2 Size Exclusion Chromatography (SEC)

To evaluate the effects of the different doses of UV radiation on the MMD of the PE pipes, thin slices (200 μm) of B_1 were peeled off from the outer surface from the exposed and unexposed side and analysed by SEC. The number and weight averages (M_n and M_w) as well as the dispersity (D) are summarised in Table 9.

Table 9: M_w and M_n and dispersity, D, of thin slices (200 μm) peeled off from the outer surface of B_1 after exposure to different UV radiation doses.

Sample	Side	M_w [g/mol]	M_n [g/mol]	D
20 000 kJ/m^2	Exposed	590.000	35.600	16.6
	Unexposed	597.000	35.800	16.7
40 000 kJ/m^2	Exposed	620.000	35.900	17.3
	Unexposed	629.000	36.800	17.1
60 000 kJ/m^2	Exposed	548.000	34.700	15.5
	Unexposed	598.000	34.600	17.3
80 000 kJ/m^2	Exposed	585.000	35.800	16.3
	Unexposed	576.000	36.200	15.9
100 000 kJ/m^2	Exposed	610.000	35.800	17.5
	Unexposed	586.000	34.800	17.5

It is observed that after exposure to UV radiation no changes in the average MM are visible. These data prove that within the reproducibility limits of SEC even after prolonged exposure to UV radiation no significant scission of polymer chains occurs.

However in the previous section (4.3.1.2) a decrease of the terminal vinyl unsaturations with the dose of UV radiation was observed and since no formation of carbonyl groups by IR-microscopy was observed it was concluded that crosslinking preferentially occurs. In other words an increase of the MM would have been expected. This contradiction can be explained by the fact that either the gel is filtered off prior to the SEC analysis by the guard column or its amount is not significant and the resulting changes to the MM are within the limitations of the SEC measurement.

4.2.3 Characterisation of the artificially aged B_2

It is common practice to protect polymers against UV radiation by adding HALS and UV-absorbers. The aim of this section is to show how a HALS interacts with the AO, Irganox 1010, and how this affects the depletion of the latter. Therefore B_2 which contains Tinuvin 770 (see section 4.1.1) was exposed to different doses of UV radiation and analysed by IR-microscopy and the results compared to B_1. Complementary HPLC measurements were performed in parallel.

4.2.3.1 IR-microscopy

4.2.3.1.1 Distribution of Irganox 1010 and Tinuvin 770

Due to the overlapping of the carbonyl vibrations from Tinuvin 770, Irganox 1010 and the pigment *Yellow 13* a quantification of Irganox 1010 is impossible using the previous calibration curve. However the cumulated distribution of the stabilisers over the pipe wall on the exposed side was determined by calculating $A_{1739\ cm\text{-}1}$ using the same integration limits of section 4.1.2.2. The results are shown in Figure 58.

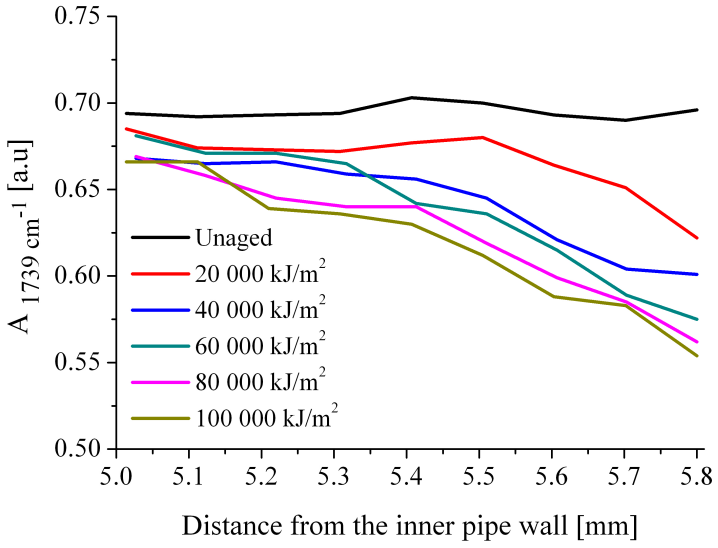

Figure 58: Profile of $A_{1739\ cm\text{-}1}$ in the wall of B_2 after exposure to different doses of UV radiation.

A decrease in the intensity of $A_{1739\ cm-1}$ towards the outer surface of the pipe can be recognised as the dose of UV radiation increases. Assuming that the pigment is not extracted, this decrease is due to the changes of the concentration of both additives (Tinuvin 770 and Irganox 1010) after exposure to different UV radiation. Since it is not possible to distinguish and quantify the two additives individually HPLC was used as complementary technique.

4.2.3.2 High performance liquid chromatography (HPLC)

To quantify the amount of the individual stabilisers present in B_2, thin slices (200 µm) of the outer pipe surface exposed and unexposed to a UV radiation dose of 100 000 kJ/m^2 were peeled off and HPLC analyses were performed. The results are summarised in Table 10.

Table 10: Comparison of stabiliser content in the outer 200 µm of the unaged B_2 and in the exposed und unexposed side of the pipe after irradiated with a UV dose of 100 000 kJ/m^2.

Sample	**Irganox 1010 [wt. %]**	**Secondary AO (Irgafos 168 as phosphite and phosphate) [wt. %]**	**Σ Irgafos 168 as phosphite and phospahte [wt. %]**	**UV protector [wt. %]**	
				Tinuvin 770	Tinuvin 327
Unaged	0.130	0.115 phosphite 0.024 phosphate	0.139	0.069	0.070
Exposed side	0.007	0.005 phosphite 0.115 phosphate	0.120	0.036	0.063
Unexposed side	0.089	0.070 phosphite 0.074 phosphate	0.144	0.044	0.068

Even in the presence of the UV protectors the depletion of Irganox 1010 and the oxidation of Irgafos 168 occur, similarly to what was found for B_1 (see Table 7 and 8) in the exposed side. Again, in the unexposed side there is a small loss of the stabilisers as previously observed due to the range of UV penetration, however these values are far smaller than for the exposed side. Additionally, Tinuvin 770 is lost as a result of the UV exposure but to a lower extent than for Irganox 1010. This loss may be due to evaporation or sublimation of the stabiliser from the pipe surface due to its low MM and due to warming up of the surface as a result of the irradiation. For the case of Tinuvin 327 there is no loss of the stabiliser as a result of the UV exposure. An interesting fact is that the addition of a UV protector neither affects the loss of Irganox 1010 as a result of photochemical degradation nor the oxidation of Irgafos 168. This may be either a result of the relatively low concentration of the Tinuvin 327 or due to the fact that the degradation of the stabilisers occurs by another mechanism, i.e. not via peroxy-radicals.

4.2.4 Characterisation of the naturally and artificially aged F

CB is widely used as a UV absorber for polyolefins [93]. But since its surface may contain a variety of functional groups such as carboxyl, phenolic hydroxyl and quinone it can interact physically and chemically with other stabilisers [230] as described in 2.4.3.2 and influence their activity. There is a wide variety of commercial CBs based on different surface chemistry and aggregate parameters. Their effectiveness as UV absorber as well as their interactions with light stabilisers and AO is depending on all these factors [231,232]. The aim of this section is to show, how the addition of CB affects the loss of the Irganox 1010, and if it can be counteracted in the same way as for B_1. Therefore, F was exposed to different weathering scenarios similar to B_1 (section 4.2.1) and samples taken after different exposure were analysed by IR-microscopy.

4.2.4.1 IR-microscopy

4.2.4.1.1 Spatial distribution of Irganox 1010

Since CB absorbs IR light, the signal-to-noise ratio in the IR measurements had to be enhanced [233] by increasing the number of scans from 100 up to 2000 *per* spectrum. In order to optimise the measurements, the focus was set on the outer 1.0 mm of the exposed pipe surface, where the major differences are expected. The concentration profiles of Irganox 1010 in the outer 1.0 mm of the side exposed to the higher UV radiation doses are shown in Figure 59a and to the lower UV radiation doses in Figure 59b.

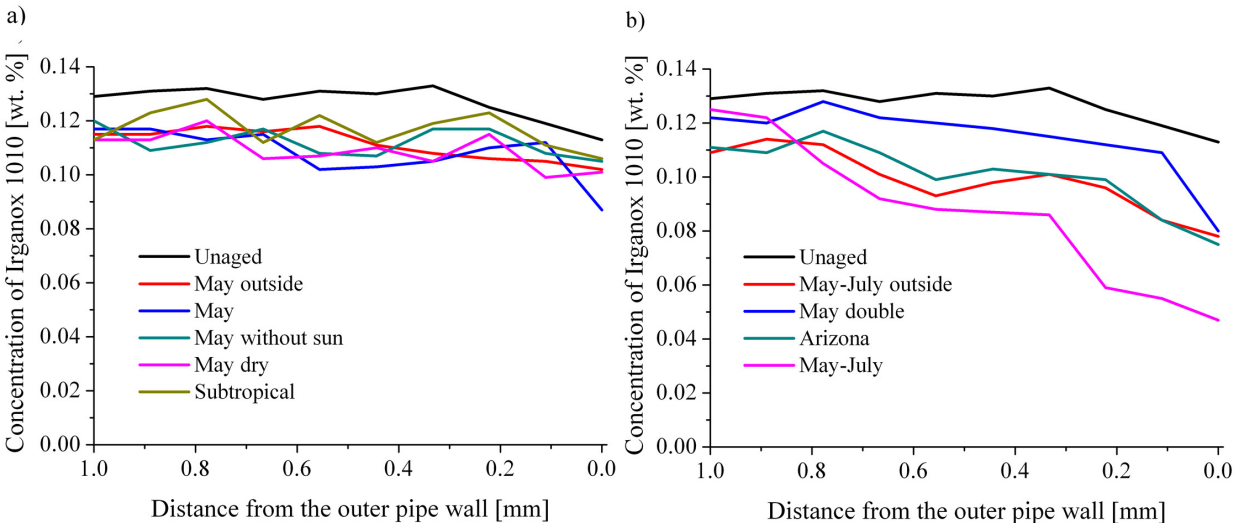

Figure 59: Concentration profiles of Irganox 1010 of the outer pipe wall of F on the side exposed to a) higher and b) lower UV-radiation doses of the different weathering conditions.

A loss of AO in the outer part of the pipe wall after natural and artificial weathering is observed. The depletion of the stabiliser is higher for the samples exposed to the higher UV doses ($F_{\mathbf{May\text{-}July}}$, $F_{\mathbf{May\text{-}July\ outside}}$ and $F_{\mathbf{Arizona}}$) similarly with B_1 (section 4.2.1.1.1).

The only difference between $F_{\mathbf{May\text{-}July}}$ and $F_{\mathbf{May\text{-}July\ outside}}$ is that $F_{\mathbf{May\text{-}July\ outside}}$ was exposed to natural and $F_{\mathbf{May\text{-}July}}$ to artificial weathering, once again showing that the depletion of the

stabiliser is higher for the artificially weathered sample than for the natural one, indicating that CB has no effect regarding the higher surface temperature in artificial weathering.
The loss of Irganox 1010 in F is lower than in B_1 proving that CB reduces the effect of UV radiation. This might be due to the UV-absorbing effect of CB and additionally be caused by physicochemical interactions between the AO and CB. Another observation is that for the humid environment without irradiation, $F_{\mathbf{Subtropical}}$, no significant changes in the concentration of Irganox 1010 appear. These results suggest that CB has no effect on the depletion of Irganox 1010 in a very humid environment.

4.2.5 Characterisation of F aged with different doses of UV radiation

In order to correlate the dose of UV radiation with the depletion of Irganox 1010 in the presence of CB, F was subjected to different doses of UV radiation (20 000 - 100 000 kJ/m^2) and the stabiliser distribution close to the surface was determined by IR-microscopy. Complementary HPLC and OIT measurements were performed.

4.2.5.1 IR-microscopy

4.2.5.1.1 Spatial concentration of Irganox 1010

The concentration profiles of Irganox 1010 in the outer surface of the pipe wall for the exposed side are shown in Figure 33a and the correlation between the dose of UV radiation and the amount of stabiliser averaged over the outer 0.4 mm of the pipe wall is shown in Figure 60b.

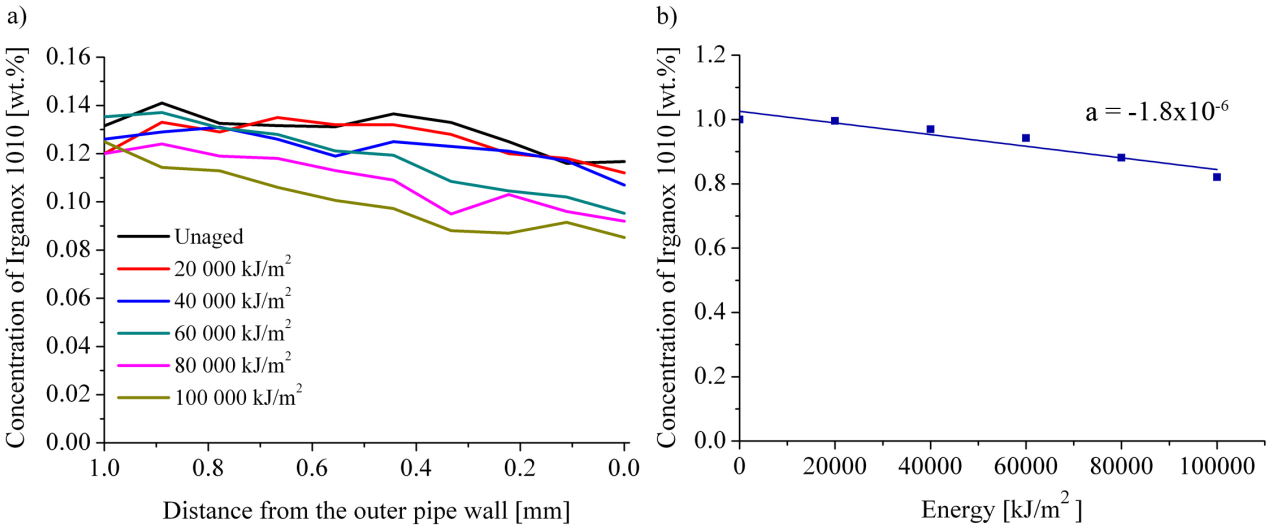

Figure 60: a) Concentration profile of Irganox 1010 in the outer surface (1.0 mm) of F on the exposed side to different UV radiation doses and b) correlation between the UV radiation dose and the stabiliser content in the outer surface (0.4 mm) of the pipe wall.

A relative decrease in the concentration of Irganox 1010 in the outer pipe wall by approximately 10 % is detected after exposure to UV radiation. This is significantly less compared to the loss of Irganox 1010 found for B_1 (approximately 30 %) (see Figure 49). These data follow the same trend as observed for naturally aged pipes (Figure 59), i.e., the presence of CB significantly prevents the loss of Irganox 1010. Two explanations are possible: *i)* that most of the UV light is absorbed by the CB and the photochemical degradation of Irganox 1010 is reduced and *ii)* that there is a physical adsorption of the AO by the CB. Some authors have pointed out that the adsorption of Irganox 1010 by CB is due mainly to the ester functionality present in the molecular structure which can interact with acidic sites of the CB surface such as carboxylic and phenolic groups [234-236]. An interaction via hydrogen bonding of the phenolic group of Irganox 1010 could be also possible. However, the latter interaction would be weak due to the steric hinderance by the tertiary butyl groups [41,237-239]. To better understand this behaviour HPLC analyses were performed.

4.2.5.2 High performance liquid chromatography (HPLC)

Thin slices of 200 µm thickness were peeled off from the outer surface of F after exposure to different doses of UV radiation and the Irganox 1010 content was determined by extraction and successive HPLC. Figure 61 shows an example of the HPLC chromatogram and the results are summarised in Table 11.

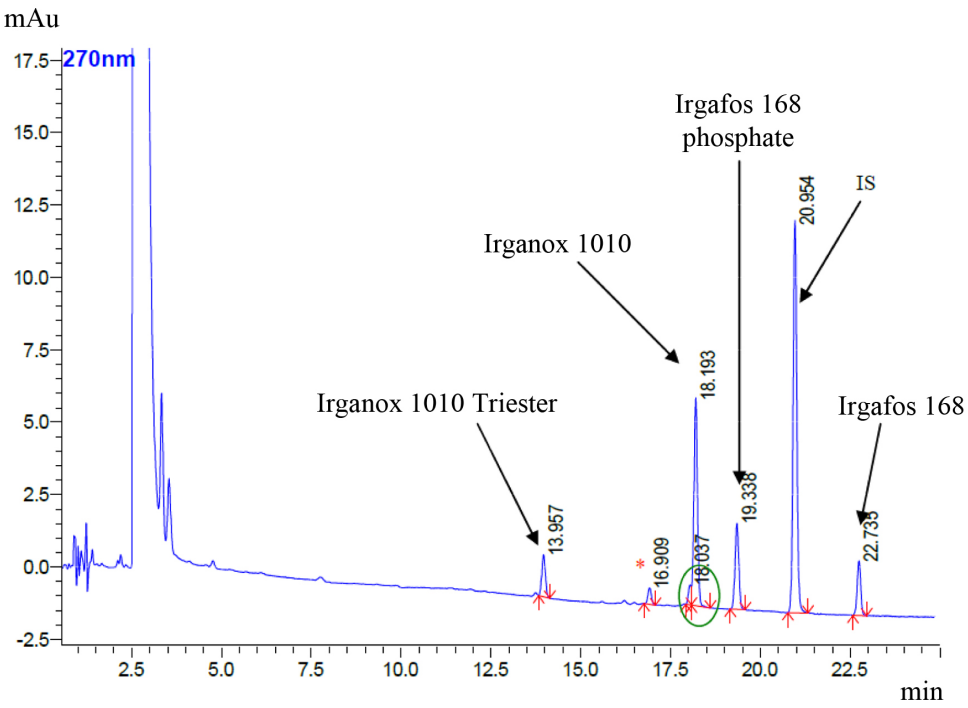

Figure 61: Example of a chromatogram of the extract of F exposed to a UV radiation of 100 000 kJ/m^2.

Table 11: Comparison between the Irganox 1010 content obtained from extraction/HPLC in the peeled outer 200 µm (exposed side) and that from averaging the Irganox 1010 content as obtained by IR-microscopy (200 µm from the surface, exposed side) for the unaged F and two representative UV radiation doses.

Sample	Extraction / HPLC		IR-microscopy
	Irganox 1010 [wt.%]	**Irganox 1010 Triester [wt. %]**	**Irganox 1010 Σ Irganox 1010 and Triester [wt. %]**
Unaged	0.123	-	0.125
60 000 kJ/m^2	0.085	0.026	0.119
100 000 kJ/m^2	0.088	0.024	0.103

It is interesting to observe the presence of the triester of Irganox 1010 in the sample. IR-microscopy is not able to distinguish between Irganox 1010 and its triester and thus the IR band is a sum of the contributions of both. Considering the sum of Irganox 1010 and the triester content from extraction/HPLC, a decrease of 10 % in the relative concentration of Irganox 1010 in the outer pipe wall is observed which is in agreement with the results from IR-microscopy. The presence of the triester in F and its absence in B_1 (section 4.2.1.2), suggests that CB, apart from being an excellent UV absorber, can slow down the loss of the low molecular cleavage products by physicochemical diffusion.

A plausible reaction mechanism for the Irganox 1010 degradation, triggered by UV radiation, can be provided by a Norrish type I reaction, i.e., the cleavage of the bond between the carbonyl-C and the α-carbon atom. This can subsequently lead to an unsaturated *di-tert* butyl phenol derivative [240]. The proposed mechanism is shown in Figure 62.

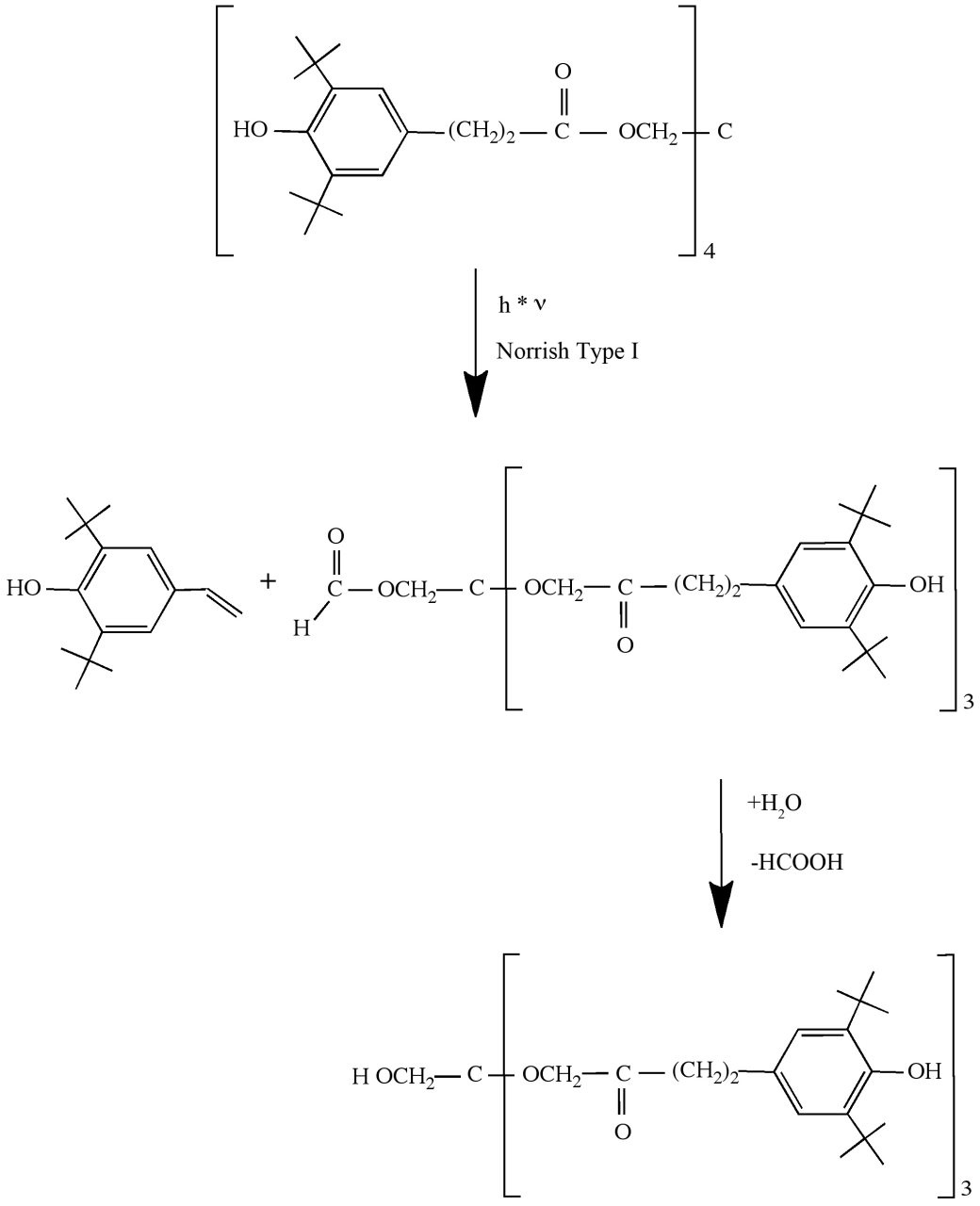

Figure 62: Proposed mechanism for the photodegradation of Irganox 1010.

Due to its low MM, the para-vinylphenol derivative is able to diffuse rapidly out of the polymer and cannot be detected in the chromatographic analysis.

Similar to B_1 the presence of the processing stabiliser (Irgafos 168 as phosphite and phosphate) was equally assessed by means of extraction/HPLC and the results are shown in Table 12.

Table 12: Content of processing stabiliser (Irgafos 168 as phosphite and phosphate) in the peeled outer 200 µm (exposed side) for the unaged F and two representative UV radiation doses by extraction/HPLC.

Sample	Extraction / HPLC	
	Secondary AO (Irgafos 168 as phosphite and phosphate) [wt. %]	**Σ Irgafos 168 as phosphite and phosphate [wt. %]**
Unaged	0.081 phosphite 0.031 phosphate	0.112
60 000 kJ/m^2	0.037 phosphite 0.065 phosphate	0.102
100 000 kJ/m^2	0.030 phosphite 0.069 phosphate	0.099

Comparing these results with those from B_1 (see Table 8) it is interesting to observe that the CB retards the degradation of the Irgafos 168. Some authors have studied the adsorption behaviour of phosphite stabilisers on CB by flow micro-calorimetry (FMC) and FTIR and showed that the phosphite and phenyl groups form strong interactions with CB [241]. The authors compared the behaviour of two phosphite stabilisers, Irgafos 168 and Alkanox TNPP, with the difference being that Alkanox TNPP has a more sterically exposed disposition of the phosphite group compared to Irgafos 168. Within these, the Alkanox TNPP has a greater adsorption on the CB, i.e. lower obstruction of the phosphite groups by alkyl groups enables better interaction with the CB surface.

4.2.5.3 Oxidative induction time (OIT)

OIT measurements were carried out on thin slices (200 µm) from the exposed outer pipe surface. The results are shown in Figure 63.

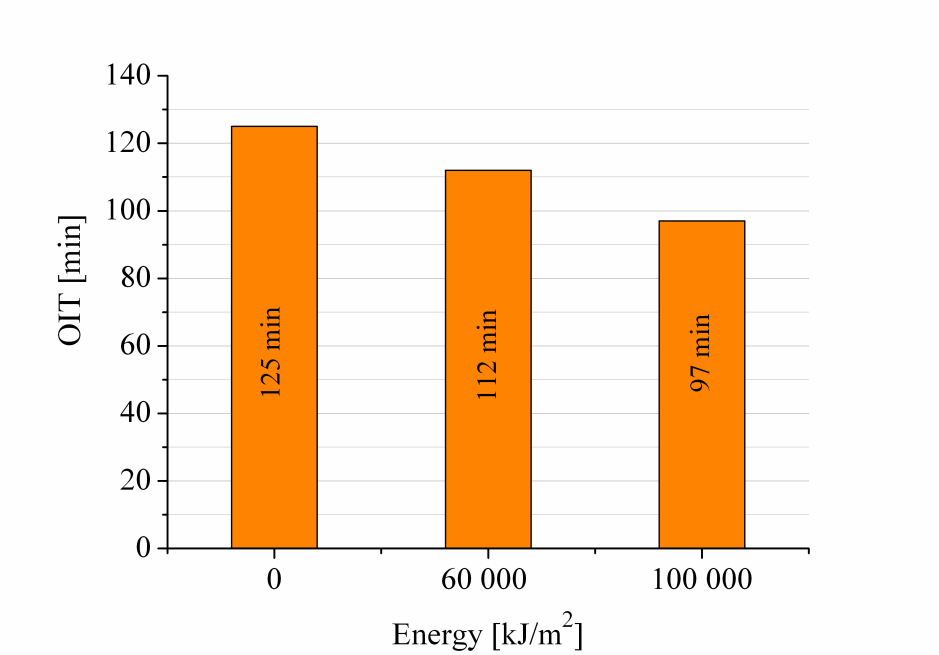

Figure 63: OIT measurements in the peeled outer 200 µm (exposed side) of the unaged F and two representative UV radiation dose.

The OIT values decrease with increasing radiation dose, thereby confirming the results from both IR-microscopy and HPLC analysis. In comparison with B_1 ($B_{\mathbf{1May\text{-}July}}$ exposed to 100 000 kJ/m^2, Figure 48) an increase of the OIT from 72 to 96 minutes can be observed for the corresponding sample. This means that after prolonged exposure to UV radiation, the decrease in the content of Irganox 1010 is lower in the presence of CB. Since by HPLC (section 4.2.5.2) a decrease in the concentration of of Irganox 1010 and its triester was found it can be concluded that both species have a stabilising effect. This confirms the observation of various authors [242] that hindered phenolic AO as a consequence of their interceding in the protection of the polymer against oxidation undergo chemical transformations and the transformation products can also be effective as polymer stabiliser.

To confirm the stabiliser effectiveness of such products Klemchuck *et. al* [243] stabilised PP and HDPE with Irganox 1010 and its triester and diester, exposed the samples to 150 ° C and 120 °C and determined the time to embrittlement. It was shown that the embrittlement time was almost equal for the samples stabilised with Irganox 1010 and those stabilised with the tri- and diester.

5. Conclusions

Plastic pipes are often exposed to a range of environmental conditions which may lead to their degradation. The most important influence factors are UV radiation, humidity and temperature. These can cause leaching of long-term and light stabilisers and finally oxidation of the polymer.

In this study the main objective was to demonstrate how the elemental steps of the photooxidative degradation of PE pipes could be monitored by IR-microscopy. In detail the influence of UV radiation on the depletion of the phenolic long-term stabiliser, Irganox 1010, and how the depletion is affected by the presence of a light stabiliser and UV absorber. The oxidation of the polymer and consequently the morphological changes intrinsically associated were also studied. For this purpose, commercial HDPE pipes were stabilised with Irganox 1010 as primary stabiliser, Irgafos 168 as secondary stabiliser, Tinuvin 770 as light stabiliser, CB and Tinuvin 327 as UV absorber.

Since Irganox 1010 presents a characteristic carbonyl absorption $\nu_{C=O}$ at 1739 cm^{-1} which can be used for its quantitative determination, a calibration curve was constructed with PE standards of well-defined concentrations of Irganox 1010 and a linear correlation between the IR absorbance and the additive concentration was established.

To study the effect of UV radiation, humidity and temperature the pipe stabilised only with Irganox 1010 and Irgafos 168 was exposed to natural and artificial weathering.

A directly dependency of the loss of AO with the climate conditions was shown. It was visible a loss of the AO in the outer pipe wall after natural and artificial weathering in all samples pronouncedly on the side that was directly exposed to UV radiation.

Since there were no visible changes in the content of the AO for the samples exposed only to humidity and no UV radiation it could be concluded that both temperature and UV radiation played an important role in the AO loss and a correlation between the amount of UV radiation and the amount of stabiliser was found.

During photodegradation of PE, carbonyl functionalities as well *trans*-vinylene groups can be formed. It was found that no additional carbonyl functionalities were formed after exposure to the different climate scenarios but on the other hand *trans*-vinylene groups were formed as the pipe ages under all weathering conditions.

A decrease of the content of vinyl groups with prolonged UV exposure was also observed.

Regarding to morphological changes it could be concluded that UV radiation does not affect the crystallinity since no significant changes of the spectral crystallinity profile was observed as a result of weathering.

Complementary HPLC measurements on the outer pipe surface of the exposed side were performed to determine the content of Irganox 1010 and once again it was shown that the extent of AO depletion depends directly on the climate conditions especially the UV radiation. It was also observed by extraction/HPLC that the ratio of phosphite/phosphate decreases as a consequence of the exposure to UV radiation and the content of Irgafos 168 decreases upon ageing in the same extent as that of the phosphate increases, and the total molar concentration of both components is equivalent to the original Irgafos 168 (as phosphite and phosphate) content.

OIT measurements showed the major differences in the samples exposed to high UV radiation doses proving once more that UV radiation plays an important role in the depletion of the AO.

For exploiting in detail the correlation between the exposure to UV radiation and the loss of AO, the pipe stabilised only with Irganox 1010 and Irgafos 168 was subjected to different doses of UV radiation (20 000 - 100 000 kJ/m^2). A linear correlation between the loss of the AO and the radiation dose was found. The slope was significantly higher for the side exposed to radiation than for the unexposed one and rate constants were calculated for the first time.

The disappearance of vinyl unsaturations originally present in PE, as well the formation of *trans*-vinylene as unsaturated degradation product of PE could also be observed. Additionally, the concentration profile of the *trans*-vinylene group passes a maximum at a certain depth, and then decreases towards the surface. With increasing dose of UV radiation the onset of the profile as well as the maximum are located deeper in the pipe wall. It could be assumed that the decrease of the *trans*-vinylene content towards the wall surface is due to secondary reactions like oxidation or crosslinking.

Since the HPLC measurements revelead that during ageing the phosphite was degraded to the corresponding phosphate the absorbance that was expected to be only due to *trans*-vinylene was indeed the sum of the contributions of the absorbance of the phosphate and the *trans*-vinylene groups. Due to this fact a method was developed to determine the amount of

reacted phosphate during the oxidation of Irgafos 168 which made it possible to single out the distinguished contributions.

After singling out the contributions of the *trans*-vinylene a correlation between the dose of UV radiation and the formation of the vinyl groups was established. It was found that the content of terminal vinyl unsaturations decreases with the dose of UV radiation. Since there was no increase in the content of carbonylic oxidation products at higher radiation it could be concluded that crosslinking occurs preferentially.

For the *trans*-vinylene double bonds initially an almost linear increase with the UV radiation dose takes place on the exposed side that is less pronounced after a certain dose of UV radiation.

To evaluate the effects of the different UV radiation doses on the MMD, SEC measurements were performed and it was found that after prolonged exposure to UV radiation no significant scission of polymer chains occurs.

It is common practice to protect polymers against UV radiation by adding HALS and UV-absorbers. In this work was also purpose to show how the combination of the UV absorber Tinuvin 327 and the HALS Tinuvin 770 interacts with Irganox 1010, and how this affects his depletion.

Therefore the pipe containing Tinuvin 770 and Tinuvin 327, in addition to the Irganox 1010 and Irgafos 168, was exposed to different UV radiation doses (20 000 - 100 000 kJ/m^2) and the results compared to the pipe stabilised only with Irganox 1010 and Irgafos 168.

Due to the overlapping of the carbonyl vibrations from Tinuvin 770, Irganox 1010 and the pigment *Yellow 13* a quantification of Irganox 1010 was impossible using the calibration curve, however the cumulated distribution of the stabilisers over the pipe wall on the exposed side was determined.

A decrease in the intensity of the carbonyl absorbance towards the outer surface of the pipe was recognised with the increase of the dose of UV radiation. Assuming that the pigment was not extracted, the decrease was due to changes of the concentration of both additives (Tinuvin 770 and Irganox 1010) after exposure to different UV radiation. Since it was not possible to distinguish and quantify the two additives individually HPLC was used as complementary technique and it was shown that even in the presence of the UV protectors the depletion of Irganox 1010 and the degradation of Irgafos 168 occured, similarly to what was found for the pipe stabilised only with Irganox 1010 and Irgafos 168.

It could be concluded that the combination of UV absorber Tinuvin 327 and the hindered amine stabiliser Tinuvin 770 had no measurable effect on the loss of Irganox 1010.

However, interestingly results were showed by HPLC analysis where it was visible a loss of Tinuvin 770 as a result of the UV exposure but to a lower extent than Irganox 1010. For the case of Tinuvin 327 no loss was observed as a result of the UV exposure.

To study the influence of CB in the loss of the Irganox 1010 the pipe stabilised with Irganox 1010, Irgafos 168 and CB was exposed to different weathering scenarios similarly to the pipe stabilised only with Irganox 1010 and Irgafos 168.

A loss of the AO in the outer pipe wall after natural and artificial weathering in all samples on the side directly exposed to UV radiation was visible. However the loss was lower than the one found for the pipe stabilised only with Irganox 1010 and Irgafos 168.

It could be concluded that CB reduces the effect of UV radiation and slows down the depletion of Irganox 1010.

For exploiting in detail the correlation between the exposure to UV radiation and the loss of AO, the pipe stabilised with Irganox 1010, Irgafos 168 and CB was subjected to different doses of UV radiation (20 000 - 100 000 kJ/m^2). It was found that the relative decrease in the concentration of Irganox 1010 in the outer pipe wall was approximately 10 % after exposure to UV radiation, which was significantly less compared with the 30 % loss of Irganox 1010 found for the pipe stabilised without CB. Complementary HPLC measurements of the outer pipe surface of the exposed side were performed and the presence of the triester of Irganox 1010 in the sample was observed.

The presence of the triester and its absence in pipe stabilised without CB, suggested that CB, apart from being an excellent UV absorber, could also slow the loss of the low molecular cleavage products by physicochemical diffusion.

Based on these results a mechanism for the photodegradation of Irganox 1010 in the presence of CB triggered by Norrish cleavage could be proposed.

Another interesting observation was that the presence of CB reduced also the degradation of the Irgafos 168.

An increase of the OIT could be observed for the sample stabilised with CB compared with the one without CB. It could be concluded that after prolonged exposure to UV radiation, the decrease in the content of Irganox 1010 was lower in the presence of CB.

Since by HPLC it was found a decrease of the concentration of Irganox 1010 and the correspondent triester it could be concluded that the triester has also a stabilisation effect.
These findings can be considered as a significant contribution for the manufacturers optimise the stabiliser recipe concerning the final application and thus to prolong their life time.
The development of an IR-microscopic method can be very useful for manufacturers since they can use it as part of their quality assurance and for the material development, as well they are able to create meaningful analysis of the stabilisation conditions of PE pipes. The time and cost of sample preparation compared with the routine methods (extraction and abrasion of layers) is greatly reduced and since with IR-microscopy it is possible to quantify AO as well analyse the spatial structure it is not necessary to spend time with other techniques.

Recommendations for future work

The current study has opened several potential fields of study. The current investigation can be extended to other type of pipes and additives. It would be interesting to compare the behaviour of different stabilised systems.

PE for pipe applications is rated by it's pressure resistance. However the large majority of failures occur as a result of thermo-oxidative ageing. Consequently it would be an important challenge to study the elemental processes which lead to the thermo-oxidative failure of PE and it is great stimulus to evaluate the potential of IR-microscopy for this purpose.

6. References

1. L. Hubert, L. David, R. Séguéla, G. Vigier, D. Degoulet, Y. Germain, *Polymer*, 42 (2001) 8425-8434

2. J. Lacoste, D. J. Carwon, *J. Polym. Sci.: Part A: Polym. Chem.,* 30 (1992) 493-500

3. R. Dhib, N. Al-Nidawy, *Chem. Eng. Sci.,* 57 (2002) 2735-2746

4. H. Knuuttila, A. Lehtinen, A. Nummila-Pakarinen, *Adv. Polym. Sci.,* 169 (2004) 13-27

5. J. P. Hogan, *J. Polym. Sci.*: A-1, 8 (1970) 2637-2652

6. D. Singh, R. P. Merrill, *Macromolecules*, 4 (1971) 599-604

7. N. Platzer, *Ind. Eng. Chem. Prod. Res. Dev.,* 22 (1983) 158-160

8. J. B. P. Soares, J. D. Kim, G. L. Rempel, *Ind. Eng. Chem. Res.,* 36 (1997) 1144-1150

9. H. G. Alt, *J. Chem. Soc*., *Dalton Trans*., (1999) 1703-1709

10. A. Malmberg, J. Liimatta, A. Lehtinen, B. Löfgren**,** *Macromolecules,* 32 (1999) 6687-6696

11. K. M. Drummond, J. L. Hopewell, R. A. Shanks, *J. Appl. Polym. Sci.,* 78 (2000) 1009-1016

12. A. A. S. Fialho, J. B. P. Soares, G. B. Galland, *Macromol. Chem. Phys.,* 201 (2000) 1226-1234

13. H. S. Cho, J. S. Chung, W. Y. Lee, *J. Mol. Catal. A Chem.,* 159 (2000) 203-213

14. W. Kaminsky, *J. Polym. Sci.: Part A: Polym. Chem.,* 42 (2004) 3911-3921

15. H. Münstedt, T. Steffl, A. Malmberg, *Rheol. Acta*, 45 (2005) 45 14-22

16. B. M. Weckhuysen, R. A. Schoonheydt, *Catal. Today*, 51 (1999) 215-221.

17. M. P. McDaniel, *Ind. Eng. Chem. Re*s., 27 (1988) 1559-1564

18. S. Mecking, *Angew. Chem. Int. Ed*., 40 (2001) 534-540

19. E. Löckenhoff, Marktentwicklung und Bedeutung der Kunststoffrohre heute, Information des Kunststoffrohrverbandes e.V. Bonn (2003)

20. A. Bos, Werkstoffe in Kunststoffrohr Handbuch, Kap. 2, 8-65, Vulkan Verlag, Essen (2000)

21. L. E. Janson, *Plastic Pipes for Water Supply and Sewage Disposal*. Borealis, Stockholm, Sweden (1996)

22. L. Böhm, H. F. Enderle, M. Fleißner, *Adv. Mater*., 4 (1992) 234-238

23. J. B. P. Soares, J. D. Kim, *J. Appl. Polym. Sci. Part A,* 32 (2000) 1408-1416

24. P. J. DesLauriers, M. P. McDaniel, D. C. Rohlfing, R. K. Krishnaswamy, S. J. Secora, E. A. Benham, P. L.Maeger, A. R. Wolfe, A. M. Sukhadia, B. B. Beaulieu, *Polym. Eng. Sci.,* 45 (2005) 1203-1213

25. ISO 12162 - Thermoplastics materials for pipes and fittings for pressure applications

26. Information der Arbeitsgemeinschaft ProKunststoffrohrsysteme GmbH, 40233 Düsseldorf

27. A. L. Andrady, H. S. Hamid, A. Torikai, *Photochem. Photobiol. Sci*., 2 (2003) 68-72

28. A. L. Bhuiyan, *Ultraviol. Rad. Polym.*, Chapter 51, 857-866

29. P. Gisjman, *e-Polymer*, 65 (2008) 1-34

30. M. Hakkarainen, A. C. Albertsson, *Adv. Polym. Sci.*, 169 (2004) 177-199

31. G. Scott, *Polym. Degrad. Stab.,* 10 (1985) 97-125

32. L. C. Mendes, E. S. Rufino, F. O. C. Paula, J. R. Torres, *Polym. Degrad. Stab.,* 79 (2003) 371-383

33. R. Mani, R.P. Singh, S. Sivaram, *Polym. Int.,* 44 (1997) 137-142

34. D. Feldman, *J. Polym. Environ.,* 10 (2002) 163-173

35. F. Genova, T. Gancheva, A. Marinova, *Angew. Makromol. Chem.,* 158/159 (1988) 71-86

36. A. Holmstrom, E. M. Sorvik, *J. Appl. Polym. Sci.,* 18 (1974) 761-778

37. M. Jerry, *Advanced Organic Chemistry: Reactions, Mechanisms, and Structure,* 3rd ed, Wiley, New York (1985)

38. F. Gugumus, *Angew. Makromol. Chem.,* 158/159 (1988) 151-176

39. F. Gugumus, *Angew. Makromol. Chem.,* 182 (1990) 85-109

40. F. Gugumus, *Angew. Makromol. Chem.,* 182 (1990) 111-134

41. F. Gugumus, *Polym. Degrad. Stab.,* 55 (1997) 21-43

42. F. Gugumus, *Polym. Degrad. Stab.,* 66 (1999) 161-172

43. F. Gugumus, *Polym. Degrad. Stab.,* 68 (2000) 21-33

44. A. Torikai, H. Shirakawa, S. Nagaya, K. Fueki, *J. Appl. Polym. Sci.,* 40 (1990) 1637-1646

45. E. Epacher, C. Kröhne, B. Pukánszky, *Polym. Eng. Sci.,* 40 (2000) 1458-1468

46. K. T. Sánchez, N. S. Allen, C. M. Liauw, B. Johnson, *J. Vinyl Addit. Techn.,* 17 (2011) 28-39

47. S. Al-Malaika, C. Goodwin, S. Issenhuth, D. Burdick, *Polym. Degrad. Stab.,* 64 (1999) 145-156

48. R. Arnaud, J. Moisan, J. Lemaire, *Macromolecules,* 17 (1984) 332-336

49. J. Lacoste, D. J. Carlsson, S. Falicki, D. M. Wiles, *Polym. Degrad. Stab.,* 34 (1991) 309-323

50. M. E. S. Carvalho, J. J. C. Pinto, *Polym. Eng. Sci.,* 32 (1992) 567-572

51. A. Tidjani, Y. Watanabe, *Polym. Degrad. Stab.,* 49 (1995) 299-304

52. J. J. C. Pinto, M. E. S. Carvalho, J. F. A. Ferreira, *Angew. Makromol. Chem.,* 216 (1994) 113-133

53. H. Zweifel, *Stabilisation of Polymeric Materials*, Springer, Berlin, Heidelberg, New York (1998)

54. A. Bravo A, J. H. Hotchkiss, *J. Appl. Polym. Sci.,* 47 (1993) 1741-1748

55. J. Lemaire, R. Arnaud, J. L. Gardette, *Pure Appl. Chem.,* 55 (1983) 1603-1614

56. J. Pospisil, *Angew. Makromol. Chem.,* 158/159 (1988) 221-231

57. F. Gugumus, *Angew. Makromol. Chem.,* 137 (1985) 189-225

58. G. Scott, *Pure Appl. Chem.,* 30 (1972) 267-289

59. L. Tamir, J. Pospisil, *Angew. Makromol. Chem.,* 52 (1976) 31-38

60. J. Pospisil, *Polym. Degrad. Sta*b., 20 (1988) 181-202

61. S. Jipa, R. Setnescu, T. Setnescu, M. Dumitru, I. Mihalcea, C. Podina, Z. Osawa, *Pure Appl. Chem.,* A35 (1998) 1103-1115

62. J. Pilar, J. Rotschova, J. Pospisil, *Angew. Makromol. Chem.,* 200 (1992) 147-161

63. J. Pospisil, *Polym. Degrad. Stab.,* 39 (1993) 103-115

64. J. Pospisil, *Polym. Degrad. Stab.,* 40 (1993) 217-232

65. H. Zweifel, *Plastic Additives Handbook* , Hanser, Munich (2001)

66. A. F. Bickel, E.C. Kooyman. *J. Chem. Soc.,* (1956) 2215-2221

67. P. P. Klemchuck, M. E. Gande, *Polym. Degrad. Stab.,* 22 (1988) 241-274

68. F. Gugumus, *Polym. Degrad. Stab.,* 24 (1989) 289-299

69. J. Pospisil, W. D. Habicher, S. Al-Malaika, H. Zweifel, S. Nesprek, *Macromol. Symp.,* 176 (2001) 55-63

70. R. Gensler, C.J.G. Plummer, H. H. Kausch,, E. Kramer, J. R. Pauquet, H. Zweifel, *Polym. Degrad. Stab.,* 67 (2000) 195-208

71. A. F. Bickel, E.C. Kooyman, *J. Chem. Soc.,* (1957) 2217-2221

72. D. B. Denney, W. F. Goodyear, B. Goldstein, *J. Am. Chem. Soc.,* 82 (1960) 1393-1395

73. T. G. Driver, J. R. Harris, K. A. Woerpel, *J. Am. Chem. Soc.,* 129 (2007) 3836-3837

74. C. Walling, R. Rabinowitz*, J. Am. Chem. Soc.,* 81 (1959) 1243-1249

75. P. J. Krusic, J. K. Kochi, *J. Am. Chem. Soc.*, 91 (1969) 3944-3946

76. K. Schwetlick, W. D. Habicher, *Angew. Makromol. Chem.,* 232 (1995) 239-246

77. T. Haruna, *Angew. Makromol. Chem.,* 232 (1995) 119-131

78. C. Neri, S. Constanzi, R. M. Riva, R. Farris, R. Colombo, *Polym. Degrad. Stab.,* 49 (1995) 65-69

79. W. L. Hawkins, H. Sautter, *J. Polym. Sci., Part A*, 1 (1963) 3499- 3509

80. F. Gugumus, *Angew. Makromol. Chem.,* 176/177 (1990) 241-28

81. K. N. Shyamal, J. J. de Pablo, A. D. DeBellis, *J. Am. Chem. Soc.,* 121 (1999) 4252-4261

82. P. Gijsman, M. Gitton, *Polym. Degrad. Stab.,* 66 (1999) 365-371

83. T. Zaharescu, M. Kaci, G. Hebal, R. Setnescu, T. Setnescu, R. Khima, C. Remili, S. Jipa, *Macromol. Mater. Eng.,* 289 (2004) 524–530

84. J. Sedlar, J. Marchal, J. Petruj, *Polym. Photochem.,* 2 (1982) 175-207

85. N. S. Allen, *Makromol. Chem.*, 181 (1980) 2413-2420

86. G. Scott, Developments in Polymer Stabilisation - 3, Applied Science Publishers, London (1980)

87. J. E. Pickett, J.E. Moore, *Polym. Degrad. Stab.,* 42 (1993) 231-244

88. J. E. Pickett, *Macromol. Symp.,* 115 (1997) 127-14

89. F. Waiblinger, F. Keck, M. Wtein, A. P. Fluegge, H. E. A. Kramer, D. Leppard, *J. Phys. Chem. A,* 104 (2000) 1100 - 1106

90. M. Stein, F. Keck, F. Waiblinger, A. P. Flugge, H. E. A. Kramer, A. Hartschuh, H. Port, D. Leppard, G. Rytz, *J. Phys. Chem. A,* 106 (2002) 2055-2066

91. G. Rytz, R. Hilfiker, E. Schmidt, A. Schmitter, *Ang. Makromol. Chem.,* 247 (1997) 213-224

92. G. J. Stueber, M. Kieninger, H. Schetteler, W. Busch, B. Goeller, J. Franke, H. E. A. Kramer, H. Hoir, S. Henkel, P. Fischer, H. Port, T. Hirsch, G. Rytz, J-L, Birbaum, *J. Phys. Chem.,* 99 (1995) 10097-10109

93. A. R. Horrocks, J. Mwila, M. L. Miraftab, S. S. Chohan, *Polym. Deg. Stab.,* 65 (1999) 25-36

94. S. W. Bigger, O. Delatyckij, *J. Mater. Sci.,* 24 (1989) 1946-1952

95. J. Mwila, M. Miraftab, A. R. Horrocks, *Polym. Degrad. Stab.,* 44 (1994) 351-356

96. N. C. Billingham, Atmospheric oxidation and antioxidants, G. Scott (Ed.), Elsevier, Vol. II, 219-244, London (1993)

97. R. Spatafore, L. T. Pearson, *Polym. Eng. Sci.,* 31 (1991) 1610-1617

98. R. Spatofore, K. Schultz, T. Thompson, L. T. Pearson, *Polym. Bull.,* 28 (1992) 467-472

99. J. J. Moisan, R. Lever, *Eur. Polym, J.,* 18 (1982) 407-411

100. J. Malik, D. Q. Tuan, E. Spirk, *Polym. Degrad. Stab.,* 47 (1985) 1-8

101. B. Bell, D. E. Beyer, N. L. Maecker, R. R. Papenfus, D. B. Priddy, *J. Appl. Polym. Sci.,* 54 (1994) 1605-1612

102. ASTM D5510-94, Standard Practice for Heat Aging of Oxidatively Degradable Plastics (Withdrawn 2010), Book of Standards (2001)

103. ASTM D3826-98, Standard Practice for Determining Degradation End Point in Degradable Polyethylene and Polypropylene Using a Tensile Test, Book of Standards (2008)

104. ASTM E313-10, Standard Practice for Calculating Yellowness and Whiteness Indices from Instrumentally Measured Colour Coordinates, Book of Standards (2010)

105. ASTM D1925-70, Test Method for Yellowness Index of Plastics (Withdrawn 1995), Book of Standards (1988)

106. D. M. Bigg, K. J. Heater, B. L. Grunden, D. E. Badowski, J. G. Ricks, J. Brasch, *Adv. Polym. Techn.,* 24 (2005) 215-225

107. V. M. Litvinov, M. Soliman, *Polymer,* 46 (2005) 3077-3089

108. ASTM D3895-07, Standard Test Method for Oxidative-Induction Time of Polyolefins by Differential Scanning Calorimetry, Book of Standards (2001)

109. N. Billingham, D. Bott, A. Manke, Application of Thermal Analysis Methods to Oxidation and Stabilization of Polymers in Developments in Polymer Degradation-3, N. Grassie (ed.), Applied Science Publishers, London (1981)

110. E. Kramer, J. Koppelmann, *J. Polym. Eng Sci.,* 27 (1987) 945-954

111. F. Gugumus, The use of Accelerated Tests in the Evaluation of Antioxidants and Light Stabilizers in Developments in Polymer Stabilization-8, G. Scott (ed.), Elsevier, 239, London, New York, (1987)

112. J. R. Pauquet, R.V. Todesco, O. W. Drake, Limitations and Applications of Oxidative Induction Time (OIT) to Quality Control of Polyolefins 42nd Int. Cable & Wire Symposium (1993)

113. T. L. Phease, N. C. Billingham, SW. Bigger, *Polymer,* 41 (2000) 9123-9130

114. R. C. Nielsen, *J. Liquid. Chromat.,* 14 (1991) 503-519

115. R. C. Nielsen*, J. Liquid. Chromat.,* 16 (1993) 1625-1638

116. H. E. Mansouri, N. Yagoubi, D. Ferrier, *Chromat*., 48 (1998) 491-496

117. H. E. Mansouri, N. Yagoubi, D. Scholler, A. Feigenbaum, D. Ferrier, *J. Appl. Polym. Sci.,* 71 (1999) 371-375

118. L. Coulier, E. R. Kaal, M. Tienstra, T. Hankemeier, *J. Chromatogr. A,* 1062 (2005) 227-238

119. E. Reingruber, W. Buchberger, *J. Sep. Sci.,* 33 (2010) 3463-3475

120. W. Camacho, S. Karlsson, *Int. J. Polym. Anal. Charact.,* 7 (2002) 41-51

121. E. Thuet, J. P. Pauquet, R. V. Todesco, Determination of Stabilizers in Polyolefins by FTIR-Spectroscopy, Ciba Specialty Chemicals (1997)

122. B. Vigerust, K. Kolset, S. Nordenson, A. Henriksen, K. Kleveland, *Appl. Spectros.,* 2 (1991) 173-177

123. T. V. Karstang**,** A. Henriksen, *Chemom. Intell. Lab. Syst.,* 14 (1992) 331-339

124. B. Mailhot, J. L. Gardette, *Macromolecules,* 25 (1992) 4127-4133

125. X. Colom, J. Canavate, J. J. Sunol, P. Pages, J. Saurina, F. Carrasco, *J. Appl. Polym. Sci.,* 87 (2003) 1685-1692

126. E. Epacher, J. Tolveth, K. Stoll, B. Pukansky, *J. Appl. Polym. Sci.,* 74 (1999) 1596-1605

127. R. P. Singh, R. Mani, S. Sivaram, J. Lacoste, D. Vaillant, *J. Appl. Polym. Sci.,* 50 (1993) 1871-1881

128. J. P. Blitz, D. C. Mc Faddin, *J. Appl. Polym. Sci.,* 51 (1994) 13-20

129. J. R. Nielsen, A. H. Woollett, *J. Chem. Phys.,* 26 (1957) 1391-1400

130. B. Fanconi, *Ann. Rev. Phys. Chern.,* 31 (1980) 265-291

131. G. Ellis, M. A. Gómez, C. Marco, *Int. J. Vibr. Spec.,* [www.ijvs.com] 5, 4, 7 (2001)

132. H. Hagemann, R. G. Snyder, A. J. Peacock, L. Mandelkern, *Macromolecules,* 22 (1989) 3600-3606

133. B. E. Read, R. S. Stein, *Macromolecules,* 1 (1968) 116-126

134. D. R. Burfield, P. S. T. Loi, *J. Appl. Polym. Sci.,* 36 (1988) 279-293

135. F. Mirabella, *J. Polym. Sci., Part B: Polym. Phys.,* 25 (1987) 591-602

136. M. Houska, M. Brummell, *Polym. Eng. Sci.,* 27 (1987) 917-924

137. F. M. Rugg, J. J Smith, R. C. Bacon, *J. Polym. Sci.,* 13 (1954) 535-547

138. E. Andreassen, Infrared and Raman spectroscopy of polypropylene. In Polypropylene: An A-Z reference, J. Karger-Kocsis, Ed. Kluwer Publishers, 320, Dordrecht (1999)

139. N. Olivares, P. Tiemblo, M. J. Gòmez-Elvira, *Polym. Degrad. Stab.,* 65 (1999) 297-302

140. A. L. Andrady, J. E. Pegram, Y. Tropsha**,** *J. Env. Polym. Degrad.,* 1 (1993) 171-179

141. H. D. Hoekstra, J. L. Spoomaker, J. Breen, L. Audouin, J. Verdu, *Polym. Degrad. Stab.,* 49 (1995) 251-262

142. T. Matsui, T. Takano, S. Takayama, M. Ito, I. Narisawa, *Rad. Phys. Chem.,* 63 (2002) 193-200

143. N. Kang, Y. Z. Xu, J. G. Wu,W. Feng, S. F. Weng, D. F. Xu, *Phys. Chem. Chem. Phys.,* 2 (2000) 3627-3630

144. P. J. Miller, J. F. Jackson, R. S. Porter, *J. Polym. Sci.: Polym. Phys. Ed.,* 11 (1973) 2001-2012

145. C. V**.** Stephenson, B. C. Moses, R. E. Burks, W. C. Coburn, W. S. Wilcox, *J. Polym. Sci***.**, 55 (1961) 465-475

146. V. A. González-Gonzalez, G. Neira-Velázquez, J. L. Angulo-Sánchez, *Polym. Degrad. Stab.,* 60 (1998) 33-42

147. D. L. Tabb, J. J. Sevcik, J. L. Koenig, *J. Polym Sci.: Polym. Phys. Ed*., 13 (1975) 815-824

148. A. Holmström, E. Sörvik, *J. Chromatogr.,* 53 (1970) 95-108

149. A. M. Kotliar, S. Podgor, *J. Polym. Sci.,* 55 (1961) 423-436

150. P. J. Perrono, P. B. Lederman, *Polym. Eng. Sci.,* 12 (1972) 340-345

151. R. Lew, D. Suwanda, S. T. Balke, *J. Appl. Polym. Sci.,* 35 (1988) 1049-1063

152. C. David, M. Trojan, A. Daro, *Polym. Degrad. Stab.,* 37 (1992) 233-245

153. P. D. Iedema, C. Willems, G. van Vliet, W. Bunge, S. M. P. Mutsers, H. C. J. Hoefsloot, *Chem. Eng. Sci.,* 56 (2001) 3659-3669

154. E. Gaube, G. Diedrich, W. Müller, *Kunststoffe,* 66 (1976) 2-8

155. M. Ifwarson, *Kunststoffe,* 79 (1989) 525-529

156. K. Karlsson, G. D. Smith, U.V Gedde, *Polym Eng. Sci.,* 32 (1992) 649-657

157. J. Viebke, E. Elble, M. Ifwarson, U.W. Gedde, *Polym. Eng. Sci.,* 34 (1994) 1354-1361

158. DIN EN ISO 1167-1, Thermoplastics pipes, fittings and assemblies for the conveyance of fluids - Determination of the resistance to internal pressure - Part 1: General method, Beuth-Verlag, Berlin (2006)

159. E. M. Hoàng, D. Lowe*, Polym. Degrad. Stab.,* 93 (2008) 1496-1503

160. J. Viebke, U. Gedde, *Polym. Eng. Sci.,* 37 (1997) 896-911

161. J. Viebke, U. Gedde, *Polym. Eng. Sci.,* 38 (1998) 1244-1250

162. K. Karlsson, G. D. Smith, U. W. Gedde, *Polym Eng. Sci.,* 32 (1992) 649-657

163. B. Terselius, U. W. Gedde, J. F. Jansson, *Polym. Eng. Sci.,* 22 (1982) 422 - 431

164. L. Peeva, B. Fileva, S. Evtimova, V. Tsveteva, *Angew. Makromol. Chem.,* 176/177 (1990) 79-86

165. E. K. Figueroa, *Thermoch. Acta,* 114 (1987) 115-124

166. U. W. Gedde, J. Viebke, H. Leijstrom, M. Ifwarson, *Polym. Eng. Sci.,* 34 (1994) 1773-1787

167. N. S. Allen, S. J. Palmer, G. P. Marshall, J. L.Gardette, *Polym. Degrad. Stab.,* 56 (1997) 264-274

168. E. Kramer, J. Koppelmann, *J. Polym. Eng. Sci.,* 27 (1987) 945-954

169. E. Kramer, J. Koppelmann, *Polym. Degr. Stab.,* 16 (1986) 261-275

170. E. Kramer, J. Koppelmann, N. Guendouz*, Angew. Makromol. Chem*., 176 (1990) 55-63

171. N. S. Allen, L. M. Moore, G. P Marshall, C. Vasiliou, J. Kotecha, B. Valange, *Polym. Degr. Stab.,* 27 (1990) 145-157

172. K. Karlsson, P. A. Eriksson, M. Hedenqvist, M. Ifwarson, G. D. Smith, U. W. Gedde, *Polym. Eng. Sci.,* 33 (1993) 303-310

173. U. W. Gedde, M. Ifwarson, *Polym. Eng. Sci.,* 30 (1990) 202-210

174. G. D. Smith, K. Karlsson, U. W. Gedde, *Polym. Eng. Sci.,* 32 (1992) 658-667

175. K. Thörnblom, M. Palmlöf, T. Hjertberg, *Polym. Degrad. Stab.,* 96 (2011) 1751-1760

176. N. S. Allen, G. P. Marshall, C. Vasiliou, L. M. Moore, J. L. Kotecha, J. L. Gardette, *Polym. Degrad. Stab.,* 20 (1988) 315-324

177. T. Schwarz, G. Steiner, J. Koppelmann, *J. Therm. Anal.,* 55 (1989) 481-496

178. M. Schmid, A. Ritter, S. Affolter, *J. Therm. Anal. Calorim.,* 83 (2006) 367-371

179. R. Bhargava, S. Q. Wang, J. L. König, *Adv. Polym. Sci.,* 163 (2003) 137-191

180. G. Ellis, C. Marco, M. Gomez, *Infrared Phys. Technol.,* 45 (2004) 349-364

181. P. J. Treado, M. D. Morris**,** *Appl. Spectrosc. Rev.,* 29 (1994) 1-38

182. H. Belz, Thermo Fisher Presentation (2008)

183. P. A. M. Smith, *Vib. Spectrosc.,* 24 (2000) 47-62

184. C. G. Smith, P. B. Smith, A. J. Pasztor, M. L. McKelvy, D. M. Meunier, S. W. Froelicher, A. S. Ellaboudy, *Anal. Chem.,* 65 (1993) 217-243

185. C. G. Smith, P. B. Smith, A. J. Pasztor, M. L. McKelvy, D. M. Meunier, S. W. Froelicher, *Anal. Chem.,* 67 (1995) 97-126

186. P. B. Smith, A. J. Pasztor, M. L. McKelvy, D. M. Meunier, S. W. Froelicher, F. C. Y. Wang, *Anal. Chem.,* 71 (1999) 61-80

187. J. E. Katon, *Micron,* 27 (1996) 303-314

188. D. Garcia, *J. Vinyl Addit. Techn.,* 3 (1997) 126-129

189. K. Sheu, S. J. Huang, J. F. Johnson, *Polym. Eng. Sci.,* 29 (1997) 77-85

190. J. L. Gardette, *Angew. Makromol. Chem.,* 232 (1995) 85-103

191. D. E. Gavrila, *J. Appl. Polym. Sci.,* 59 (1996) 71-76

192. D. Garcia, J. Black *J. Vinyl. Add.,* 5 (1999) 81-86

193. J. M. Chalmers, N. J. Everall, *Analusis,* 28 (2000) 53-64

194. D. E. Gravila, B. Gosse, *J. Radioanal. Nucl. Chem,* 185 (1994) 311-317

195. S. C. Hsu, D. Lin-Vien, R. N. French, *Appl. Spectros.,* 46 (1992) 187-381

196. N. B. Joshi, D. E. Hirt, *Appl. Spectrosc.,* 53 (1999) 11-16

197. S. Y. Sankhe, D. E. Hirt, *Appl. Spectrosc.,* 56 (2002) 205-211

198. S. Y. Sankhe, D. E. Hirt, *Appl. Spectrosc.,* 57 (2003) 37-43

199. R. Brüll, G. Geertz, H. Kothe, T. Macko, M. Rudschuck, M. Wenzel, K. Engelsing, J. Wüst, M. Bastian, *Macromol. Mater. Eng.,* 293 (2008) 400-408

200. R. Brüll, G. Geertz, R. Maria, K. Rode, *Nachr. aus der Chemie,* 58 (2010)

201. G. Geertz, R. Brüll, J. Wieser, R. Maria, M. Wenzel, K. Engelsing, J. Wüst, M. Bastian, M. Rudschuck, *Polym. Degr. Stab.,* 94 (2009) 1092-1102

202. DIN EN 728, Plastics piping and ducting systems - Polyolefin pipes and fittings - Determination of oxidation induction time, Berlin: Beuth-Verlag (1997)

203. S. Krimm, C. Y. Liang, G. B. B. M. Sutherland, *J. Chem. Phys.,* 25 (1956) 549-562

204. N. Marabayashi, Y. Ishida, M. Haratakea, *Anal. Sci.,* 7 (1991) 665-668

205. R. Milini, G. D. Piero, *Acta Cryst.,* C48 (1992) 696-699

206. C. Wu, T. Yamagishi, Y. Nakamoto, *Polym. Int.,* 50 (2001) 1095-1102

207. C. Wu, T. Kuriyama, T. Inoue, *J. Mater. Sci.,* 39 (2004) 1249 -1254

208. E. Földes, B. Turcsanyi, *J. Appl. Polym. Sci.,* 46 (1992) 505-515

209. E. Földes, J. Lohmeijer, *J. Appl. Polym. Sci.,* 65 (1997) 761-775

210. A. Bigotto, V. Galasso, *Spectroch. Acta Part A: Mol. Spectros.,* 35 (1979) 725-732

211. T. Matsuo, *Bull Chem Soc. Japan*, 37 (1964) 1844-1848

212. G. Socrates, Infrared and Raman characteristic group frequencies, Wiley, New York (2001)

213. S. A. Jabarin, *J. Appl. Polym. Sci.,* 34 (1987) 85-96

214. A. J. C. Padron, M. A. Colmenares, Z. Rubinztain, L. A. Albornoz, E*ur. Polym. J.,* 23 (1987) 723-727

215. A. Tanaka, G. Chen, Y. Zhao, A. E. Davies, A. S. Vaughan, T. Takada, *IEEE Trans. Dielectr. Electr. Insul.*, 10 (2003) 148-154

216. Y. S. Suzuki, J. Mizuguchi, *Dyes Pigm.*, 61 (2004) 69-77

217. D. L. Wo, R. I. Tanner, *Rheol. Acta,* 49 (2010) 75-88

218. F. R. Williams, *J. Appl. Polym. Sci.,* 9 (1965) 861-886

219. E. Kovacs, Z. Wolkober, *J. Polym. Sci., Symposium*, 57 (1976) 171-180

220. N. S. Allen, C. Vasiliou, G. P. Marshall, *Polym. Degrad. Stab.,* 24 (1989) 17-31

221. H. Yamashita, Y. Ohkatsu, *Polym. Degrad. Stab.,* 80 (2003) 421–426

222. J. R. Pauquet, R.V. Todesco, O.W. Drake, Limitations and Applications of Oxidative Induction Time (OIT) to Quality Control of Polyolefins 42nd Int. Cable & Wire Symposium (1993)

223. F. Gugumus, *Polym. Degrad. Stab.,* 27 (1990) 19-34

224. J. P. Luongo, R. Salovey, *J. Appl. Polym Sci.,* 7 (1963) 2307-2318

225. M. Dole, D.C Milner, T. F. Williams, *J. Am. Chem. Soc.,* 80 (1958) 1580-1588

226. A. A. Miller, E. J. Lawton, J.S Balwit , *J. Phys. Chem.,* 60 (1956) 599-604

227. G. Dörner, R. W. Lang, *Polym. Degrad. Stab.,* 62 (1998) 431-440

228. M. Tsuboi, *J. Am. Chem. Soc*. 79 (1957) 1351-1354

229. R. A. Nyquist, *Spectrochim. Acta*, 22 (1963) 1315-1323

230. N. S. Allen, M. Edge, Fundamentals of Polymer Degradation and Stabilisation, Elsevier Applied Science, New York (1992)

231. B. Randy, J. F. Rabek, Photodegradation, Photo-oxidation and Photostabilization of Polymers, Principles and Applications, Wiley, New York (1975)

232. A. P. D'Silva, *Carbon,* 36 (1998) 1317-1325

233. I. W. Levin, R. Bhargava, *Annu. Rev. Phys. Chem.*, 56 (2005) 429-474

234. J. M. Pena, N. S. Allen, C. M. Liauw, M. Edge, B. Valange, *J. Vinyl Addit. Techn.,* 6 (2000) 62-68

235. J. M. Pena, N. S. Allen, M. Edge, C. M. Liauw, F. Santamaria, *J. Mater. Sci.,* 36 (2001) 2885-2898

236. J. M. Pena, N. S. Allen, M. Edge, C. M. Liauw , B. Valange, *Polym. Degrad. Stab*., 72 (2001) 259-270

237. W. L. Hawkins, *J. Polym. Sci. Polym. Symp.,* 57 (1976) 319-328

238. J. Y. Moisan, Polymer Permeability, Elsevier, London (1988)

239. J. M. Pena, N. S. Allen, M. Edge, C. M. Liauw, B. Valange, *Polym. Degrad. Stab.,* 72 (2001) 163-174

240. W. M. Horspool*, ChemInform*., 34 (2003) 124-158

241. J. M. Pena, N.S. Allen, M. Edge, C.M. Liauw, B. Valange, *Polym. Degrad. Stab.,* 72 (2001) 31-45

242. J. C. Bart, Polymer Additive Analytics, Industrial Practise and Case Studies, University Press, Firenze (2006)

243. P. P. Klemchuck, P-L. Horning, *Polym. Degrad. Stab.,* 34 (1991) 333-346

7. List of abbreviations

A

A	absorbance
AO	antioxidant
a-PP	atactic polypropylene
ASTM	American Society for Testing and Materials
ATR	Attenuated total reflectance

C

c	concentration
°C	centigrade
CB	carbon black
CI	carbonyl index

D

DSC	Differential scanning calorimetry

E

ε	absorptivity or extinction coefficient

F

FTIR	Fourier transform infrared spectroscopy

H

h	hour
HAS	hindered amine stabiliser
HALS	hindered amine light stabiliser
HDPE	high density polyethylene
HD	hydroperoxide decomposer

Hi-PP	high impact polypropylene
HPLC	high performance liquid chromatography

K

kJ/m^2	kilo joule per square meter

I

i-PP	isotactic polypropylene
IR	infrared
IS	internal standard
ISO	International Organisation for Standardisation

M

MCT	mercury cadmium telluride
MM	molar mass
mm	millimeter
MMD	molar mass distribution
M_n	number average molar mass
M_w	weight average molar mass
M_z	z-average molar mass

N

NO·	nitroxyl radical

O

OIT	Oxidation induction time

P

PB	poly-1-butene
PDI	Polydispersity index
PE	polyethylene
PEX	crosslinked polyethylene

PP	polypropylene
PP-H	homo-polypropylene
PP-R	random-polypropylene
PTFE	politetrafluoretileno

R

R·	alkyl radical
ROOH	hydroperoxide
ROO·	peroxy radical

L

l	lenght
LDPE	low density polyethylene
LLDPE	linear low density polyethylene

S

SAAO	secondary aromatic antioxidant
SCG	slow crack grow
SCB	short-chain branches
SEC	Size exclusion chromatography
s-PP	syndiotactic polypropylene

T

TCB	1,2,4-trichlorobenzene
TLC	Thin layer chromatography

U

UV	Ultraviolet

Y

YI	Yellowness index

8. Curriculum Vitae

Name: Raquel Maria
Date of Birth: 19 September 1979
Place of Birth: Lisbon, Portugal
Nationality: Portuguese
Marital status: Married

Education

1989-1997	High School Rainha Dona Leonor, Lisbon, Portugal

Academic career

September 1997-Juni 2004	Licentiate in Chemistry, Department of Chemistry and Biochemistry, Faculty of Sciences, University of Lisbon, Lisbon, Portugal Thesis title: "Influence of the cerium substitution on the structure and electrical conductivity of the $CaMnO_3$ perovskite"
Since Juli 2008	Doctoral thesis under the supervision of Prof. Dr. M. Rehahn at Technical University Darmstadt, Germany

Publications:

R. Maria, K. Rode, R. Brüll, F. Dorbath, B. Baudrit, M. Bastian, E. Brendlé, *Polym. Degrad. Stab.*, 96 (2011) 1901-1910

R. Brüll, R. Maria, K. Rode, *Macromol. Chem. Phys.,* 211 (2010) 2233-2239

R. Brüll, G. Geertz, R. Maria, K. Rode, *Nachrichten aus der Chemie*, 58 (2010) 675-688

G. Geertz, R. Brüll, J. Wieser, R. Maria, M. Wenzel, K. Engelsing, et al., *Polym. Degrad. Stab*., 94 (2009) 1092-1102

Presentations:

R. Maria, K. Rode, R. Brüll, "*Monitoring the degradation of PE-pipes by IR-Microscopy*" ACS Seminar, Darmstadt, Germany, 06th July, 2010

R. Maria, K. Rode, R. Brüll, "*Monitoring the degradation of PE-pipes by IR-Microscopy*", Doktorandentag, Darmstadt, Germany, 14th December, 2011

Posters:

R. Maria, R. Brüll, G. Geertz, J. Wüst, K. Engelsing, M. Wenzel,*"Imaging techniques as tools for studying the ageing behaviour of PP-pipes",* Advances in Polymer Science and Technology (APST), Linz, Austria, 8th-10th July, 2009

R. Maria, R. Brüll, K. Rode, G. Geertz, R. Kleppinger, J. Wüst, K. Engelsing, M. Wenzel,*"Imaging techniques as tools for studying the ageing behaviour of PP-pipes",* Material and Science Engeneering*,* Darmstadt, Germany, 24th-26th August, 2010

R. Maria, R. Brüll, K. Rode, G. Geertz, R. Kleppinger, J. Wüst, K. Engelsing, M. Wenzel,*"Imaging techniques as tools for studying the ageing behaviour of PP-pipes",* 3rd Internacional Conference on Polyolefins Characterisation*,* Shangai, China, 7th-10th November, 2010

R. Maria, T. Schuster, K. Rode, S. Damodaran, R. Brüll, M. Wenzel, K. Engelsing, Martin Bastian*,"Imaging techniques: Understanding the ageing of pipe grade polyethylene",* Eurotec 2011, Barcelona, Spain, 14th -15th November, 2011

R. Maria, T. Schuster, K. Rode, S. Damodaran, R. Brüll, M. Wenzel, K. Engelsing, M. Bastian*,"Imaging techniques: Understanding the ageing of pipe grade polyethylene",* Chemelot International Polyolefins Symposium, CIPS, Maastricht, Holland, 7th-10th October, 2012

R. Maria, K. Rode, T. Schuster, R. Brüll, F. Dorbath, B. Baudrit, M. Wenzel, J. Wüst, M. Bastian,*"Imaging Techniques: Innovative Tools for Failure Analysis"*, International Conference for Polyolefin Characterisation (ICPC), Houston, USA, 21st-24th October, 2012

Raquel Maria
Wilhelm Kuelz Strasse 17
06108 Halle (Saale)

27th September 2013

Eidesstattliche Erklärung

Ich erkläre hiermit an Eides Statt, dass ich meine Dissertation selbstständig und nur mit den angegebenen Hilfsmitteln angefertigt habe.

Raquel Maria

Raquel Maria
Wilhelm Kuelz Strasse 17
06108 Halle (Saale)

27th September 2013

Erklärung

Ich erkläre hiermit, noch keinen Promotionsversuch unternommen zu haben.

Raquel Maria